Nonlinear Projective-Iteration Methods for Solving Transport Problems on Regular and Unstructured Grids

Dmitriy Y. Anistratov, PI,
Adrian Constantinescu, Loren Roberts and William Wieselquist, graduate students

Department of Nuclear Engineering
North Carolina State University

Final Technical Report

Apri 30, 2007

Contents

List of Figures

List of Tables

Chapter 1

Preface

This is a project in the field of fundamental research on numerical methods for solving the particle transport equation. Numerous practical problems require to use unstructured meshes, for example, detailed nuclear reactor assembly-level calculations, large-scale reactor core calculations, radiative hydrodynamics problems, where the mesh is determined by hydrodynamic processes, and well-logging problems in which the media structure has very complicated geometry. Currently this is an area of very active research in numerical transport theory. Main issues in developing numerical methods for solving the transport equation are the accuracy of the numerical solution and effectiveness of iteration procedure. The problem in case of unstructured grids is that it is very difficult to derive an iteration algorithm that will be unconditionally stable. It is vital to develop novel computational transport methods that will be able to fit accurately asymptotics of the transport equation, mimic various important features of the transport solution, adapt to significantly different behavior of the solution without loss of accuracy, and converge fast. The project focuses on development of unconditionally stable methods for solving the multidimensional transport equation on unstructured grids and new nonlinear methods with advanced properties for regular meshes, based on nonlinear projective-iterative methods, namely, the Quasidiffusion and Flux methods.

Three graduate students were involved in this NEER project:

1. Adrian Constantinescu

   - Thesis title: "Analysis of Projective-Iterative Methods for Solving Multidimensional Transport Problems,"
   - M.S. in Nuclear Engineering, Dept. of Nuclear Eng., NC State University,
   - graduated in August 2006.

2. Loren Roberts

   - Dissertation title: "Nonlinear Weighted Flux Methods for Solving the Multidimensional Transport Equation,"
   - Ph.D. student, May 2003 - present, Dept. of Nuclear Eng., NC State University,
   - preliminary exam was passed on April 23, 2007,

- to graduate in fall 2007.

3. William Wieselquist

   - Dissertation title: "The Quasidiffusion Method for Solving Transport Problems on Unstructured Grids,"
   - Ph.D. student, January 2005 - present, Dept. of Nuclear Eng., NC State University,
   - to graduate in summer 2008.

The results of this research project are presented in the following publications:

1. A. Constantinescu and D.Y. Anistratov, "Stability Analysis of the Quasidiffusion Method for 1D Periodic Heterogeneous Problems," *Trans. Am. Nucl. Soc.,* **95**, 565-567 (2006).

2. A. Constantinescu, "Analysis of Projective-Iterative Methods for Solving Multidimensional Transport Problems," Master Thesis, Scientific Advisor: D.Y. Anistratov, Department of Nuclear Engineering, North Carolina State University, August 2006.

3. L. Roberts & D.Y. Anistratov, "Nonlinear Weighted Flux Methods for Particle Transport Problems," *M&C 2005*, International Conference on Mathematics and Computations, Supercomputing, Reactor Physics and Nuclear Biological Applications, American Nuclear Society Topical Meeting of M&C Division, Avignon, France, September, 2005, 10 pp.

4. L. Roberts & D.Y. Anistratov, "Nonlinear Weighted Flux Methods for Solving Transport Equation," *Transport Theory and Statistical Physics.*

5. L. Roberts & D.Y. Anistratov, "Nonlinear Weighted Flux Methods for Solving the Transport Equation in 2D Cartesian Geometry," *Proceedings of M&C + SNA 2007, Joint International Topical Meeting on Mathematics & Computations and Supercomputing in Nuclear Applications*, Monterey, CA, April, 2007, 13 pp.

6. A. Constantinescu & D.Y. Anistratov, "Stability Analysis of the Quasidiffusion Method for Multidimensional Problems with Material Discontinuities," *Proceedings of M&C + SNA 2007, Joint International Topical Meeting on Mathematics & Computations and Supercomputing in Nuclear Applications*, Monterey, CA, April, 2007, 11 pp.

7. W. A. Wieselquist and D.Y. Anistratov, "The Quasidiffusion Method for 2D Transport Problems on AMR Grids," *Trans. Am. Nucl. Soc.,* **96** (2007) (to appear).

Chapter 2

Stability Analysis of the Quasidiffusion Method for 1D Periodic Heterogeneous Problems

2.1　Introduction

Recently it has been observed that some acceleration methods for transport iterations lose effectiveness in problems with strongly heterogeneous media. To understand this phenomenon and theoretically predict the convergence properties of linear transport iteration methods, problems with spatially periodic heterogeneous media have been studied by means of a Fourier analysis [1, 5, 2].

There exists a group of nonlinear methods for solving transport problems [4, 5]. In the light of the new results on performance of the diffusion synthetic acceleration and transport synthetic acceleration methods [5, 2], it is interesting to study the nonlinear methods for this special class of problems. Note that the Fourier analysis cannot be directly applied to study these methods even in homogeneous medium problems, because of their nonlinearity. For this case, they have been analyzed on special infinite medium problems with a constant source for which the analytic solution is known [6]. The equations of nonlinear methods are linearized about the solution. As a result, it became possible to predict the convergence rates of the nonlinear methods in the vicinity of the solution in homogeneous media. It has been shown also that the theoretically estimated spectral radius is close to the numerically evaluated one [5, 6]. However, in the case of heterogeneous media the analytic solution is not known. In this paper, to analyze nonlinear transport iteration methods for problems with infinite periodic heterogeneous media, we propose to use a numerical solution generated in a finite period-wide domain with periodic boundary conditions. A study of the quasidiffusion (QD) method [4] is presented. The results of theoretical analysis and computations are shown to demonstrate the power of prediction.

The results of the research presented in this chapter were published in

- A. Constantinescu (*graduate student*) and D.Y. Anistratov, "Stability Analysis of the Quasidiffusion Method for 1D Periodic Heterogeneous Problems," *Trans. Am. Nucl. Soc.*, **95**, 565-567 (2006).

- A. Constantinescu, "Analysis of Projective-Iterative Methods for Solving Multidimensional Transport Problems," Master Thesis, Scientific Advisor: D.Y. Anistratov, Department of Nuclear Engineering, North Carolina State University, August 2006.

2.2   The QD Method

We consider a one group transport problem with isotropic scattering and source in 1D slab geometry ($0 \leq x \leq X$). The QD method is defined by [4]:

$$\mu \frac{\partial}{\partial x} \psi^{(s+1/2)} + \sigma_t \psi^{(s+1/2)} = 0.5(\sigma_s \phi^{(s)} + q) \,, \tag{2.1}$$

$$E^{(s+1/2)}(x) = \frac{\int_{-1}^{1} \mu^2 \psi^{(s+1/2)}(x,\mu) d\mu}{\int_{-1}^{1} \psi^{(s+1/2)}(x,\mu) d\mu} \,, \tag{2.2}$$

$$\frac{d}{dx} J^{(s+1)} + \sigma_a \phi^{(s+1)} = q \,, \tag{2.3}$$

$$\frac{d}{dx} \left(E^{(s+1/2)} \phi^{(s+1)} \right) + \sigma_t J^{(s+1)} = 0 \,, \tag{2.4}$$

and corresponding boundary conditions. Standard notations are used. s is the iteration index.

2.3   The Discretized QD Equations and Linearization

The transport equation (2.1) is discretized by the step characteristic method. To approximate the low-order QD equations (2.3) and (2.4), we use independent discretization by means of a second-order finite volume (FV) scheme. A spatial mesh is defined so that $x_{j+1/2}$ ($1 \leq j \leq N$) correspond to the cell edges, where $x_{1/2}=0$, $x_{N+1/2}=X$, and $\Delta x_j = x_{j+1/2} - x_{j-1/2}$. The discretized QD equations have the following form ($j=1,...,N$, $m=1,...,M$):

$$\mu_m(\psi_{m,j+1/2} - \psi_{m,j-1/2}) + \sigma_{t,j} \Delta x_j \psi_{m,j} \tag{2.5}$$
$$= 0.5(\sigma_{s,j} \phi_j + q_j) \Delta x_j \,,$$

$$\psi_{m,j} = \alpha_{m,j} \psi_{m,j-1/2} + (1 - \alpha_{m,j}) \psi_{m,j+1/2} \,, \tag{2.6}$$

$$\alpha_{m,j} = \frac{1}{\tau_{m,j}} - \frac{1}{e^{\tau_{m,j}} - 1} \,, \ \tau_{m,j} = \frac{\sigma_{t,j} \Delta x_j}{\mu_m} \,, \tag{2.7}$$

$$E_j = \sum_m \mu_m^2 \psi_{m,j} w_m / \sum_m \psi_{m,j} w_m \,, \tag{2.8}$$

$$J_{j+1/2} - J_{j-1/2} + \sigma_{a,j} \Delta x_j \phi_j = q_j \Delta x_j \,, \tag{2.9}$$

$$E_{j+1} \phi_{j+1} - E_j \phi_j + \sigma_{t,j+1/2} \Delta x_{j+1/2} J_{j+1/2} = 0 \,, \tag{2.10}$$

$$\sigma_{t,j+1/2} = \frac{\sigma_{t,j} \Delta x_j + \sigma_{t,j+1} \Delta x_{j+1}}{\Delta x_j + \Delta x_{j+1}} \,. \tag{2.11}$$

Cell-average and cell-edge quantities have integer and half-integer subscripts, correspondingly. Here w_m is a quadrature weight, $\Delta x_{j+1/2} = 0.5(\Delta x_j + \Delta x_{j+1})$.

The Eqs. (2.5)-(2.11) are solved according to the QD iteration scheme given by Eqs. (2.1)-(2.4). Assuming that the solution on s-th iteration is close to the converged one, we

11

define

$$\psi_{m,j}^{(s+1/2)} = \psi_{m,j} + \varepsilon\delta\psi_{m,j}^{(s+1/2)} \,, \tag{2.12}$$

$$\psi_{m,j+1/2}^{(s+1/2)} = \psi_{m,j+1/2} + \varepsilon\delta\psi_{m,j+1/2}^{(s+1/2)} \,, \tag{2.13}$$

$$\phi_j^{(s)} = \phi_j + \varepsilon\delta\phi_j^{(s)} \,, \quad J_j^{(s)} = J_j + \varepsilon\delta J_j^{(s)} \,, \tag{2.14}$$

where $\varepsilon \ll 1$. Introducing Eqs. (2.12)-(2.14) into Eqs. (2.5)-(2.10), we linearize the discretized QD equations and get the following equations for the variations:

$$\mu_m(\delta\psi_{m,j+1/2}^{(s+1/2)} - \delta\psi_{m,j-1/2}^{(s+1/2)}) + \sigma_{t,j}\Delta x_j\delta\psi_{m,j}^{(s+1/2)} \tag{2.15}$$
$$= 0.5\sigma_{s,j}\delta\phi_j^{(s)}\Delta x_j \,,$$

$$\delta\psi_{m,j}^{(s+1/2)} = \alpha_{m,j}\delta\psi_{m,j-1/2}^{(s+1/2)} + (1 - \alpha_{m,j})\delta\psi_{m,j+1/2}^{(s+1/2)} \,, \tag{2.16}$$

$$\delta J_{j+1/2}^{(s+1)} - \delta J_{j-1/2}^{(s+1)} + \sigma_{a,j}\Delta x_j\delta\phi_j^{(s+1)} = 0 \,, \tag{2.17}$$

$$E_{j+1}\delta\phi_{j+1}^{(s+1)} - E_j\delta\phi_j^{(s+1)} + \sigma_{t,j+1/2}\Delta x_{j+1/2}\delta J_{j+1/2}^{(s+1)} \tag{2.18}$$
$$= \frac{\phi_j}{\phi_j^*}\delta P_j^{(s+1/2)} - \frac{\phi_{j+1}}{\phi_{j+1}^*}\delta P_{j+1}^{(s+1/2)} \,,$$

$$\delta P_j^{(s+1/2)} = \sum_m \left(\mu_m^2 - E_j\right)\delta\psi_{m,j}^{(s+1/2)}w_m \,, \tag{2.19}$$

$$\phi_j^* = \sum_m \psi_{m,j}w_m \,. \tag{2.20}$$

Note that the resulting linearized QD equations depend on the solution of the original discretized QD equations (2.5)-(2.11) in terms of ϕ_j, ϕ_j^*, and E_j, where generally $\phi_j \neq \phi_j^*$ due to independent discretization of the transport and low-order QD equations.

2.4   Fourier Analysis and Numerical Results

We consider an infinite medium problem that is formed by two layers of different materials periodically repeated. The spatial mesh consists of one cell per layer. To generate the solution necessary for the analysis, we solve the corresponding finite problem with two cells (layers) and periodic boundary conditions. To perform the Fourier analysis of the QD method in the vicinity of the solution, we introduce the following ansatz (j=1,2):

$$\delta\psi_{m,j}^{(s+1/2)} = \omega^s a_{m,j}e^{i\lambda x_j}, \delta\psi_{m,j-1/2}^{(s+1/2)} = \omega^s b_{m,j}e^{i\lambda x_{j-1/2}}, \tag{2.21}$$

$$\delta\psi_{m,5/2}^{(s+1/2)} = \omega^s b_{m,1}e^{i\lambda x_{5/2}} \,, \delta\phi_j^{(s)} = \omega^s A_j e^{i\lambda x_j} \,, \tag{2.22}$$

$$x_j = 0.5(x_{j-1/2} + x_{j+1/2}) \,.$$

We eliminate $\delta J_{j+1/2}^{(s+1)}$ from Eqs. (2.15)-(2.20), substitute Eqs. (2.21)-(2.22) into them and get an equation for the eigenvalue ω. The spectral radius is defined by $\rho = \sup_\lambda|\omega(\lambda)|$.

The convergence rate depends on parameters of materials $\sigma_{t,j}$, $c_j = \frac{\sigma_{t,j}}{\sigma_{s,j}}$, spatial intervals Δx_j (j=1,2), and the angular quadrature set. The spectral radius is evaluated for problems with various combinations of $\sigma_{t,1}$ and $\sigma_{t,2}$. The lower-triangular part of Table 1 contains theoretical estimates of ρ versus $\sigma_{t,1}$ and $\sigma_{t,2}$, for $c_1 = c_2 = 0.9999$ and $\Delta x_1 = \Delta x_2 = 1$. The double S_4 Gauss-Legendre quadrature set was used.

To evaluate how the obtained theoretical results of the Fourier analysis for infinite media predict the performance of the QD method in finite media, we compare them with numerically estimated values of ρ for problems with non-periodic boundary conditions. The upper-triangular part of Table 1 presents the results of numerical solution of problems with 1000 layers ($0 \leq x \leq 1000$), vacuum boundary conditions and source $q=1$ everywhere. The spectral radii were evaluated in L_2-norm by last 3 iterations. The point-wise convergence criterion for ϕ with a parameter equal to 10^{-10} was used. Note that the problem is symmetric with respect to $\sigma_{t,1}$ and $\sigma_{t,2}$. The graphs of theoretically and numerically estimated ρ versus $\sigma_{t,1}$ and $\sigma_{t,2}$ for the QD method are shown on Figure 1.

In infinite spatially homogeneous problems with a constant source the QD method converges in the vicinity of the solution in the same way as the linear second moment (SM) method [6]. To compare these methods in the case of heterogeneous problems, we performed the Fourier analysis of the SM method on the same class of problems with spatially periodic media. The low-order SM equations are discretized with the FV scheme used for the QD method. The same transport discretization was utilized. The results of the Fourier analysis and numerical calculations are presented on Figure 2, where the corresponding spectral radii are plotted.

2.5   Conclusions

We have developed an approach for stability analysis of nonlinear transport iteration methods for infinite medium problems with spatially periodic material composition and applied it to the QD method in 1D slab geometry. The numerical results showed that the analysis predicts well the convergence rates of the QD method in the vicinity of the solution for this class of problems. Some differences between numerically and theoretically evaluated ρ can be explained by leakage effects in finite domains. We note also that due to these effects the solution in such problems is different from the one in infinite medium that has been used to get theoretical evaluation of ρ. In some cases, theoretical results are sensitive to this difference.

The presented analysis was able to reveal fine details of the convergence properties of the QD method as a function of problem parameters characterized by $\rho(\sigma_{t,1}\Delta x_1, \sigma_{t,2}\Delta x_2)$. In the range of $10^{-4} \leq \sigma_{t,1} \leq 10$ and $10^2 \leq \sigma_{t,2} \leq 10^4$, this function for the QD method is qualitatively different compared to the one for the SM method. Note that the analysis of either the QD method for homogeneous medium problems or the linear SM method for heterogeneous problems does not enable us to find and predict such an effect in convergence behavior of the QD method.

We work now on the analysis of the QD method for 2D heterogeneous problems, and study as well other nonlinear methods such as the nonlinear diffusion acceleration method [7].

Table 2.1: Theoretically and Numerically Estimated Spectral Radii for the QD Method $c_1 = c_2 = 0.9999$.

$\sigma_{t,1}$	$\sigma_{t,2}$								
	1.00e-4	1.00e-3	1.00e-2	1.00e-1	1.00e+0	1.00e+1	1.00e+2	1.00e+3	1.00e+4
1.00e-4		8.86e-2*	2.04e-1	2.06e-1	1.84e-1	4.46e-2	1.82e-4	4.75e-3	1.40e-1
1.00e-3	2.25e-1		2.04e-1	2.06e-1	1.84e-1	4.46e-2	1.81e-3	4.48e-2	6.76e-2
1.00e-2	2.25e-1	2.25e-1		2.06e-1	1.85e-1	1.28e-2	1.73e-2	2.25e-1	8.17e-3
1.00e-1	2.23e-1	2.24e-1	2.24e-1		1.19e-1	8.94e-2	1.14e-1	7.90e-2	3.51e-2
1.00e+0	1.99e-1	2.09e-1	2.18e-1	2.09e-1		1.63e-1	1.40e-1	8.73e-2	3.51e-2
1.00e+1	4.96e-2	4.96e-2	4.96e-2	9.38e-2	1.63e-1		4.05e-2	1.01e-2	8.51e-4
1.00e+2	2.84e-3	2.84e-3	2.36e-2	1.15e-1	1.33e-1	2.04e-2		1.09e-4	8.62e-6
1.00e+3	6.62e-3	6.01e-2	2.27e-1	5.14e-2	8.41e-3	8.92e-4	1.08e-4		1.21e-7
1.00e+4	1.44e-1	1.32e-1	9.08e-2	1.19e-2	2.31e-4	1.26e-5	1.31e-6	1.21e-7	

*Read as 8.86×10^{-2}
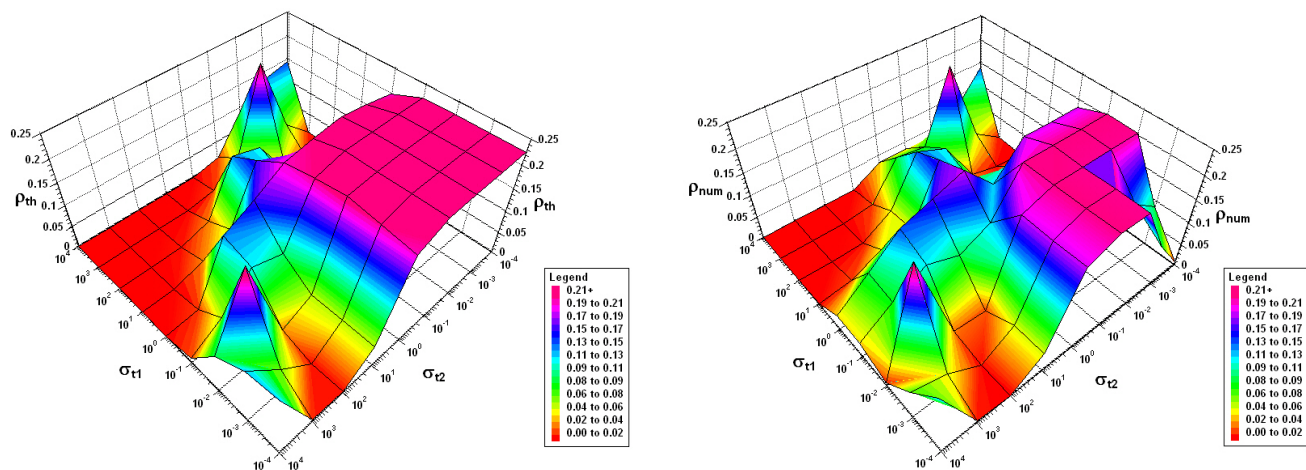
Figure 2.1: Theoretically (ρ_{th}) and numerically (ρ_{num}) estimated spectral radii for the QD method.
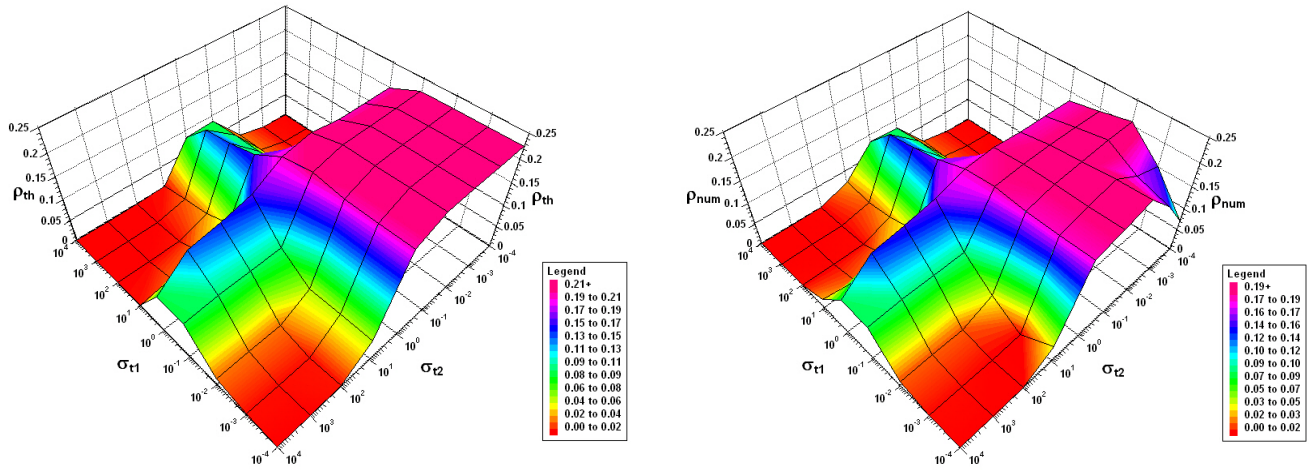
Figure 2.2: Theoretically (ρ_{th}) and numerically (ρ_{num}) estimated spectral radii for the SM method.

Chapter 3

Nonlinear Weighted Flux Methods for Particle Transport Problems

Abstract

A new parameterized family of iterative methods for the 1D slab geometry transport equation is proposed. The new methods are derived by integrating the transport equation over $-1 \leq \mu \leq 0$ and $0 \leq \mu \leq 1$ with weight $1 + \beta |\mu|^{\alpha}$, where $\alpha \geq 0$. The asymptotic diffusion analysis enabled us to determine a particular method of this family the solution of which satisfies a good approximation of both the diffusion equation and asymptotic boundary condition in the diffusive regions. Note that none of the α-weighted nonlinear methods possesses this combination of properties. The convergence properties of the proposed method are similar to the properties of the diffusion-synthetic acceleration (DSA), quasidiffusion, and DSA-like α-weighted nonlinear methods. Numerical results are presented to demonstrate the performance of the derived method.

The results of the research presented in this chapter were published in

- L. Roberts (*Ph.D. student*) & D.Y. Anistratov, "Nonlinear Weighted Flux Methods for Particle Transport Problems," *M&C 2005*, International Conference on Mathematics and Computations, Supercomputing, Reactor Physics and Nuclear Biological Applications, American Nuclear Society Topical Meeting of M&C Division, Avignon, France, September, 2005, 10 pp.

and submitted for publication in

- L. Roberts (*Ph.D. student*) & D.Y. Anistratov, "Nonlinear Weighted Flux Methods for Solving Transport Equation," *Transport Theory and Statistical Physics.*

16

3.1 Introduction

The particle transport (linear Boltzmann) equation is an integro-differential equation. To solve it, iteration methods must be utilized. To accelerate transport iterations, nonlinear projective-iteration methods have been developed [8, 5]. Among these methods are the quasidiffusion method [4], the first-flux (FF) (averaged flux) method [9, 10], second-flux (SF) method [11], α-weighted nonlinear (α-WN) methods [12], nonlinear S_2-like methods [13, 14] and others [5].

The low-order equations of the flux methods are formulated for the partial scalar fluxes. The attractive feature of the flux methods is that discretization schemes similar to transport differencing schemes can be used to approximate their low–order equations. For stability of these methods, there is no need to discretize the transport and low-order equations consistently. However, neither the FF method nor the SF method satisfies the diffusion limit unless the discretization of the low–order equations is consistent with the transport differencing scheme, which itself satisfies the diffusion limit [8, 12].

The family of the nonlinear α-weighted methods is the generalization of the flux methods [12]. In case of 1D slab geometry, these methods are derived by integrating the transport equation over $-1 \leq \mu \leq 0$ and $0 \leq \mu \leq 1$ with weight $|\mu|^\alpha$, $\alpha \geq 0$. The method with $\alpha = 0$ reduces to the FF method, and the method with $\alpha = 1$ is equivalent to the SF method. The study of the nonlinear α-weighted methods showed that the method with $\alpha \approx 0.366$ has properties similar to the DSA method, and the equations of this method can be reduced to the diffusion equation in the diffusive regions. However, the solution of this method does not satisfy an accurate approximation of the asymptotic boundary condition in the diffusive problems.

We consider a new parameterized family of nonlinear projective-iteration methods that uses a different weight function, namely, $1+\beta|\mu|^\alpha$. The analysis of this new family of methods enabled us to derive a method for solving particle transport problems that satisfies a good approximation of both the diffusion equation and asymptotic diffusion boundary condition in the diffusive regions. As a result, the developed method possesses a combination of properties necessary for producing accurate numerical solutions of the transport problems with diffusive regions using independent discretization of the transport and low-order equations of the method.

The remainder of the paper is organized as follows. In Section 3.2 we formulate the new parameterized family of methods. In Section 3.3 we describe the discretization of the equations of the methods. In Section 3.4 we perform the asymptotic diffusion analysis of the considered methods. In Section 3.5 the Fourier analysis of the proposed methods is performed. In Section 3.6 the numerical results are presented. We conclude with the summary in Section 7.

3.2 Formulation of the Family of 1D NWF Methods

Let us consider the one-group transport equation for 1D slab geometry with isotropic scattering:

$$\mu\frac{\partial}{\partial x}\psi(x,\mu) + \sigma_t(x)\psi(x,\mu) = \frac{1}{2}\sigma_s(x)\int_{-1}^{1}\psi(x,\mu')d\mu' + \frac{1}{2}q(x)\,, \tag{3.1}$$

$$-1 \le \mu \le 1\,, \quad 0 \le x \le L\,,$$

with the reflective boundary condition at $x = 0$

$$\psi(0,\mu) = \psi(0,-\mu)\,, \quad \text{for} \quad \mu > 0\,, \tag{3.2}$$

and an incident flux at $x = L$

$$\psi(L,\mu) = \Psi_{in}(\mu)\,, \quad \text{for} \quad \mu < 0\,. \tag{3.3}$$

Here $\psi(x,\mu)$ is the angular flux, σ_t and σ_s are total and scattering cross sections, correspondingly, q is an external source of particles.

To derive the new family of methods, we formulate the low-order equations for the partial scalar fluxes

$$\phi(x)^- = \int_{-1}^{0}\psi(x,\mu)d\mu\,, \quad \phi(x)^+ = \int_{0}^{1}\psi(x,\mu)d\mu \tag{3.4}$$

by operating on the transport equation (Eq. (3.1)) by $\gamma\int_{0}^{1}(1 + \beta\mu^\alpha)(\cdot)d\mu$ and $\gamma\int_{-1}^{0}(1 + \beta|\mu|^\alpha))(\cdot)d\mu$, where $\alpha \ge 0$ and β are parameters, and

$$\gamma = \left(1 + \frac{\beta}{\alpha + 1}\right)^{-1}. \tag{3.5}$$

The resulting low-order equations are

$$-\frac{d}{dx}\left(F^-(x)\phi^-(x)\right) + \left(\sigma_t(x)G^-(x) - \frac{1}{2}\sigma_s(x)\right)\phi^-(x) = \frac{1}{2}\left(\sigma_s(x)\phi^+(x) + q(x)\right)\,, \tag{3.6}$$

$$\frac{d}{dx}\left(F^+(x)\phi^+(x)\right) + \left(\sigma_t(x)G^+(x) - \frac{1}{2}\sigma_s(x)\right)\phi^+(x) = \frac{1}{2}\left(\sigma_s(x)\phi^-(x) + q(x)\right)\,, \tag{3.7}$$

where we defined the factors

$$G^\pm(x) = \frac{\gamma\int_{0}^{\pm 1}(1 + \beta|\mu|^\alpha)\psi(x,\mu)d\mu}{\int_{0}^{\pm 1}\psi(x,\mu)d\mu}\,, \tag{3.8}$$

$$F^\pm(x) = \frac{\gamma\int_{0}^{\pm 1}|\mu|(1 + \beta|\mu|^\alpha)\psi(x,\mu)d\mu}{\int_{0}^{\pm 1}\psi(x,\mu)d\mu}\,, \tag{3.9}$$

18

which nonlinearly depend on the transport solution. These factors are used to close the system of equations.

The nonlinear weighted flux (NWF) methods are defined by the following set of equations:

$$\mu \frac{\partial}{\partial x} \psi^{(k+1/2)} + \sigma_t \psi^{(k+1/2)} = \frac{1}{2} \left(\sigma_s \phi^{(k)} + q \right) , \tag{3.10}$$

$$\psi^{(k+1/2)}(0, \mu) = \psi^{(k+1/2)}(0, -\mu), \quad \text{for } \mu > 0 , \tag{3.11}$$

$$\psi^{(k+1/2)}(L, \mu) = \Psi_{in}(\mu), \quad \text{for } \mu < 0 , \tag{3.12}$$

$$G^{\pm(k+1/2)} = \frac{\gamma \int\limits_0^{\pm 1} (1 + \beta|\mu|^\alpha)\psi^{(k+1/2)}d\mu}{\int\limits_0^{\pm 1} \psi^{(k+1/2)}d\mu} , \tag{3.13}$$

$$F^{\pm(k+1/2)} = \frac{\gamma \int\limits_0^{\pm 1} |\mu|(1 + \beta|\mu|^\alpha)\psi^{(k+1/2)}d\mu}{\int\limits_0^{\pm 1} \psi^{(k+1/2)}d\mu} , \tag{3.14}$$

$$-\frac{d}{dx}\left(F^{-(k+1/2)} \phi^{-(k+1)} \right) + \left(\sigma_t G^{-(k+1/2)} - \frac{1}{2}\sigma_s \right) \phi^{-(k+1)} = \frac{1}{2}\left(\sigma_s \phi^{+(k+1)} + q \right) , \tag{3.15}$$

$$\frac{d}{dx}\left(F^{+(k+1/2)} \phi^{+(k+1)} \right) + \left(\sigma_t G^{+(k+1/2)} - \frac{1}{2}\sigma_s \right) \phi^{+(k+1)} = \frac{1}{2}\left(\sigma_s \phi^{-(k+1)} + q \right) , \tag{3.16}$$

$$\phi^{+(k+1)}(0) = \phi^{-(k+1)}(0) , \tag{3.17}$$

$$\phi^{-(k+1)}(L) = \Phi_{in}^-, \quad \text{where} \quad \Phi_{in}^- = \int_{-1}^0 \Psi_{in}(\mu)d\mu , \tag{3.18}$$

$$\phi^{(k+1)} = \phi^{+(k+1)} + \phi^{-(k+1)} . \tag{3.19}$$

Here k is the iteration index. The nonlinear iteration scheme consists of three stages:

1. A transport sweep to calculate the angular flux $\psi^{(k+1/2)}$ (Eqs. (3.10)-(3.12)).

2. The calculation of the factors $G^{\pm(k+1/2)}$ and $F^{\pm(k+1/2)}$ from $\psi^{(k+1/2)}$ (Eqs. (3.13)-(3.14)).

3. Solving the low-order problem (Eqs. (3.15)-(3.18)) for $\phi^{\pm(k+1)}$ using $G^{\pm(k+1/2)}$ and $F^{\pm(k+1/2)}$.

We are interested in the methods the low-order equations of which can be reduced to the diffusion equation in an optically thick medium. To perform a preliminary analysis, let us consider the case when the angular flux is isotropic. Then, $G^\pm = 1$ and $F^\pm = \zeta$, where

$$\zeta = \left(\frac{1}{2} + \frac{\beta}{\alpha + 2} \right) \left(1 + \frac{\beta}{\alpha + 1} \right)^{-1} \tag{3.20}$$

19

and the low-order equations (3.15) and (3.16) can be reduced to the following second-order equation for the partial scalar fluxes:

$$-\zeta^2 \frac{d}{dx}\frac{1}{\sigma_t}\frac{d}{dx}(\phi^- + \phi^+) + \sigma_a(\phi^- + \phi^+) = q\,, \tag{3.21}$$

where

$$\sigma_a = \sigma_t - \sigma_s \tag{3.22}$$

is the absorption cross section. If

$$\zeta = \frac{1}{\sqrt{3}}\,, \tag{3.23}$$

then Eq. (3.21) is equivalent to the diffusion equation. Equation (3.23) is the first condition on the α and β parameters of the methods. Another important issue of the asymptotic diffusion limit is related to boundary conditions. The detailed asymptotic analysis presented below (see Section 3.4) provides the second condition on these parameters.

3.3 Discretization

We now spatially discretize the equations of the NWF methods using independent differencing schemes for the transport and low-order equations. The approximation of the low-order equations is based on the linear discontinuous (LD) method that was formulated for the transport equation [18, 19, 15]. We introduce the spatial mesh $\{x_{j-1/2},\ j = 1, ..., N,\ x_{1/2} = 0,\ x_{N+1/2} = L\}$. The equations (3.15) and (3.16) are integrated over the ith cell with weights 1 and $x - x_j$, where $x_j = 0.5(x_{j+1/2} + x_{j-1/2})$. Then, the auxiliary conditions are formulated using the assumption that $\phi^\pm$ in the cell are linear functions defined by their zeroth and first spatial moments. The resulting discretized low-order equations of the NWF methods have the following form:

$$-(F^-_{j+1/2}\phi^-_{j+1/2} - F^-_{j-1/2}\phi^-_{j-1/2}) + (\sigma_{t,j}G^-_j - 0.5\sigma_{s,j})\phi^-_j\Delta x_j = 0.5(\sigma_{s,j}\phi^+_j + q_j)\Delta x_j\ , \tag{3.24}$$

$$F^+_{j+1/2}\phi^+_{j+1/2} - F^+_{j-1/2}\phi^+_{j-1/2} + (\sigma_{t,j}G^+_j - 0.5\sigma_{s,j})\phi^+_j\Delta x_j = 0.5(\sigma_{s,j}\phi^-_j + q_j)\Delta x_j\ , \tag{3.25}$$

$$-\theta_j(F^-_{j+1/2}\phi^-_{j+1/2} + F^-_{j-1/2}\phi^-_{j-1/2} - 2F^-_j\phi^-_j) + (\sigma_{t,j}G^-_j - 0.5\sigma_{s,j})\hat\phi^-_j\Delta x_j$$
$$= 0.5(\sigma_{s,j}\hat\phi^+_j + \hat q_j)\Delta x_j\ , \tag{3.26}$$

$$\theta_j(F^+_{j+1/2}\phi^+_{j+1/2} + F^+_{j-1/2}\phi^+_{j-1/2} - 2F^+_j\phi^+_j) + (\sigma_{t,j}G^+_j - 0.5\sigma_{s,j})\hat\phi^+_j\Delta x_j$$
$$= 0.5(\sigma_{s,j}\hat\phi^-_j + \hat q_j)\Delta x_j\ , \tag{3.27}$$

$$\hat\phi^-_j = \phi^-_j - \phi^-_{j-1/2}\,, \tag{3.28}$$

$$\hat\phi^+_j = \phi^+_{j+1/2} - \phi^+_j\,, \tag{3.29}$$

$$\phi^+_{1/2} = \phi^-_{1/2}\,, \tag{3.30}$$

20

$$\phi^-_{N+1/2} = \Phi^-_{in} \, , \tag{3.31}$$

$$F^\pm_j = 0.5(F^\pm_{j+1/2} + F^\pm_{j-1/2}) \, , \tag{3.32}$$

$$G^\pm_j = 0.5(G^\pm_{j+1/2} + G^\pm_{j-1/2}) \, , \tag{3.33}$$

where

$$\hat{\phi}^\pm_j = \frac{6}{\Delta x_j^2} \int\limits_{x_{j-1/2}}^{x_{j+1/2}} (x - x_j)\phi^\pm(x)dx \, , \tag{3.34}$$

$$\hat{q}_j = \frac{6}{\Delta x_j^2} \int\limits_{x_{j-1/2}}^{x_{j+1/2}} (x - x_j)q(x)dx \, , \tag{3.35}$$

$$\Delta x_j = x_{j+1/2} - x_{j-1/2} \, . \tag{3.36}$$

Integer $\pm\frac{1}{2}$ subscripts refer to cell-edge quantities, and integer subscripts refer to cell-average quantities. Here θ_j is a "lumping" parameter; $\theta_j = 3$ corresponds to the standard LD method; $\theta_j = 1$ corresponds to a lumped LD method [15] that is used for optically thick cells. In case the ith interval is optically thick, the values of the cell-average factors are defined as

$$F^-_j = F^-_{j-1/2}, \quad G^-_j = G^-_{j-1/2}, \tag{3.37}$$

$$F^+_j = F^+_{j+1/2}, \quad G^+_j = G^+_{j+1/2}. \tag{3.38}$$

To solve the transport equation, we use the Step Characteristic (SC) method

$$\mu_m(\psi_{m,j+1/2} - \psi_{m,j-1/2}) + \sigma_{t,j}\Delta x_j(T_{m,j}\psi_{m,j-1/2} + (1 - T_{m,j})\psi_{m,j+1/2})$$
$$= 0.5(\sigma_{s,j}\phi_j + q_j)\Delta x_j \, , \tag{3.39}$$

$$T_{m,j} = \frac{1}{\tau_{m,j}} - \frac{1}{e^{\tau_{m,j}} - 1} \, , \quad \text{where} \quad \tau_{m,j} = \frac{\sigma_{t,j}\Delta x_j}{\mu_m} \, . \tag{3.40}$$

$$m = 1, ..., M \, . \tag{3.41}$$

The subscript m denotes the discrete ordinates number.

3.4 Asymptotic Diffusion Analysis

We now perform the asymptotic diffusion analysis [16] of the discretized equations of the NWF methods considering that the lumping parameter $\theta_j=1$ and the cell-average factors are defined by Eqs. (3.37) and (3.38). We define a small parameter ε, introduce the scaled cross sections and sources

$$\sigma_{t,j} = \frac{\bar{\sigma}_{t,j}}{\varepsilon} \, , \quad \sigma_{a,j} = \varepsilon\bar{\sigma}_{a,j} \, , \quad q_j = \varepsilon\bar{q}_j \, , \quad \hat{q}_j = \varepsilon\breve{q}_j \, , \tag{3.42}$$

and the following ansatz:

$$\psi_{m,j+1/2} = \sum_{l=0}^{\infty} \varepsilon^l \psi^{[l]}_{m,j+1/2}, \quad \phi_j^{\pm} = \sum_{l=0}^{\infty} \varepsilon^l \phi_j^{\pm[l]}, \quad \phi_{j+1/2}^{\pm} = \sum_{l=0}^{\infty} \varepsilon^l \phi^{\pm[l]}_{j+1/2}, \quad \hat{\phi}_j^{\pm} = \sum_{l=0}^{\infty} \varepsilon^l \hat{\phi}_j^{\pm[l]}$$

(3.43)

into Eqs. (3.24)-(3.31) and (3.37)-(3.40). Then, we equate the coefficients of different powers of ε. The analysis of the obtained scaled equations shows that the leading-order solution satisfies the following equation in the interior of the diffusion region:

$$-\zeta^2 \left(\frac{1}{\sigma_{t,j+1}\Delta x_{j+1}} (\phi^{[0]}_{j+3/2} - \phi^{[0]}_{j+1/2}) - \frac{1}{\sigma_{t,j}\Delta x_j}(\phi^{[0]}_{j+1/2} - \phi^{[0]}_{j-1/2}) \right)$$

(3.44)

$$+0.5(\sigma_{a,j}\Delta x_j + \sigma_{a,j+1}\Delta x_{j+1})\phi^{[0]}_{j+1/2} = 0.5\left((q_j + \hat{q}_j)\Delta x_j + (q_{j+1} - \hat{q}_{j+1})\Delta x_{j+1} \right),$$

$$\phi^{\pm[0]}_{j+1/2} = 0.5\phi^{[0]}_{j+1/2},$$

(3.45)

with the boundary condition defined as

$$\phi^{[0]}_{N+1/2} = \frac{2}{\frac{1}{2} + \frac{\beta}{\alpha+2}} \sum_{\mu_m \leq 0} \left(|\mu_m| + \beta|\mu_m|^{\alpha+1} \right) \Psi_{in}(\mu_m)w_m,$$

(3.46)

where w_m are quadrature weights.

These results demonstrate that if $\zeta = \frac{1}{\sqrt{3}}$, the leading-order solution meets a reasonable spatial approximation of the correct diffusion equation that represents stable and consistent discretization of this partial differential equation. From Eq. (3.46) we notice that the leading-order solution in the boundary cell satisfies the boundary condition of the form

$$\phi^{[0]}(L) = 2 \int_{-1}^{0} \widetilde{W}(-\mu)\Psi_{in}(\mu)d\mu,$$

(3.47)

where

$$\widetilde{W}(\mu) = \frac{1}{\frac{1}{2} + \frac{\beta}{\alpha+2}} (\mu + \beta\mu^{\alpha+1}).$$

(3.48)

The asymptotic diffusion analysis of the transport equation in the continuous form yields that the leading-order solution meets the Dirichlet boundary condition [20, 21, 32]

$$\phi(L) = 2 \int_{-1}^{0} W(-\mu)\Psi_{in}(\mu)d\mu,$$

(3.49)

where

$$W(\mu) = \frac{\mu}{X(-\mu)} \left(\int_0^1 \frac{s}{X(-s)}ds \right)^{-1} \approx 0.956\mu + 1.565\mu^2.$$

(3.50)

The function $X(-\mu)$ is tabulated in [32].

We note that the NWF method with $\alpha = 1$ and $\beta = \sqrt{3}$ gives rise to

$$\zeta = \frac{1}{\sqrt{3}},$$

(3.51)

$$\widetilde{W}(\mu) = \frac{2\sqrt{3}}{2+\sqrt{3}}(\mu + \sqrt{3}\mu^2) \approx 0.928\mu + 1.608\mu^2 \,. \tag{3.52}$$

The comparison between functions $W(\mu)$ and $\widetilde{W}(\mu)$ shows that

$$\max_{0 \leq \mu \leq 1} |W(\mu) - \widetilde{W}(\mu)| = 0.018 \,. \tag{3.53}$$

Thus, the NWF method with such set of parameters α and β generates the solution in the diffusive regions that satisfies reasonable approximation of the diffusion equation. Also, the numerical diffusion boundary condition closely agrees with the analytic asymptotic boundary condition.

3.5 Fourier Analysis

To analyze the convergence properties of the NWF methods in the discretized form, we use the special class of infinite medium problems with a flat source and constant cross sections and linearize the equations around the solution [6]. The exact solution has the following form:

$$\psi_{m,j+1/2} = \frac{q}{2\sigma_a} \,. \tag{3.54}$$

We consider such iterations that the estimation of the solution is close to the exact solution and assume that

$$\psi_{m,j+1/2}^{(k+1/2)} = \frac{q}{\sigma_a}\left(\frac{1}{2} + \epsilon\eta_{m,j+1/2}^{(k+1/2)}\right), \tag{3.55}$$

$$\phi_{j+1/2}^{\pm(k)} = \frac{q}{\sigma_a}\left(\frac{1}{2} + \epsilon\xi_{j+1/2}^{\pm(k)}\right), \tag{3.56}$$

$$\phi_j^{\pm(k)} = \frac{q}{\sigma_a}\left(\frac{1}{2} + \epsilon\xi_j^{\pm(k)}\right), \tag{3.57}$$

$$\phi_j^{(k)} = \frac{q}{\sigma_a}\left(1 + \epsilon\xi_j^{(k)}\right), \tag{3.58}$$

where $\epsilon \ll 1$. We introduce this ansatz (Eqs. (3.55)-(3.58)) into Eqs. (3.24)-(3.29), and (3.39), taking into account the iteration process (3.10)-(3.19). The equations are expanded in powers of ϵ. The O(1) terms cancel out. We neglect the $O(\epsilon^2)$ terms and obtain the following set of O(ϵ) equations:

$$\mu_m(\eta_{m,j+1/2}^{(k+1/2)} - \eta_{m,j-1/2}^{(k+1/2)}) + \sigma_t\Delta x_j(T_m\eta_{m,j-1/2}^{(k+1/2)} + (1 - T_m)\eta_{m,j+1/2}^{(k+1/2)}) = 0.5\sigma_s\Delta x_j\xi_j^{(k)} \,, \tag{3.59}$$

$$-\zeta(\xi_{j+1/2}^{-(k+1)} - \xi_{j-1/2}^{-(k+1)}) + (\sigma_t - 0.5\sigma_s)\Delta x_j\xi_j^{-(k+1)} - 0.5\sigma_s\Delta x_j\xi_j^{+(k+1)}$$
$$= f_{j+1/2}^{-(k+1/2)} - f_{j-1/2}^{-(k+1/2)} - 0.5\sigma_t\Delta x_j(g_{j-1/2}^{-(k+1/2)} + g_{j+1/2}^{-(k+1/2)}) \,, \tag{3.60}$$

$$\zeta(\xi_{j+1/2}^{+(k+1)} - \xi_{j-1/2}^{+(k+1)}) + (\sigma_t - 0.5\sigma_s)\Delta x_j\xi_j^{+(k+1)} - 0.5\sigma_s\Delta x_j\xi_j^{-(k+1)}$$
$$= f_{j-1/2}^{+(k+1/2)} - f_{j+1/2}^{+(k+1/2)} - 0.5\sigma_t\Delta x_j(g_{j-1/2}^{+(k+1/2)} + g_{j+1/2}^{+(k+1/2)}) \,, \tag{3.61}$$

$$-\theta\zeta(\xi_{j+1/2}^{-(k+1)} + \xi_{j-1/2}^{-(k+1)} - 2\xi_j^{-(k+1)}) + (\sigma_t - 0.5\sigma_s)\Delta x_j(\xi_j^{-(k+1)} - \xi_{j-1/2}^{-(k+1)})$$
$$-0.5\sigma_s\Delta x_j(\xi_{j+1/2}^{+(k+1)} - \xi_j^{+(k+1)}) = 0 \,, \tag{3.62}$$

$$\theta\zeta(\xi_{j+1/2}^{+(k+1)} + \xi_{j-1/2}^{+(k+1)} - 2\xi_j^{+(k+1)}) + (\sigma_t - 0.5\sigma_s)\Delta x_j(\xi_{j+1/2}^{+(k+1)} - \xi_j^{+(k+1)})$$
$$-0.5\sigma_s\Delta x_j(\xi_j^{-(k+1)} - \xi_{j-1/2}^{-(k+1)}) = 0 \,, \tag{3.63}$$

$$\xi_j^{(k+1)} = \xi_j^{-(k+1)} + \xi_j^{+(k+1)}, \tag{3.64}$$

where

$$g_{j+1/2}^{\pm(k+1/2)} = \sum_{\mu_m \gtrless 0} (\gamma(1 + \beta|\mu_m|^\alpha) - 1)\eta_{m,j+1/2}^{(k+1/2)} w_m \,, \tag{3.65}$$

$$f_{j+1/2}^{\pm(k+1/2)} = \sum_{\mu_m \gtrless 0} (\gamma|\mu_m|(1 + \beta|\mu_m|^\alpha) - \zeta)\eta_{m,j+1/2}^{(k+1/2)} w_m \,. \tag{3.66}$$

We now apply a Fourier analysis to the linearized discretized equations in the case of a uniform spatial mesh. We introduce the following Fourier ansatz:

$$\eta_{m,j+1/2}^{(k+1/2)} = a_m \omega^k e^{i\lambda\sigma_t x_{j+1/2}} \,, \tag{3.67}$$

$$\xi_{j+1/2}^{\pm(k)} = A^\pm \omega^k e^{i\lambda\sigma_t x_{j+1/2}} \,, \tag{3.68}$$

$$\xi_j^{\pm(k)} = B^\pm \omega^k e^{i\lambda\sigma_t x_j} \,, \tag{3.69}$$

$$\xi_j^{(k)} = \omega^k e^{i\lambda\sigma_t x_j} \tag{3.70}$$

into Eqs. (3.59)-(3.66) and obtain a system of equations for ω, $A^\pm$ and $B^\pm$. Solving this system for ω, we get

$$\omega = \frac{\sigma_s}{\sigma_t} \frac{P\left(\zeta\nu_t\nu_a(0.5\sigma_t\Delta x g_1 - f_0)\tan^2\chi - \sigma_t\Delta x(0.5\sigma_t\Delta x g_0 + f_1\tan^2\chi)(P + 2\zeta\nu_a\tan^2\chi)\right)}{\sigma_t\sigma_a\Delta x^2(P + 2\zeta\nu_t\tan^2\chi)(P + 2\zeta\nu_a\tan^2\chi) + 4\zeta^2\nu_t^2\nu_a^2\tan^2\chi} \,, \tag{3.71}$$

$$\chi = 0.5\lambda\sigma_t\Delta x \,, \tag{3.72}$$

$$\nu_t = 2\zeta\theta + \sigma_t\Delta x \,, \tag{3.73}$$

$$\nu_a = 2\zeta\theta + \sigma_a\Delta x \,, \tag{3.74}$$

$$P = \nu_t\nu_a + \sigma_t\sigma_a\Delta x^2\tan^2\chi \,, \tag{3.75}$$

$$g_n = \sum_{\mu_m \geq 0} (\gamma(1 + \beta\mu_m^\alpha) - 1)\, b_{n,m} w_m \,, \quad n = 0, 1 \,, \tag{3.76}$$

$$f_n = \sum_{\mu_m \geq 0} (\gamma\mu_m(1 + \beta\mu_m^\alpha) - \zeta)\, b_{n,m} w_m \,, \quad n = 0, 1 \,, \tag{3.77}$$

$$b_{0,m} = \left(1 + \left(\frac{1 + e^{-\tau_m}}{1 - e^{-\tau_m}}\right)^2 \tan^2\chi\right)^{-1} \,, \tag{3.78}$$

$$b_{1,m} = \frac{1 + e^{-\tau_m}}{1 - e^{-\tau_m}} b_{0,m} \,, \tag{3.79}$$

$$\tau_m = \frac{\sigma_t \Delta x}{\mu_m}. \tag{3.80}$$

The spectral radius is defined by

$$\rho = \sup_{0 \le \chi \le \frac{\pi}{2}} |\omega(\chi)| . \tag{3.81}$$

Table 3.1 contains the theoretically estimated spectral radii of the NWF method with $\alpha = 1$ and $\beta = \sqrt{3}$ using the formula (3.71). The double S_5 Gauss-Legendre quadrature set was utilized to calculate Eqs. (3.76) and (3.77). These results demonstrate theoretically that the convergence is fast for the important range of scattering ratios and optical thicknesses of mesh intervals.

Table 3.1: Theoretically Estimated Spectral Radii ρ for the Discretized NWF Method with $\alpha = 1$ and $\beta = \sqrt{3}$ versus $\sigma_t h$ and c.

c	$\sigma_t h$						
	0.01	0.1	1.	2.	3.	5.	10
0.9999	2.2 10^{-1}	2.2 10^{-1}	1.5 10^{-1}	8.5 10^{-2}	5.9 10^{-2}	1.8 10^{-2}	3.2 10^{-4}
0.99	2.2 10^{-1}	2.2 10^{-1}	1.4 10^{-1}	7.6 10^{-2}	4.0 10^{-2}	7.9 10^{-3}	6.3 10^{-5}
0.9	1.9 10^{-1}	1.9 10^{-1}	1.1 10^{-1}	4.5 10^{-2}	1.7 10^{-2}	1.9 10^{-3}	9.8 10^{-6}
0.7	1.4 10^{-1}	1.4 10^{-1}	7.0 10^{-2}	2.3 10^{-2}	7.1 10^{-3}	6.9 10^{-4}	3.1 10^{-6}

Note that similar Fourier analysis of the convergence properties of the NWF methods in the differential form shows that in the vicinity of the solution of the considered special class of infinite medium problems one gets

$$\omega(\lambda) = c\left(\frac{1}{1 + \lambda^2 \zeta^2 - c}\right)\left[(1 + \lambda^2 \zeta^2)\frac{\tan^{-1}\lambda}{\lambda} - 1\right], \quad c = \frac{\sigma_s}{\sigma_t}. \tag{3.82}$$

If the condition (3.23) is met, then Eq. (3.82) leads to the formula for the DSA method and linearized QD method [6]. In such case the value of the spectral radius as $c \to 1$ equals 0.2247.

3.6 Numerical Results

To demonstrate the performance of the proposed NWF method with the particular linear weight function ($\alpha = 1$ and $\beta = \sqrt{3}$), we present numerical results of problems that test the convergence properties of the proposed method and its behavior in the diffusive domains. Note that in the calculations below the lumping parameter $\theta_j = 1$ if $\sigma_{t,j}\Delta x_j \ge 5$.

Problem 1. We consider slab geometry problems: $\sigma_t = 1$, $\sigma_s = 0.99$, $q = 1$, a reflecting boundary $x = 0$, and a vacuum boundary $x = L$ [6]. We use $L = 10^3 h$, where h is the width of the spatial cell. The angular mesh for the transport equation and quadrature weights for integration with respect to μ correspond to the double S_5 Gauss-Legendre quadrature set. The relative pointwise convergence criterion

$$\max_j \left|1 - \frac{\phi_j^{(k)}}{\phi_j^{(k-1)}}\right| < \tilde{\epsilon} \tag{3.83}$$

with $\tilde{\epsilon} = 10^{-12}$ is used.

Table 3.2 contains the numerically estimated spectral radii that were determined by means of the formula

$$\rho = \frac{\|\phi^{(k)} - \phi^{(k-1)}\|_{L_2}}{\|\phi^{(k-1)} - \phi^{(k-2)}\|_{L_2}} \tag{3.84}$$

for the last iteration in each problem. These results enable us to compare theoretically and numerically estimated values. We note that the Fourier analysis approximately predicts the values of the spectral radii for the proposed NWF method.

Table 3.2: Numerically Estimated Spectral Radii ρ for the Discretized NWF Method with $\alpha = 1$ and $\beta = \sqrt{3}$ versus $\sigma_t h$ for Problem No. 1 (c=0.99).

$\sigma_t h$	0.01	0.1	1.	2.	3.	5.	10
ρ	$1.9\ 10^{-1}$	$1.9\ 10^{-1}$	$1.4\ 10^{-1}$	$8.0\ 10^{-2}$	$4.2\ 10^{-2}$	$4.2\ 10^{-3}$	$4.9\ 10^{-4}$

Problem 2. We consider a slab $0 \leq x \leq 20$ having $\sigma_t = 1$, $\sigma_s = 0.97$, $q = 0$. The left boundary has an isotropic incident flux with magnitude unity, and the right boundary is reflecting [17]. A spatial mesh consisting of J equal cells with cell width $h = 20/J$ is used. The double S_4 Gauss-Legendre quadrature set is utilized. The relative pointwise convergence criterion with $\tilde{\epsilon} = 10^{-12}$ is imposed.

Table 3.3 shows the numbers of iterations for the proposed NWF method, as well as for the α-WN method with α=0.366, the QD and DSA methods that were taken from [12, 17]. The results of problems 1 and 2 show that the developed method converges fast, and its convergence properties are close to those of the α-WN method with α=0.366, the QD and DSA methods.

Problem 3. We consider a slab $0 \leq x \leq 11$ with pure absorbing ($0 \leq x \leq 1$) and diffusive ($1 \leq x \leq 11$) regions [15]. The parameters of the problem are listed in Table 3.4. The right boundary is vacuum. There is an isotropic incident angular flux $\psi(x, \mu)$=1 on the left boundary. A spatial mesh has 10 uniform cells in each region. The double S_8 Gauss-Legendre quadrature set is utilized.

The numerical solution obtained with the proposed NWF method is demonstrated in Figure 3.1. Both the cell-edge and cell-average scalar fluxes calculated from the low-order equations are plotted. The markers that indicate the cell-average values have smaller size compared to those for the cell-edge values. We also show the results calculated by means of other flux methods, namely, the FF, SF, and α-WN (α=0.366) methods. The low-order equations of these methods were discretized by the lumped LD method, and the SC method was used for the transport equation [12]. The relative pointwise convergence criterion with $\tilde{\epsilon} = 10^{-7}$ is used. All methods converged in 3 iterations.

These results show that the proposed NWF method with α=1 and $\beta = \sqrt{3}$ performs very well in the thick diffusive region. We note that the solutions of FF and SF methods have large errors in the diffusive region. The reason is that the low-order equations of these methods do not reduce to the diffusion equation in this case. The solution of the α-WN method (α=0.366) is considerably better, because it satisfies a good discretization of the diffusion

26

equation. However, it is not well enough due to inaccurate asymptotic boundary condition that this method generates at the interface with the diffusive region. The relative errors in the scalar flux in the diffusive region versus position for the NWF and α-WN methods are presented in Table 3.5. These data show that in the thick diffusive region (after the boundary layer) the new method generates the solution with significantly higher accuracy than the α-WN method with α=0.366.

Table 3.3: Number of Iterations for Problem No. 2.

$\sigma_t h$	5.	2.	1.	0.5	0.25	0.125
NWF Method ($\alpha = 1$, $\beta = \sqrt{3}$)	7	12	15	17	17	17
α-WN method (α=0.366)	7	11	13	15	16	16
QD method	10	14	14	15	15	15
DSA Method	14	16	16	16	16	16

Table 3.4: Parameters of Problem No. 3.

Region	Domain	σ_t	σ_s	q	h
1	$0 \leq x \leq 1$	2	0	0	0.1
2	$1 \leq x \leq 11$	100	100	0	1

Table 3.5: Problem 3. Relative Errors in the Scalar Flux in the Diffusive Region.

x	α-WN (α=0.366)	NWF (α=1, β=$\sqrt{3}$)
1.	-4.1 10^{-2}	-7.1 10^{-2}
2.	2.6 10^{-2}	8.2 10^{-5}
3.	2.5 10^{-2}	9.2 10^{-5}
4.	2.5 10^{-2}	-1.1 10^{-4}
5.	2.5 10^{-2}	-3.1 10^{-4}
6.	2.4 10^{-2}	-5.0 10^{-4}
7.	2.4 10^{-2}	-5.5 10^{-4}
8.	2.4 10^{-2}	-4.9 10^{-4}
9.	2.3 10^{-2}	-3.7 10^{-4}
10.	2.4 10^{-2}	-3.7 10^{-4}

3.7   Conclusions

We have considered a new parameterized family of nonlinear iterative methods for solving particle transport problems. The low-order problems of these methods are based on the equations for the partial scalar fluxes, and hence they are similar to the flux and α-WN methods. The new methods use different weight functions to derive the low-order equations.
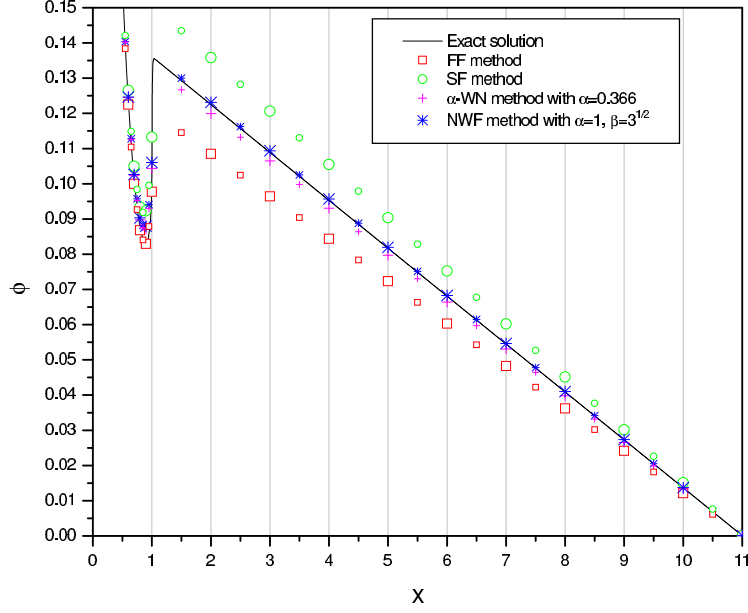
Figure 3.1: Problem 3. The scalar flux ϕ obtained by the NWF, FF, SF, and α-WN methods discretized with the lumped LD method.

To approximate the equations of the considered methods, we utilized independent discretization of the low-order and high-order equations. The asymptotic diffusion analysis enabled us to find a particular method of this family the solution of which satisfies a good approximation of the diffusion equation and asymptotic boundary condition in the diffusive regions. The convergence properties of this method are close to the properties of the QD, DSA and α-WN (with α=0.366) methods. As a result, we developed a flux method with the combination of features that are important for solving transport problems with optically thick regions and that none of the α-WN methods (including the FF and SF methods) possesses.

Chapter 4

Nonlinear Weighted Flux Methods for Particle Transport Problems in 2D Cartesian Geometry

Abstract

The family of nonlinear weighted flux methods for solving the transport equation is derived for 2D Cartesian geometry. A linear polynomial weight is considered. An asymptotic diffusion limit analysis is performed on the discretized method. The analysis reveals conditions on the weight necessary for an accurate approximation of the diffusion equation. As a result, we developed a new weighted flux method, the equations of which give rise to the diffusion equation in optically thick diffusive regions. Numerical results are presented to confirm the theoretical results and demonstrate performance of the proposed method.

The results of the research presented in this chapter were published in

- L. Roberts (Ph.D. student) & D.Y. Anistratov, "Nonlinear Weighted Flux Methods for Solving the Transport Equation in 2D Cartesian Geometry," *Proceedings of M&C + SNA 2007, Joint International Topical Meeting on Mathematics & Computations and Supercomputing in Nuclear Applications*, Monterey, CA, April, 2007, 13 pp.

4.1   Introduction

The nonlinear weighted flux (NWF) methods for solving the transport equation belong to a group of nonlinear projective-iterative (NPI) methods. These are also known as projected discrete ordinates (PDO) methods [5]. The NPI methods are defined by a system of nonlinearly coupled high-order and low-order problems that is equivalent to the original linear transport problem. The equations of NPI methods are closed by a defining of linear-fractional factors. These factors are weakly dependent on the angular flux. NPI methods possess certain advantages for their use in multiphysics applications. NPI methods have

some flexibility in coupling, for instance, radiative transfer and hydrodynamics equations. For stability, the low-order equations of these methods need not be discretized consistently with the spatial discretization of the transport equation. Examples of NPI methods are the quasidiffusion (QD) method [4], flux methods [9, 10, 11], α-weighted methods [12], nonlinear S_2-like methods [13, 14] and others [5]. These methods differ from each other by the definition of the low-order equations which results in differences in features of these methods. In this paper, we derive new low-order equations of the flux methods such that the resulting discretized NWF method has the desired properties of an accurate approximation of the diffusion equation in the diffusion limit and fast convergence [15].

The low-order problem of the QD method is an elliptic one, i.e. the solution in any spatial point depends on the solution in all other points. However, when particles stream without scattering in some direction, the nature of the relationship of the solution amongst various spatial points is different and based on the properties of the hyperbolic differential operator of the transport equation. The low-order equations of the flux and α-weighted methods are formulated for the partial scalar fluxes and possess such a feature. The flux methods have been used successfully, for instance, to solve electron transport problems with highly anisotropic scattering and radiative transfer problems [23].

In many cases, practical radiative transfer problems contain optically thick diffusive regions in which the leading-order transport solution satisfies the diffusion equation. An asymptotic analysis has been previously developed to assess a discretized method's ability to reproduce the diffusion equation in diffusive regions [15, 16, 24]. This analysis also determines the leading-order boundary condition for the resulting diffusion equation for the case of numerically unresolved boundary layers of the diffusive region. The structure of the flux method equations is similar to that of the transport equation. This asymptotic analysis can be well utilized in the development of the NWF methods with these necessary properties.

Recently, a new parameterized family of NWF methods for the 1D slab geometry transport equation was proposed [25]. The asymptotic diffusion analysis enabled us to determine a particular method of this family the solution of which satisfies a good approximation of both the diffusion equation and asymptotic boundary condition in the diffusive regions. Note that none of the α-weighted nonlinear methods possesses this combination of properties. The convergence properties of this method are close to the properties of the diffusion-synthetic acceleration (DSA) and QD methods.

In this paper, we consider the NWF methods for 2D Cartesian geometry and analyze them to derive a method that possesses a combination of properties necessary for producing accurate numerical solutions of multidimensional transport problems with diffusive regions. We present a NWF method derived with a polynomial weight function whose leading-order solution reproduces an accurate discretization of the diffusion equation in the diffusion limit. Numerical results are presented to illustrate the method's properties.

The remainder of this paper is organized as follows. The family of 2D NWF methods is formulated in Sec. 4.2. The discretization of the proposed methods is presented in Sec. 4.3. In Sec. 4.4, we describe the asymptotic diffusion analysis of the NWF methods in continuous and discrete forms. In Sec. 4.5, the numerical results are presented. We conclude, in Sec. 4.6, with a discussion on the developed methods.

4.2 Formulation of the Family of 2D NWF Methods

Let us consider the one-group steady-state transport equation in 2D Cartesian geometry with isotropic scattering and source:

$$\Omega_x \frac{\partial}{\partial x}\psi(\vec{r},\vec{\Omega}) + \Omega_y \frac{\partial}{\partial y}\psi(\vec{r},\vec{\Omega}) + \sigma_t(\vec{r})\psi(\vec{r},\vec{\Omega}) = \frac{1}{4\pi}\sigma_s(\vec{r})\int_{4\pi}\psi(\vec{r},\vec{\Omega}')d\vec{\Omega}' + \frac{1}{4\pi}q(\vec{r}), \quad \vec{r}\in\mathcal{D},$$
(4.1)

$$\psi(\vec{r},\vec{\Omega})\Big|_{\vec{r}\in\partial\mathcal{D}} = \psi^{in}(\vec{r}_b,\vec{\Omega}), \quad \vec{\Omega}\cdot\vec{n}<0, \quad \vec{r}_b\in\partial\mathcal{D},$$
(4.2)

where $\mathcal{D} = \{0\le x\le X,\ 0\le y\le Y\}$.

To derive the low-order equations of the NWF family of methods, we operate on the transport equation (4.1) by $\gamma_m\int_{\omega_m}w(\Omega_x,\Omega_y)(\bullet)d\vec{\Omega}$ over spherical angular quadrants ω_m, $m=1,\ldots,4$, where $w(\Omega_x,\Omega_y)$ is a weight function and

$$\gamma_m = \frac{\int_{\omega_m}d\vec{\Omega}}{\int_{\omega_m}w(\Omega_x,\Omega_y)d\vec{\Omega}} \ .$$
(4.3)

The family of 2D NWF methods are then defined by the following high-order problem for the angular flux ψ and low-order problem for the partial scalar fluxes $\phi_m = \int_{\omega_m}\psi d\vec{\Omega}$:

$$\Omega_x \frac{\partial}{\partial x}\psi^{(k+1/2)} + \Omega_y\frac{\partial}{\partial y}\psi^{(k+1/2)} + \sigma_t\psi^{(k+1/2)} = \frac{1}{4\pi}\sigma_s\phi^{(k)} + \frac{1}{4\pi}q,$$
(4.4)

$$G_m^{(k+1/2)} = \gamma_m\int_{\omega_m}w(\Omega_x,\Omega_y)\psi^{(k+1/2)}d\vec{\Omega}\bigg/\int_{\omega_m}\psi^{(k+1/2)}d\vec{\Omega},$$
(4.5)

$$F_m^{\alpha(k+1/2)} = \gamma_m\int_{\omega_m}|\Omega_\alpha|w(\Omega_x,\Omega_y)\psi^{(k+1/2)}d\vec{\Omega}\bigg/\int_{\omega_m}\psi^{(k+1/2)}d\vec{\Omega},$$
(4.6)

$$\alpha = x,y, \quad m = 1,\ldots,4,$$

$$\frac{\partial}{\partial x}(F_1^{x(k+1/2)}\phi_1^{(k+1)}) + \frac{\partial}{\partial y}(F_1^{y(k+1/2)}\phi_1^{(k+1)}) + \sigma_t G_1^{(k+1/2)}\phi_1^{(k+1)} = \frac{1}{4}(\sigma_s\phi^{(k+1)}+q),$$
(4.7)

$$-\frac{\partial}{\partial x}(F_2^{x(k+1/2)}\phi_2^{(k+1)}) + \frac{\partial}{\partial y}(F_2^{y(k+1/2)}\phi_2^{(k+1)}) + \sigma_t G_2^{(k+1/2)}\phi_2^{(k+1)} = \frac{1}{4}(\sigma_s\phi^{(k+1)}+q),$$
(4.8)

$$-\frac{\partial}{\partial x}(F_3^{x(k+1/2)}\phi_3^{(k+1)}) - \frac{\partial}{\partial y}(F_3^{y(k+1/2)}\phi_3^{(k+1)}) + \sigma_t G_3^{(k+1/2)}\phi_3^{(k+1)} = \frac{1}{4}(\sigma_s\phi^{(k+1)}+q),$$
(4.9)

$$\frac{\partial}{\partial x}(F_4^{x(k+1/2)}\phi_4^{(k+1)}) - \frac{\partial}{\partial y}(F_4^{y(k+1/2)}\phi_4^{(k+1)}) + \sigma_t G_4^{(k+1/2)}\phi_4^{(k+1)} = \frac{1}{4}(\sigma_s\phi^{(k+1)}+q),$$
(4.10)

$$0\le x\le X,\ 0\le y\le Y,$$

$$\phi^{(k+1)} = \sum_{m=1}^{4}\phi_m^{(k+1)},$$
(4.11)

with the following boundary conditions for the low-order equations (4.7)-(4.11):

$$\phi_m^{(k+1)}\big|_{x=0} = \int_{\omega_m} \psi^{in}\big|_{x=0} \, d\vec{\Omega}\,, \;\; m=1,4\,, \;\; 0 \le y \le Y\,, \tag{4.12}$$

$$\phi_m^{(k+1)}\big|_{x=X} = \int_{\omega_m} \psi^{in}\big|_{x=X} \, d\vec{\Omega}\,, \;\; m=2,3\,, \;\; 0 \le y \le Y\,, \tag{4.13}$$

$$\phi_m^{(k+1)}\big|_{y=0} = \int_{\omega_m} \psi^{in}\big|_{y=0} \, d\vec{\Omega}\,, \;\; m=1,2\,, \;\; 0 \le x \le X\,, \tag{4.14}$$

$$\phi_m^{(k+1)}\big|_{y=Y} = \int_{\omega_m} \psi^{in}\big|_{y=Y} \, d\vec{\Omega}\,, \;\; m=3,4\,, \;\; 0 \le x \le X\,. \tag{4.15}$$

Standard notations are used. k is the iteration index.

The iterative process is defined by the following three stages:

1. A transport sweep to calculate the angular flux $\psi^{(k+1/2)}$ (Eq. (4.4)).

2. The calculation of the factors $G_m^{(k+1/2)}$ and $F_m^{\alpha(k+1/2)}$ from $\psi^{(k+1/2)}$ (Eqs. (4.5)-(4.6)).

3. Solving the low-order problem (Eqs. (4.7)-(4.15)) for $\phi_m^{(k+1)}$ using $G_m^{(k+1/2)}$ and $F_m^{\alpha(k+1/2)}$.

On the first iteration ($k = 0$) the transport sweep is not performed. The factors $G_m^{(1/2)}$ and $F_m^{\alpha(1/2)}$ are calculated using an isotropic angular flux.

4.3   Discretization of the 2D NWF Methods

The structure of the operator of the low-order NWF equations has some features that make them similar to the transport equation. This enables one to use transport differencing methods as a basis for development of a discretization of the low-order NWF equations.

We consider orthogonal spatial grids

$$x_{i+1/2} = x_{i-1/2} + \Delta x_i, \;\; i=1,\ldots,N_x; \;\; x_{1/2} = 0, \;\; x_{N_x+1/2} = X\,,$$

$$y_{j+1/2} = y_{j-1/2} + \Delta y_j, \;\; j=1,\ldots,N_y; \;\; y_{1/2} = 0, \;\; y_{N_y+1/2} = Y\,.$$

The low-order equations are discretized by the lumped bilinear-discontinuous (BLD) method [26, 27]. The BLD approximation of the partial scalar fluxes in the (i,j)-cell is

$$\phi_m(x,y) = \phi_{m,i,j} + \frac{2}{\Delta x_i}(x-x_i)\phi_{m,i,j}^x + \frac{2}{\Delta y_j}(y-y_j)\phi_{m,i,j}^y + \frac{4}{\Delta x_i \Delta y_j}(x-x_i)(y-y_j)\phi_{m,i,j}^{xy}\,, \tag{4.16}$$

where x_i and y_j are midpoints of the corresponding intervals. The discretized low-order equations of the NWF method are:

$$\nu_m^x \Delta y_j (F_{m,i+1/2,j}^x \phi_{m,i+1/2,j} - F_{m,i-1/2,j}^x \phi_{m,i-1/2,j}) + \nu_m^y \Delta x_i (F_{m,i,j+1/2}^y \phi_{m,i,j+1/2} - F_{m,i,j-1/2}^y \phi_{m,i,j-1/2})$$

$$+ \sigma_{t,i,j} G_{m,i,j} \phi_{m,i,j} \Delta x_i \Delta y_j = \frac{1}{4} \Delta x_i \Delta y_j (\sigma_{s,i,j} \phi_{i,j} + q_{i,j}) , \qquad (4.17)$$

$$\theta_x \nu_m^x \Delta y_j (F_{m,i+1/2,j}^x \phi_{m,i+1/2,j} + F_{m,i-1/2,j}^x \phi_{m,i-1/2,j} - 2 F_{m,i,j}^x \phi_{m,i,j}) + \gamma_y \nu_m^y \Delta x_i (F_{m,i,j+1/2}^y \phi_{m,i,j+1/2}^x$$

$$- F_{m,i,j-1/2}^y \phi_{m,i,j-1/2}^x) + \sigma_{t,i,j} G_{m,i,j} \phi_{m,i,j}^x \Delta x_i \Delta y_j = \frac{1}{4} \Delta x_i \Delta y_j (\sigma_{s,i,j} \phi_{i,j}^x + q_{i,j}^x) , \qquad (4.18)$$

$$\gamma_x \nu_m^x \Delta y_j (F_{m,i+1/2,j}^x \phi_{m,i+1/2,j}^y - F_{m,i-1/2,j}^x \phi_{m,i-1/2,j}^y) + \theta_y \nu_m^y \Delta x_i (F_{m,i,j+1/2}^y \phi_{m,i,j+1/2}$$

$$+ F_{m,i,j-1/2}^y \phi_{m,i,j-1/2} - 2 F_{m,i,j}^y \phi_{m,i,j}) + \sigma_{t,i,j} G_{m,i,j} \phi_{m,i,j}^y \Delta x_i \Delta y_j = \frac{1}{4} \Delta x_i \Delta y_j (\sigma_{s,i,j} \phi_{i,j}^y + q_{i,j}^y) ,$$
$$(4.19)$$

$$\delta_x \nu_m^x \Delta y_j (F_{m,i+1/2,j}^x \phi_{m,i+1/2,j}^y + F_{m,i-1/2,j}^x \phi_{m,i-1/2,j}^y - 2 F_{m,i,j}^x \phi_{m,i,j}^y) + \delta_y \nu_m^y \Delta x_i (F_{m,i,j+1/2}^y \phi_{m,i,j+1/2}^x$$

$$+ F_{m,i,j-1/2}^y \phi_{m,i,j-1/2}^x - 2 F_{m,i,j}^y \phi_{m,i,j}^x) + \sigma_{t,i,j} G_{m,i,j} \phi_{m,i,j}^{xy} \Delta x_i \Delta y_j = \frac{1}{4} \Delta x_i \Delta y_j (\sigma_{s,i,j} \phi_{i,j}^{xy} + q_{i,j}^{xy}) ,$$
$$(4.20)$$

$$i = 1, \dots, N_x , \quad j = 1, \dots, N_y \quad m = 1, \dots, 4 ,$$

where

$$\nu_1^x = \nu_4^x = 1 , \quad \nu_2^x = \nu_3^x = -1 , \qquad (4.21)$$
$$\nu_1^y = \nu_2^y = 1 , \quad \nu_3^y = \nu_4^y = -1 . \qquad (4.22)$$

The BLD auxiliary equations are given by

$$\phi_{1,i+1/2,j} = \phi_{1,i,j} + \phi_{1,i,j}^x , \qquad \phi_{3,i-1/2,j} = \phi_{3,i,j} - \phi_{3,i,j}^x ,$$
$$\phi_{1,i+1/2,j}^y = \phi_{1,i,j}^y + \phi_{1,i,j}^{xy} , \qquad \phi_{3,i-1/2,j}^y = \phi_{3,i,j}^y - \phi_{3,i,j}^{xy} ,$$
$$\phi_{1,i,j+1/2} = \phi_{1,i,j} + \phi_{1,i,j}^y , \qquad \phi_{3,i,j-1/2} = \phi_{3,i,j} - \phi_{3,i,j}^y ,$$
$$\phi_{1,i,j+1/2}^x = \phi_{1,i,j}^x + \phi_{1,i,j}^{xy} , \qquad \phi_{3,i,j-1/2}^x = \phi_{3,i,j}^x - \phi_{3,i,j}^{xy} ,$$

$$\phi_{2,i-1/2,j} = \phi_{2,i,j} - \phi_{2,i,j}^x , \qquad \phi_{4,i+1/2,j} = \phi_{4,i,j} + \phi_{4,i,j}^x ,$$
$$\phi_{2,i-1/2,j}^y = \phi_{2,i,j}^y - \phi_{2,i,j}^{xy} , \qquad \phi_{4,i+1/2,j}^y = \phi_{4,i,j}^y + \phi_{4,i,j}^{xy} ,$$
$$\phi_{2,i,j+1/2} = \phi_{2,i,j} + \phi_{2,i,j}^y , \qquad \phi_{4,i,j-1/2} = \phi_{4,i,j} - \phi_{4,i,j}^y ,$$
$$\phi_{2,i,j+1/2}^x = \phi_{2,i,j}^x + \phi_{2,i,j}^{xy} , \qquad \phi_{4,i,j-1/2}^x = \phi_{4,i,j}^x - \phi_{4,i,j}^{xy} . \qquad (4.23)$$

Lumping parameters are denoted by θ_α, γ_α, and δ_α ($\alpha = x, y$). The standard BLD equations are obtained by setting the lumping parameters to 3, 1, and 3, respectively. For mass-lumped BLD, the parameters become 1, 1/3, and 1/3. For fully lumped BLD, the parameters all have values of 1.

The transport equation is approximated by the method of short characteristics [40, 41, 42], from which the factors are calculated on vertices. Cell-average factors, $F_{m,i,j}^\alpha$ and $G_{m,i,j}$, are calculated as averages of factors evaluated on the four cell vertices. Face-average factors, $F_{m,i+1/2,j}^\alpha$ and $F_{m,i,j+1/2}^\alpha$, are averages of the two nearest vertex values.

4.4 Analysis of Asymptotic Diffusion Limit

4.4.1 NWF Methods in Continuous Form

To meet the diffusion limit, the leading-order solution of the low-order equations (4.7)-(4.10) must give rise to the diffusion equation [16, 24]. In order to develop a NWF method that satisfies this condition, we perform an asymptotic diffusion limit analysis of the low-order equations of the NWF methods for general weight $w(\Omega_x, \Omega_y)$ under the assumption that the angular flux is isotropic. Then, the factors are

$$G_m = 1, \quad F_m^\alpha = \tilde{F}_m^\alpha, \quad \alpha = x, y, \quad m = 1, \ldots, 4,$$

where

$$\tilde{F}_m^\alpha = \gamma_m \int_{\omega_m} |\Omega_\alpha| w(\Omega_x, \Omega_y) d\vec{\Omega} \Big/ \int_{\omega_m} d\vec{\Omega}. \tag{4.24}$$

The analysis shows that the leading-order solution of the low-order equations (4.7)-(4.10) satisfies the following second-order PDE in the interior of the optically thick diffusive region:

$$-\frac{1}{4} \left(\sum_{m=1}^{4} (\tilde{F}_m^x)^2 \right) \frac{\partial}{\partial x} \frac{1}{\sigma_t} \frac{\partial \phi^{[0]}}{\partial x} - \frac{1}{4} \left(\sum_{m=1}^{4} (\tilde{F}_m^y)^2 \right) \frac{\partial}{\partial y} \frac{1}{\sigma_t} \frac{\partial \phi^{[0]}}{\partial y}$$

$$-\frac{1}{4} \left(\tilde{F}_1^x \tilde{F}_1^y - \tilde{F}_2^x \tilde{F}_2^y + \tilde{F}_3^x \tilde{F}_3^y - \tilde{F}_4^x \tilde{F}_4^y \right) \left(\frac{\partial}{\partial x} \frac{1}{\sigma_t} \frac{\partial \phi^{[0]}}{\partial y} + \frac{\partial}{\partial y} \frac{1}{\sigma_t} \frac{\partial \phi^{[0]}}{\partial x} \right)$$

$$+\frac{1}{4} \left(\tilde{F}_1^x + \tilde{F}_4^x - \sum_{m=2}^{3} \tilde{F}_m^x \right) \frac{\partial \phi^{[1]}}{\partial x} + \frac{1}{4} \left(\sum_{m=1}^{2} \tilde{F}_m^y - \sum_{m=3}^{4} \tilde{F}_m^y \right) \frac{\partial \phi^{[1]}}{\partial y} + \sigma_a \phi^{[0]} = q. \tag{4.25}$$

The equation (4.25) results in the diffusion equation and hence the leading-order solution satisfies the diffusion equation, if the following five conditions are met:

$$\frac{1}{4} \sum_{m=1}^{4} (\tilde{F}_m^x)^2 = \frac{1}{3}, \tag{4.26}$$

$$\frac{1}{4} \sum_{m=1}^{4} (\tilde{F}_m^y)^2 = \frac{1}{3}, \tag{4.27}$$

$$\tilde{F}_1^x \tilde{F}_1^y - \tilde{F}_2^x \tilde{F}_2^y + \tilde{F}_3^x \tilde{F}_3^y - \tilde{F}_4^x \tilde{F}_4^y = 0, \tag{4.28}$$

$$\tilde{F}_1^x + \tilde{F}_4^x - \sum_{m=2}^{3} \tilde{F}_m^x = 0, \tag{4.29}$$

$$\sum_{m=1}^{2} \tilde{F}_m^y - \sum_{m=3}^{4} \tilde{F}_m^y = 0. \tag{4.30}$$

The results of this analysis allow an evaluation of NWF methods with various weights. Note that if a weight satisfies only Eqs. (4.28)-(4.30), then Eq. (4.25) leads to a diffusion-like equation with a wrong diffusion coefficient, D.

34

Let us consider methods with a general linear weight function of directional cosines

$$w(\Omega_x, \Omega_y) = 1 + \beta_x |\Omega_x| + \beta_y |\Omega_y| \,. \tag{4.31}$$

For the weight (4.31) and specified above ranges for the partial fluxes (i.e. ω_m), we get

$$\tilde{F}_m^\alpha = \tilde{F}\,, \quad m = 1, \ldots, 4\,, \tag{4.32}$$

where

$$\tilde{F} = \frac{\frac{1}{2} + \frac{1}{3}(\beta_x + \frac{2}{\pi}\beta_y)}{1 + \frac{1}{2}(\beta_x + \beta_y)} \,. \tag{4.33}$$

Note that the use of a general constant term in (4.31) will not result in a different NWF method.

The above five requirements (5.21)-(4.30) are met if the following two conditions on the weight (4.31) are true:

$$\beta_x = \beta_y = \beta\,, \tag{4.34}$$

where

$$\beta = \frac{\pi\sqrt{3}(\sqrt{3}-2)}{2(\pi(\sqrt{3}-1)-2)} \approx -2.43\,. \tag{4.35}$$

The weight (4.31) and parameter β determine a specific method within the family of NWF methods for which the low-order equations lead to the correct diffusion equation in the diffusion limit provided that the factors are calculated with an isotropic angular flux. The low-order equations of methods with $w = 1$, $w = |\Omega_x| + |\Omega_y|$, and $w = 1 + |\Omega_x| + |\Omega_y|$ give rise to a diffusion-like equation, but with a wrong diffusion coefficient. The values of the diffusion coefficients for these methods are shown in Table 4.1.

Table 4.1: Values of the Diffusion Coefficients (D) for Specific NWF Methods

Weight	$w = 1$	$w=|\Omega_x|+|\Omega_y|$	$w=1+|\Omega_x|+|\Omega_y|$	$w=1+\beta(|\Omega_x|+|\Omega_y|)$
D	$\frac{1}{4\sigma_t}$	$\left(\frac{\pi+2}{3\pi}\right)^2\frac{1}{\sigma_t} \approx \frac{1}{3.36\sigma_t}$	$\left(\frac{4+5\pi}{12\pi}\right)^2\frac{1}{\sigma_t} \approx \frac{1}{3.66\sigma_t}$	$\frac{1}{3\sigma_t}$

4.4.2 NWF Methods in Discretized Form

We now perform an asymptotic diffusion limit analysis of the NWF methods approximated by means of the discretization described above (see Sec. 4.3) on a uniform rectangular spatial grid. The analysis showed that the equation for the leading-order solution can be reduced to a diffusion-like equation provided that in the cells at the interior of the interfaces of the thick diffusive regions, cell-average factors and downstream face-average factors are defined

by the corresponding downstream vertex value, namely, given by:

$$G_{1,i,j} = G_{1,i+1/2,j+1/2} ,$$
$$G_{2,i,j} = G_{2,i-1/2,j+1/2} ,$$
$$G_{3,i,j} = G_{3,i-1/2,j-1/2} ,$$
$$G_{4,i,j} = G_{4,i+1/2,j-1/2} , \tag{4.36}$$

$$F_{1,i,j}^\alpha = F_{1,i+1/2,j}^\alpha = F_{1,i,j+1/2}^\alpha = F_{1,i+1/2,j+1/2}^\alpha ,$$
$$F_{2,i,j}^\alpha = F_{2,i-1/2,j}^\alpha = F_{2,i,j+1/2}^\alpha = F_{2,i-1/2,j+1/2}^\alpha ,$$
$$F_{3,i,j}^\alpha = F_{3,i-1/2,j}^\alpha = F_{3,i,j-1/2}^\alpha = F_{3,i-1/2,j-1/2}^\alpha ,$$
$$F_{4,i,j}^\alpha = F_{4,i+1/2,j}^\alpha = F_{4,i,j-1/2}^\alpha = F_{4,i+1/2,j-1/2}^\alpha . \tag{4.37}$$

If these conditions are met, then the low-order NWF equations discretized by the BLD method lead to the same discrete equation for the leading-order solution as the BLD discretization of the transport equation [24]. However, the resulting discretized diffusion equation has the diffusion coefficient

$$D = \frac{\tilde{F}^2}{\sigma_t} , \tag{4.38}$$

and hence in general it is not a correct one. In case of the weight $w(\Omega_x, \Omega_y) = 1 + \beta(|\Omega_x| + |\Omega_y|)$, we have $\tilde{F}^2 = \frac{1}{3}$ and obtain the right diffusion coefficient.

We now analyze the behavior of the discretized NWF methods in the presence of a boundary layer that is not resolved by the spatial grid. The asymptotic analysis of the boundary-layer solution of the transport equation in the differential form showed that the leading-order scalar flux meets the following boundary condition [32]:

$$\phi^{[0]}(X, y) = 2 \int_{\vec{n}\cdot\vec{\Omega}<0} W(|\vec{n}\cdot\vec{\Omega}|)\psi_{in}(X, y, \vec{\Omega})d\vec{\Omega} , \tag{4.39}$$

$$W(\mu) = \frac{\sqrt{3}}{2}\mu H(\mu) \approx 0.956\mu + 1.565\mu^2 , \tag{4.40}$$

where $H(\mu)$ is the Chandrasekhar H-function for a purely scattering medium.

Let us consider the boundary condition at $x = X$, where $\vec{n} = \vec{e}_x$. The analysis of the discretized NWF methods revealed that on the boundary of an optically thick diffusive region the leading-order scalar flux is defined by

$$\phi_{N_x,j}^{[0]} = \frac{2\pi\sum\limits_{\vec{n}\cdot\vec{\Omega}_m<0} \left[w(|\Omega_{x,m}|, |\Omega_{y,m}|)|\Omega_{x,m}|\right]\psi_{in}(\vec{\Omega}_m)\zeta_m}{\sum\limits_{m\in\omega_1} w(|\Omega_{x,m}|, |\Omega_{y,m}|)|\Omega_{x,m}|\zeta_m} , \tag{4.41}$$

where ζ_m are quadrature weights. The equation (4.41) approximates the following boundary relationship in a continuous form:

$$\phi^{[0]}(X, y) = 2 \int_{\vec{n}\cdot\vec{\Omega}<0} \widetilde{W}(|\Omega_x|, |\Omega_y|)\psi_{in}(X, y, \vec{\Omega})d\vec{\Omega} , \tag{4.42}$$

where

$$\widetilde{W}(|\Omega_x|, |\Omega_y|) = \frac{\pi w(|\Omega_x|, |\Omega_y|)|\Omega_x|}{\int_{\omega_1} w(|\Omega_x|, |\Omega_y|)|\Omega_x| d\vec{\Omega}} . \tag{4.43}$$

The asymptotic analysis of other boundaries, for instance at $y = 0$, results in a similar expression.

We now examine the resulting weight function in the boundary condition, $\widetilde{W}(|\Omega_x|, |\Omega_y|)$, for various NWF methods. For the NWF method with $w(\Omega_x, \Omega_y) = 1$ (the first flux method), we get

$$\widetilde{W}(|\Omega_x|) = 2|\Omega_x| . \tag{4.44}$$

For the case $w(\Omega_x, \Omega_y) = |\Omega_x| + |\Omega_y|$, the boundary weight function is

$$\begin{aligned}
\widetilde{W}(|\Omega_x|, |\Omega_y|) &= \frac{3\pi}{2+\pi}[|\Omega_x|^2 + |\Omega_y||\Omega_x|] \\
&\approx 1.833[|\Omega_x|^2 + |\Omega_y||\Omega_x|] .
\end{aligned} \tag{4.45}$$

The weight $w(\Omega_x, \Omega_y) = 1 + |\Omega_x| + |\Omega_y|$ results in the boundary weight function

$$\begin{aligned}
\widetilde{W}(|\Omega_x|, |\Omega_y|) &= \frac{6\pi}{5\pi+4}[|\Omega_x| + |\Omega_x|^2 + |\Omega_y||\Omega_x|] \\
&\approx 0.956[|\Omega_x| + |\Omega_x|^2 + |\Omega_y||\Omega_x|] .
\end{aligned} \tag{4.46}$$

If $w(\Omega_x, \Omega_y) = 1 + \beta\left(|\Omega_x| + |\Omega_y|\right)$, we have

$$\begin{aligned}
\widetilde{W}(|\Omega_x|, |\Omega_y|) &= \left[\frac{1}{2} + \beta(\frac{2+\pi}{3\pi})\right]^{-1}\left(|\Omega_x| + \beta|\Omega_x|^2 + \beta|\Omega_y||\Omega_x|\right) \\
&\approx -1.209|\Omega_x| + 2.942|\Omega_x|^2 + 2.942|\Omega_y||\Omega_x| .
\end{aligned} \tag{4.47}$$

The transport equation's boundary weight function (4.40) depends only on $\mu = |\vec{n}\cdot\vec{\Omega}|$, which for the boundary considered is $|\Omega_x|$. Note that the resulting boundary weight functions for the considered weights, $w(\Omega_x, \Omega_y)$, each differ from the polynomial approximation of $W(\mu)$. Higher order polynomial weights may be considered, but they are not necessary to produce the asymptotic diffusion equation and will introduce third-order and higher terms into the asymptotic boundary condition that do not exist in the analytic result of the transport equation. The following section presents numerical results that enable one to compare and analyze the properties of different NWF methods.

4.5 Numerical Results

We present numerical results of two test problems to demonstrate the performance of the proposed 2D NWF method with weight $w(\Omega_x, \Omega_y) = 1 + \beta(|\Omega_x| + |\Omega_y|)$. The first problem is designed to test the diffusion limit performance of the method in the interior of a diffusive region. The second problem investigates both the diffusion limit and the boundary condition properties of the method. We also show the results for the NWF methods with weights $w(\Omega_x, \Omega_y) = 1$, $w(\Omega_x, \Omega_y) = |\Omega_x| + |\Omega_y|$ and $w(\Omega_x, \Omega_y) = 1 + |\Omega_x| + |\Omega_y|$.

Note that the factors in the NWF methods involve integration over individual quadrants of the angular flux multiplied by polynomials of directional cosines. Taking into account this fact, we use Gauss-type quadratures [31], namely, the compatible quadruple-range quadrature with an equal number of azimuthal angles on each polar cone.

Problem 1

We consider a unit square having $\sigma_t = 1/\varepsilon$, $\sigma_a = \varepsilon$, and $q = \varepsilon$ for $\varepsilon = 10^{-2}, 10^{-3}, 10^{-4}, 10^{-5}$ [24]. Note that as $\varepsilon \to 0$ the domain becomes more and more diffusive. A uniform spatial mesh of 19x19 equal cells is used with vacuum boundary conditions. The angular discretization is 9 directions per octant, 3 per polar level. A relative pointwise convergence criterion of 10^{-8} is used.

Tables 4.2 and 4.3 show measures of the error of the NWF methods' solutions in Problem 1 as compared to the fine-mesh numerical solution obtained by the QD method. Note that the low-order equations of the QD method give rise to the diffusion equation in diffusive regions. The low-order QD equations are discretized by means of a finite-volume method of second-order accuracy. The QD solution accurately reproduces the solution of this problem. Relative errors of the cell-average scalar flux in the cell located at the center of the domain are listed in Table 4.2. The relative errors of the solution in the L_2-norm are shown in Table 4.3. These results demonstrate that the NWF method with the weight $w(\Omega_x, \Omega_y) = 1 + \beta(|\Omega_x| + |\Omega_y|)$ reproduces the maximum of the solution with small errors, especially in case of extremely diffusive regions. The proposed method also has the smallest relative errors in the L_2 norm. Larger errors of the NWF method with other weights $w(\Omega_x, \Omega_y)$ are explained by the fact that the equations of these methods lead to the diffusion equation with a wrong diffusion coefficient (Eq.(4.38) and Table 4.1) in the interior of diffusive regions.

Problem 2

We consider a boundary layer problem $0 \le x, y \le 11$ having $\sigma_t = \sigma_a = 2$, $\Delta x = 0.1$, and $q = 0$ from $0 \le x \le 1$ and $\sigma_t = \sigma_s = 100$, $\Delta x = 1$, and $q = 0$ from $1 \le x \le 11$ ($\Delta y = 1$ everywhere). There is an isotropic incoming angular flux with magnitude $\frac{1}{2\pi}$ on the left boundary and vacuum on the rest. The angular quadrature set and convergence criterion are the same as in Problem 1. This problem tests a method's ability to reproduce an accurate diffusion solution in the interior of a diffusive region with a spatially unresolved boundary layer.

Figure 4.1 shows the overall performance of the methods in an unresolved boundary layer problem. The scalar flux from the low-order problem along the middle of the spatial domain at $y = 5.5$ is plotted where the cell-average values are displayed in solid and the face-average values are in outline form. The red curve represents the fine-mesh solution obtained by the QD method. Figure 4.2 demonstrates the absolute value of the relative errors of the low-order scalar flux with respect to the fine mesh solution. Note that at the right boundary (x=11) the solution is very small ($\phi = 3.724 \times 10^{-5}$). It results in an increase of the relative error at x=11. The presented results show that the NWF method with the smallest errors in the diffusive region with highly anisotropic angular flux coming from the purely absorbing region is the method with the weight $w = 1 + \beta(|\Omega_x| + |\Omega_y|)$.

Table 4.2: Problem 1: Relative Errors of the Cell-Average Scalar Flux in the Cell Located at the Center of the Domain

Weight	$w=1$	$w=|\Omega_x|+|\Omega_y|$	$w=1+|\Omega_x|+|\Omega_y|$	$w=1+\beta(|\Omega_x|+|\Omega_y|)$
$\varepsilon = 10^{-2}$	2.57E-1	1.02E-1	1.76E-1	8.49E-3
$\varepsilon = 10^{-3}$	2.70E-1	9.97E-2	1.81E-1	-7.98E-4
$\varepsilon = 10^{-4}$	2.71E-1	1.00E-1	1.81E-1	-6.02E-4
$\varepsilon = 10^{-5}$	2.71E-1	1.00E-1	1.81E-1	-5.81E-4

Table 4.3: Problem 1: Relative Errors of the Scalar Flux in L_2 Norm

Weight	$w=1$	$w=|\Omega_x|+|\Omega_y|$	$w=1+|\Omega_x|+|\Omega_y|$	$w=1+\beta(|\Omega_x|+|\Omega_y|)$
$\varepsilon = 10^{-2}$	2.32E-1	8.56E-2	1.55E-1	1.81E-2
$\varepsilon = 10^{-3}$	2.54E-1	8.82E-2	1.67E-1	1.96E-2
$\varepsilon = 10^{-4}$	2.56E-1	8.90E-2	1.68E-1	1.99E-2
$\varepsilon = 10^{-5}$	2.56E-1	8.91E-2	1.68E-1	1.99E-2

4.6 Conclusions

A parameterized family of nonlinear weighted flux methods for solving particle transport problems in 2D Cartesian geometry has been considered. The properties of these methods for transport problems with isotropic scattering have been analyzed in differential and discretized form. Independent schemes to discretize the low-order and high-order (transport) equations are used. The performed analysis revealed a method with a particular linear weight function the low-order equations of which lead to the diffusion equation in the asymptotic diffusion limit. The resulting low-order NWF equations are discretized with the lumped BLD method. The convergence rates of the proposed iterative method are similar to those of the QD and DSA methods. We now work on further analysis and development of the NWF methods.

The proposed NWF method that meets the diffusion limit can be used for developing approximate mathematical models for radiative transfer and particle transport that are similar to the Variable Eddington Factor (VEF) approach [33]. The VEF methods are based on a set of low-order equations for moments of the angular flux and some *apriori* closure relationships, for instance, Levermore-Pomraning or Minerbo closures [34, 35]. For some class of transport problems, these approximate models can be more accurate than the flux-limited diffusion model or P_1 theory. The low-order NWF equations can be used in combination with, for example, Minerbo closure to derive a model with new features. This area of application of the NWF methods in 1D and 2D requires further studies.
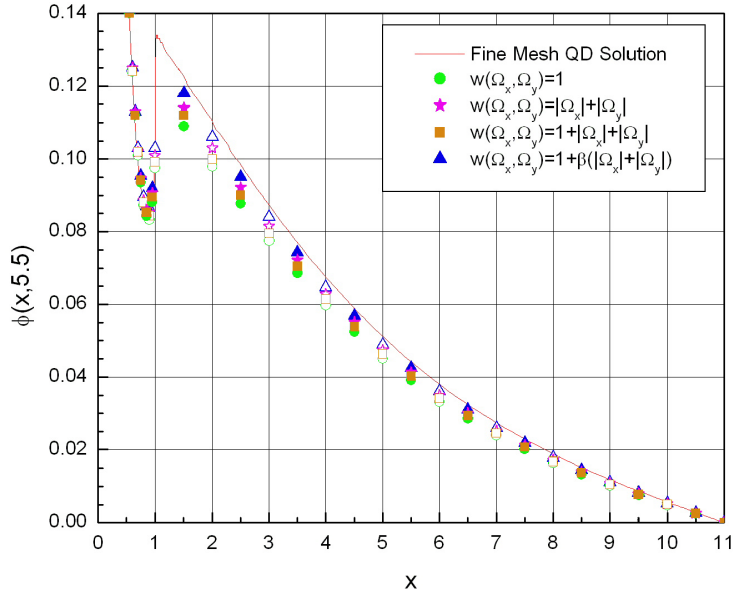
Figure 4.1: Problem 2: Cell Average and Cell Face Total Low-Order Scalar Flux.
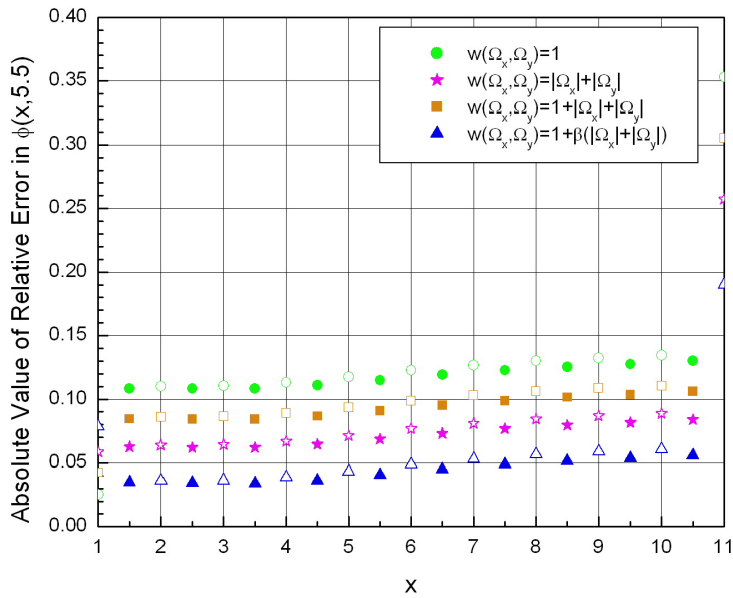
Figure 4.2: Problem 2: Absolute Value of Relative Errors of the Scalar Flux versus QD Fine Mesh Solution of Figure 4.1.

Chapter 5

Analysis of the Quasidiffusion Method on Two-Dimensional Problems with Spatially Periodic Media

Abstract

We study convergence of the quasidiffusion (QD) method on two-dimensional spatially periodic problems with strong heterogeneities. A Fourier analysis of the linearized QD equations in the vicinity of the solution is performed. The analysis shows that in Periodic Horizontal Interface (PHI) problems the QD iteration method loses its effectiveness and even diverges in some cases. Numerical results of finite-medium PHI problems are presented to demonstrate the behavior of the QD method that was theoretically predicted.

The results of the research presented in this chapter were published in

- A. Constantinescu (graduate student) & D.Y. Anistratov, "Stability Analysis of the Quasidiffusion Method for Multidimensional Problems with Material Discontinuities," *Proceedings of M&C + SNA 2007, Joint International Topical Meeting on Mathematics & Computations and Supercomputing in Nuclear Applications*, Monterey, CA, April, 2007, 11 pp.

- A. Constantinescu, "Analysis of Projective-Iterative Methods for Solving Multidimensional Transport Problems," Master Thesis, Scientific Advisor: D.Y. Anistratov, Department of Nuclear Engineering, North Carolina State University, August 2006.

5.1   Introduction

Recent research on transport acceleration methods showed that some of them lose their effectiveness in problems with strongly heterogeneous media [1, 5, 36, 2]. The diffusion synthetic acceleration (DSA) and transport synthetic acceleration (TSA) methods has been studied by means of a Fourier analysis on problems with spatially periodic media. It enabled

one to find out details of effects of material discontinuity on convergence behavior of these iterative methods.

In this paper, we analyze the convergence of the quasidiffusion (QD) method [4] for this class of transport problems in 2D geometry. The QD method is a nonlinear iteration method and hence the Fourier analysis cannot be directly applied to study its properties. The QD equations must be linearized about the solution. Then the analysis of the convergence of the method is performed in the vicinity of the solution. In case of a special problem with an infinite uniform medium and constant source, the analytic solution is known [6]. However, in heterogeneous-medium problems this is not the case.

We use an approach for stability analysis of nonlinear transport iteration methods for infinite medium problems with spatially periodic material composition that was developed and applied to the QD method in 1D slab geometry [37]. To obtain the solution of an infinite-medium problem with heterogeneous material composition, we formulate an equivalent finite-medium problem with periodic boundary conditions and generate its solution numerically. This solution is used to linearize the equations of the QD method. These studies showed that the QD method is stable and converges fast on this class of problems in 1D slab geometry. The numerical results showed that the theoretical analysis predicts well the convergence rates of the QD method in the vicinity of the solution. Note that this analysis enabled us to find and predict some effects in convergence behavior of the QD method that could not be obtained from either studying the QD method in homogeneous-medium problems or analysis of its linear version on heterogeneous problems. In this paper, we analyze the QD method on 2D problems.

The remainder of this paper is organized as follows. In Sec. 5.2, the QD method is formulated. The linearization of the discretized 2D QD equations is presented in Sec. 5.3. In Sec. 5.4, we describe the Fourier analysis. The numerical results are presented in Sec. 5.5. In Sec. 5.6, we conclude with a discussion on the obtained results of analysis of the QD method in 2D.

5.2 Formulation of the QD Method

We consider a one group transport problem with isotropic scattering and source in 2D Cartesian geometry ($0 \leq x \leq X$, $0 \leq y \leq Y$). The QD method is defined by [4]:

$$\Omega_x \frac{\partial}{\partial x} \psi^{(s+1/2)}(\vec{r}, \vec{\Omega}) + \Omega_y \frac{\partial}{\partial y} \psi^{(s+1/2)}(\vec{r}, \vec{\Omega}) + \sigma_t(\vec{r}) \psi^{(s+1/2)}(\vec{r}, \vec{\Omega}) = \frac{1}{4\pi} \sigma_s(\vec{r}) \phi^{(s)}(\vec{r}) + \frac{1}{4\pi} Q(\vec{r}) \tag{5.1}$$

$$E_{\alpha\beta}^{(s+1/2)}(\vec{r}) = \int_{4\pi} \Omega_\alpha \Omega_\beta \psi^{(s+1/2)}(\vec{r}, \vec{\Omega}) d\vec{\Omega} \bigg/ \int_{4\pi} \psi^{(s+1/2)}(\vec{r}, \vec{\Omega}) d\vec{\Omega} \,, \quad \alpha, \beta = x, y \,, \tag{5.2}$$

$$\vec{\nabla} \cdot \vec{J}^{(s+1)}(\vec{r}) + \sigma_a(\vec{r}) \phi^{(s+1)}(\vec{r}) = Q(\vec{r}) \,, \tag{5.3}$$

$$\frac{\partial}{\partial x} \left(E_{xx}^{(s+1/2)}(\vec{r}) \phi^{(s+1)}(\vec{r}) \right) + \frac{\partial}{\partial y} \left(E_{xy}^{(s+1/2)}(\vec{r}) \phi^{(s+1)}(\vec{r}) \right) + \sigma_t(\vec{r}) J_x^{(s+1)}(\vec{r}) = 0 \,, \tag{5.4}$$

$$\frac{\partial}{\partial x} \left(E_{xy}^{(s+1/2)}(\vec{r}) \phi^{(s+1)}(\vec{r}) \right) + \frac{\partial}{\partial y} \left(E_{yy}^{(s+1/2)}(\vec{r}) \phi^{(s+1)}(\vec{r}) \right) + \sigma_t(\vec{r}) J_y^{(s+1)}(\vec{r}) = 0 \,, \tag{5.5}$$

and corresponding boundary conditions. Here s is the iteration index. Standard notations are used.

5.3   Linearization of the Discretized QD Equations

We consider rectangular spatial grids $\{x_{i-1/2}, 1 \le i \le N_x+1, y_{j-1/2}, 1 \le j \le N_y+1\}$. The low-order QD equations (LOQD) (5.3)-(5.5) are discretized with a finite volume method [39, 38] and have the following form:

$$\left(J_{x,i+1/2,j}^{(s+1)} - J_{x,i-1/2,j}^{(s+1)} \right) \Delta y_j + \left(J_{x,i,j+1/2}^{(s+1)} - J_{x,i,j-1/2}^{(s+1)} \right) \Delta x_i + \sigma_{a,i,j} \Delta x_i \Delta y_j \phi_{i,j}^{(s+1)} = Q_{i,j} \Delta x_i \Delta y_j \,, \quad (5.6)$$

$$\left(E_{xx,i,j}^{(s+1/2)} \phi_{i,j}^{(s+1)} - E_{xx,i-1/2,j}^{(s+1/2)} \phi_{i-1/2,j}^{(s+1)} \right) \Delta y_j$$

$$- \left(E_{xy,i,j+1/2}^{(s+1/2)} \phi_{i,j+1/2}^{(s+1)} - E_{xy,i,j-1/2}^{(s+1/2)} \phi_{i,j-1/2}^{(s+1)} \right) \tfrac{\Delta x_i}{2} + \tfrac{1}{2} \sigma_{t,i,j} \Delta x_i \Delta y_j J_{i-1/2,j}^{(s+1)} = 0 \,, \quad (5.7)$$

$$\left(E_{xx,i+1/2,j}^{(s+1/2)} \phi_{i+1/2,j}^{(s+1)} - E_{xx,i,j}^{(s+1/2)} \phi_{i,j}^{(s+1)} \right) \Delta y_j$$

$$- \left(E_{xy,i,j+1/2}^{(s+1/2)} \phi_{i,j+1/2}^{(s+1)} - E_{xy,i,j-1/2}^{(s+1/2)} \phi_{i,j-1/2}^{(s+1)} \right) \tfrac{\Delta x_i}{2} + \tfrac{1}{2} \sigma_{t,i,j} \Delta x_i \Delta y_j J_{i+1/2,j}^{(s+1)} = 0 \,, \quad (5.8)$$

$$\left(E_{yy,i,j}^{(s+1/2)} \phi_{i,j}^{(s+1)} - E_{yy,i,j-1/2}^{(s+1/2)} \phi_{i,j-1/2}^{(s+1)} \right) \Delta x_i$$

$$- \left(E_{xy,i+1/2,j}^{(s+1/2)} \phi_{i+1/2,j}^{(s+1)} - E_{xy,i-1/2,j}^{(s+1/2)} \phi_{i-1/2,j}^{(s+1)} \right) \tfrac{\Delta y_j}{2} + \tfrac{1}{2} \sigma_{t,i,j} \Delta x_i \Delta y_j J_{i,j-1/2}^{(s+1)} = 0 \,, \quad (5.9)$$

$$\left(E_{yy,i,j+1/2}^{(s+1/2)} \phi_{i,j+1/2}^{(s+1)} - E_{yy,i,j}^{(s+1/2)} \phi_{i,j}^{(s+1)} \right) \Delta x_i$$

$$- \left(E_{xy,i+1/2,j}^{(s+1/2)} \phi_{i+1/2,j}^{(s+1)} - E_{xy,i-1/2,j}^{(s+1/2)} \phi_{i-1/2,j}^{(s+1)} \right) \tfrac{\Delta y_j}{2} + \tfrac{1}{2} \sigma_{t,i,j} \Delta x_i \Delta y_j J_{i,j+1/2}^{(s+1)} = 0 \,, \quad (5.10)$$

$$\Delta x_i = x_{i+1/2} - x_{i-1/2} \,, \quad \Delta y_i = y_{j+1/2} - y_{j-1/2} \,.$$

The transport equation (5.1) is approximated by the method of short characteristics [40, 41, 42]. The edge- and cell-average $E_{\alpha\beta}$ are calculated as arithmetic average of vertex values

$$E_{\alpha\beta,i+1/2,j+1/2}^{(s+1/2)} = \sum_m \Omega_{\alpha,m} \Omega_{\beta,m} \psi_{m,i+1/2,j+1/2}^{(s+1/2)} w_m \Big/ \sum_m \psi_{m,i+1/2,j+1/2}^{(s+1/2)} w_m \,, \quad \alpha, \beta = x, y \,, \quad (5.11)$$

where w_m is a quadrature weight that corresponds to the discrete ordinates direction $\vec{\Omega}_m$.

To study the convergence behavior of the nonlinear QD method, we linearize the equations in the vicinity of the solution. Assuming that the solution on s-th iteration is close to the converged one, we define

$$\psi_{m,i,j}^{(s+1/2)} = \psi_{m,i,j} + \delta\psi_{m,i,j}^{(s+1/2)} \,, \quad (5.12)$$

$$\psi_{m,i+1/2,j}^{(s+1/2)} = \psi_{m,i+1/2,j} + \delta\psi_{m,i+1/2,j}^{(s+1/2)} \,, \quad (5.13)$$

$$\psi_{m,i,j+1/2}^{(s+1/2)} = \psi_{m,i,j+1/2} + \delta\psi_{m,i,j+1/2}^{(s+1/2)} \,, \quad (5.14)$$

$$\phi_{i,j}^{(s)} = \phi_{i,j} + \delta\phi_{i,j}^{(s)} \,, \quad (5.15)$$

$$\phi_{i+1/2,j}^{(s)} = \phi_{i+1/2,j} + \delta\phi_{i+1/2,j}^{(s)} \,, \quad (5.16)$$

$$\phi_{i,j+1/2}^{(s)} = \phi_{i,j+1/2} + \delta\phi_{i,j+1/2}^{(s)} \,. \quad (5.17)$$

We introduce Eqs. (5.12)-(5.17) into the discretized transport and LOQD equations. The linearized LOQD equations can be reduced to the equation for the errors of cell-average

scalar fluxes $\delta\phi^{(s)}$

$$\frac{E_{xx,i,j}\delta\phi_{i,j}^{(s+1)}-E_{xx,i+1,j}\delta\phi_{i+1,j}^{(s+1)}}{\sigma_{t,i+1/2,j}\Delta x_i\Delta x_{i+1/2}} - \frac{E_{xx,i-1,j}\delta\phi_{i-1,j}^{(s+1)}-E_{xx,i,j}\delta\phi_{i,j}^{(s+1)}}{\sigma_{t,i-1/2,j}\Delta x_i\Delta x_{i-1/2}}$$

$$+\frac{E_{yy,i,j}\delta\phi_{i,j}^{(s+1)}-E_{yy,i,j+1}\delta\phi_{i,j+1}^{(s+1)}}{\sigma_{t,i,j+1/2}\Delta y_j\Delta y_{j+1/2}} - \frac{E_{yy,i,j-1}\delta\phi_{i,j-1}^{(s+1)}-E_{yy,i,j}\delta\phi_{i,j}^{(s+1)}}{\sigma_{t,i,j-1/2}\Delta y_j\Delta y_{j-1/2}} + \sigma_{a,i,j}\delta\phi_{i,j}^{(s+1)}$$

$$= -\frac{R_{i+1,j}\delta T_{xx,i+1,j}^{(s+1/2)}-R_{i,j}\delta T_{xx,i,j}^{((s+1/2))}}{\sigma_{t,i+1/2,j}\Delta x_{i+1}\Delta x_{i+1/2}} - \frac{R_{i,j+1/2}\delta T_{xy,i,j+1/2}^{(s+1/2)}-R_{i,j-1/2}\delta T_{xy,i,j-1/2}^{(s+1/2)}}{2\sigma_{t,i+1/2,j}\Delta y_j\Delta x_{i+1/2}}$$

$$-\frac{\Delta x_{i+1}}{2\Delta x_i\Delta y_j}\frac{R_{i+1,j+1/2}\delta T_{xy,i+1,j+1/2}^{(s+1/2)}-R_{i+1,j-1/2}\delta T_{xy,i+1,j-1/2}^{(s+1/2)}}{\sigma_{t,i+1/2,j}\Delta x_{i+1/2}}$$

$$+\frac{R_{i,j}\delta T_{xx,i,j}^{(s+1/2)}-R_{i-1,j}\delta T_{xx,i-1,j}^{(s+1/2)}}{\sigma_{t,i-1/2,j}\Delta x_i\Delta x_{i-1/2}} + \frac{R_{i,j+1/2}\delta T_{xy,i,j+1/2}^{(s+1/2)}-R_{i,j-1/2}\delta T_{xy,i,j-1/2}^{(s+1/2)}}{2\sigma_{t,i-1/2,j}\Delta y_j\Delta x_{i-1/2}}$$

$$+\frac{\Delta x_{i-1}}{2\Delta x_i\Delta y_j}\frac{R_{i-1,j+1/2}\delta T_{xy,i-1,j+1/2}^{(s+1/2)}-R_{i-1,j-1/2}\delta T_{xy,i-1,j-1/2}^{(s+1/2)}}{\sigma_{t,i-1/2,j}\Delta x_{i-1/2}}$$

$$-\frac{R_{i,j+1}\delta T_{yy,i,j+1}^{(s+1/2)}-R_{i,j}\delta T_{yy,i,j}^{(s+1/2)}}{\sigma_{t,i,j+1/2}\Delta y_j\Delta y_{j+1/2}} - \frac{R_{i+1/2,j}\delta T_{yx,i+1/2,j}^{(s+1/2)}-R_{i-1/2,j}\delta T_{yy,i-1/2,j}^{(s+1/2)}}{2\sigma_{t,i,j-1/2}\Delta x_i\Delta y_{j-1/2}}$$

$$-\frac{\Delta y_{j+1}}{2\Delta x_i\Delta y_j}\frac{R_{i+1/2,j+1}\delta T_{yx,i+1/2,j+1}^{(s+1/2)}-R_{i-1/2,j+1}\delta T_{yx,i-1/2,j+1}^{(s+1/2)}}{\sigma_{t,i,j+1/2}\Delta y_{j+1/2}}$$

$$+\frac{R_{i,j}\delta T_{yy,i,j}^{(s+1/2)}-R_{i,j-1}\delta T_{yy,i,j-1}^{(s+1/2)}}{\Delta y_j\Delta y_{j-1/2}\sigma_{t,i,j-1/2}} + \frac{R_{i+1/2,j}\delta T_{yx,i+1/2,j}^{(s+1/2)}-R_{i-1/2,j}\delta T_{yx,i-1/2,j}^{(s+1/2)}}{2\sigma_{t,i,j+1/2}\Delta x_i\Delta y_{j+1/2}}$$

$$+\frac{\Delta y_{j-1}}{2\Delta x_i\Delta y_j}\frac{R_{i+1/2,j-1}\delta T_{yx,i+1/2,j-1}^{(s+1/2)}-R_{i-1/2,j-1}\delta T_{yx,i-1/2,j-1}^{(s+1/2)}}{\sigma_{t,i,j-1/2}\Delta y_{j-1/2}}\,, \tag{5.18}$$

$$\sigma_{t,i+1/2,j} = \frac{\sigma_{t,i+1,j}\Delta x_{i+1}+\sigma_{t,i,j}\Delta x_i}{2\Delta x_{i+1/2}}\,, \quad \Delta x_{i+1/2} = \tfrac{1}{2}\left(\Delta x_{i+1}+\Delta x_i\right),$$

$$\sigma_{t,i,j+1/2} = \frac{\sigma_{t,i,j+1}\Delta y_{j+1}+\sigma_{t,i,j}\Delta y_j}{2\Delta y_{j+1/2}}\,, \quad \Delta y_{j+1/2} = \tfrac{1}{2}\left(\Delta y_{j+1}+\Delta y_j\right),$$

$$\delta T_{\alpha\beta,i,j}^{s+1/2} = \sum_m \left(E_{\alpha\beta,i,j}-\Omega_{\alpha,m}\Omega_{\beta,m}\right)\delta\psi_{m,i,j}^{(s+1/2)}w_m\,, \quad \alpha,\beta = x,y\,, \tag{5.19}$$

$$R_{i,j} = \frac{\phi_{i,j}}{\phi_{i,j}^*}\,, \quad R_{i,j+1/2} = \frac{\phi_{i,j+1/2}}{\phi_{i,+1/2}^*}\,, \quad R_{i+1/2,j} = \frac{\phi_{i+1/2,j}}{\phi_{i+1/2,j}^*}\,. \tag{5.20}$$

Here $\phi_{l,p}$ is the solution of the low-order problem, $\phi_{l,p}^*$ is the solution of the high-order problem, $E_{\alpha\beta,i,j}$ is the QD factor calculated by the solution of the transport equation. Note that $\phi_{i,j} \neq \phi_{i,j}^*$ because we use independent discretization of the transport and LOQD equations.

5.4 Fourier Analysis

We perform a Fourier analysis for Periodic Horizontal Interface (PHI) problems [1] in a medium that is spatially periodic in y-direction and formed by repeated layers of two different materials with cross sections $\sigma_{t,1}$ and $\sigma_{t,2}$, widths h_1 and h_2, and equal scattering ratios $c_1 = c_2 = c$. The size of the cell in y-direction (Δy_j) is equal to the width of a horizontal material layer. To generate the numerical solution necessary for the stability analysis of a given infinite-medium problem, we solve an equivalent finite-medium problem with just two material layers, 1×2 spatial grid and periodic boundary conditions. This enables us to calculate the infinite-medium solution ($\phi_{l,p}$, $\phi_{l,p}^*$ and $E_{\alpha\beta,i,j}$) which is necessary for linearization.

We now introduce the following Fourier mode ansatz:

$$\delta\psi_{m,i-1/2,j-1/2+2k}^{(s+1/2)} = \omega^s a_{m,j} e^{\hat{i}(\lambda_x x_{i-1/2} + \lambda_y y_{j-1/2+2k})}, \tag{5.21}$$

$$\delta\phi_{i,j+2k}^{(s)} = \omega^s A_j e^{\hat{i}(\lambda_x x_i + \lambda_y y_{j+2k})}, \tag{5.22}$$

$$x_i = \tfrac{1}{2}(x_{i-1/2} + x_{i+1/2}), \quad y_j = \tfrac{1}{2}(y_{j-1/2} + y_{j+1/2}).$$

$$y_{j+2k} = y_j + k(h_1 + h_2)$$

$$j = 1, 2, \quad k = 0, \pm 1, \pm 2, \dots, \quad \hat{i} = \sqrt{-1},$$

then substitute Eqs. (5.21)-(5.22) into the discretized QD equations linearized about the infinite-medium solution and solve for the eigenvalue ω. The spectral radius is defined by $\rho = \sup_\lambda |\omega(\lambda)|$.

5.5 Numerical Results

The results of the Fourier analysis are utilized to evaluate spectral radii for various combinations of layers with different material properties. The predictions based on infinite-medium problems are compared with the results of numerical tests in finite media with a periodic structure, constant source everywhere and vacuum boundary conditions. A product quadrature set with 16 directions per octant was used in all calculations. Table 5.1 and and Figure 5.1 present theoretical estimates of the spectral radius, ρ_{th}, versus $\sigma_{t,1}$ and $\sigma_{t,2}$ for $c = 0.9999$, $\Delta x = 1$, $\Delta y_1 = \Delta y_2 = 1$. We notice that the theoretical analysis in infinite media predicts that the QD method loses its effectiveness and even diverges for certain combinations of $\sigma_{t,1}$ and $\sigma_{t,2}$.

The results of the Fourier analysis of the QD method for PHI problems are obtained under the following several assumptions:

1. There is no leakage.

2. There are infinite number of spatial cells. This assumption is especially important for the x-direction for which no conditions are imposed on error modes.

3. The exact solution is the same everywhere in the sense that it is exactly periodic in any location.

However, when one considers finite-medium problems with periodic configurations and non-periodic boundary conditions, the convergence rate will be influenced by the leakage effects near boundaries. These effects destroy perfect periodicity of the solution. As a result, the solution used to perform theoretical analysis does not exactly match the finite-medium solution. The theoretical results can be rather sensitive to the solution around which the nonlinear equations are linearized. The QD method is a nonlinear one, and a special effort must be made to measure the spectral radius in the vicinity of the solution while performing calculations with finite precision arithmetic. The finite number of cells, for example, along horizontal layers (i.e. in x-direction) eliminates part of errors modes that were accounted for in the infinite-medium analysis. All these effects cause the discrepancy between theoretical

and numerical results. The value of the Fourier analysis is that it can show what happens if one considers a problem that meets close enough the above assumptions and what one should expect while approaching this limit.

We now present numerical results for a PHI problem in the square region $\{0 \leq x, y \leq 40\}$ with c=0.9999, source $Q = 1$ in the whole domain, and vacuum boundary conditions. Table 5.2 and Figure 5.2 show the spectral radii evaluated in L_2-norm. The theoretically and numerically estimated spectral radii as functions of $\sigma_{t,2}$ for different $\sigma_{t,1}$ are also plotted in Figure 5.5. The graphs provide an illustration that help one to correlate the infinite-medium theory with numerical results. For the given set of parameters of transport problems, theoretical results $\rho_{th}(\sigma_{t,1}, \sigma_{t,2})$ give very good qualitative prediction reproducing the shape of numerically estimated spectral radius $\rho_{num}(\sigma_{t,1}, \sigma_{t,2})$ for $\sigma_{t,2} \geq 10^{-1}$. In many cases, the values of ρ_{th} are close to ρ_{num} and provide good estimation of convergence rates in the considered finite-medium problems. The presented numerical results show that the convergence of the QD method slows down if σ_t of layers are significantly different from each other. For example, it happens when $\sigma_{t,1} = 10^4$ and $\sigma_{t,2} = 10^{-1}$. Figure 5.6 presents theoretically and numerically evaluated ρ for $\sigma_{t,1} = 10^{-1}$ and various scattering ratios. We notice that the QD method exhibits similar effect in case of smaller scattering ratios as well. There are cases in which ρ_{num} is close to the values of the scattering ratio. Thus, we do observe the loss of effectiveness of the QD method in this set of problems with spatial domain $\{0 \leq x, y \leq 40\}$. However, we did not encounter the phenomena of divergence in these finite-medium problems.

To demonstrate finite-medium problems in which the performance of the QD method degrades more dramatically as it predicted by infinite-medium analysis, we consider PHI test problems with significantly larger horizontal dimensions and number of cells in x-direction and fewer number of horizontal layers. We use the same sizes of cells and widths of layers as in the above PHI problems (i.e. $\Delta x = 1$, $\Delta y_1 = \Delta y_2 = 1$). Tables 5.3 and 5.4 as well as Figures 5.3 and 5.4 present the numerically estimated spectral radii in problems with rectangular domains $\{0 \leq x \leq 400, 0 \leq y \leq 12\}$ and $\{0 \leq x \leq 2000, 0 \leq y \leq 4\}$, respectively. Figure 5.5 shows also graphs of ρ_{num} for these problems.

In the case with 400×12 domain, the numerical results are in much better consistency with the theoretical prediction then the results of problems with 40×40 domain. We now observe the divergence of the QD method, $\rho_{num} > 1$ when $\sigma_{t,1} = 10^4$ and $10^{-2} \leq \sigma_{t,2} \leq 10^{-1}$. The problem with 2000×4 domain has just few horizontal layers and as a result ρ_{num} is far less than ρ_{th} when the optical thickness of the domain in y-direction is small, namely, for $1 \leq \sigma_{t,1} \leq 10^2$ and $10^{-4} \leq \sigma_{t,2} \leq 10^{-1}$. In most of other cases (for example, $\sigma_{t,1} = 10^3$), it is in a good agreement with theoretical estimations. We also notice that the QD method loses it effectiveness and even diverges, for instance, when $10^3 \leq \sigma_{t,1} \leq 10^4$ and $10^{-3} \leq \sigma_{t,2} \leq 10^{-1}$.

The essential feature of the above transport problems is the existence of a long horizontal layer of the same material. The infinite-medium PHI problem is basically a 1D transport problem in which the error modes in x-direction are not synchronized. To eliminate this feature and analyze the behavior of the QD method on a more typical 2D problem, we consider the transport problem with a checker-board configuration of two different materials with $c = 0.9999$ in the square region $\{0 \leq x, y \leq 40\}$. Each material zone is 1×1. There is one cell per zone. The unit source is defined in the whole domain. Boundary conditions are vacuum. Table 5.5 contains numerically evaluated spectral radii. These results are plotted

in Figure 5.7. In this test, the QD method converges fast in strongly heterogeneous problems for any combination of materials. The spectral radius reaches its maximum value of 0.239 in the case $\sigma_{t,1} = 10^{-2}$ and $\sigma_{t,2} = 10$.

To present the performance of the QD method in problems with heterogeneous media and non-periodic configuration, we show the results of a two-region test problem [2] in the square region $\{0 \leq x, y \leq 40\}$ having $\sigma_{t,1}$ and $Q = 1$ for $\{10 \leq x, y \leq 30\}$ and $\sigma_{t,2}$ and $Q = 0$ outside of this inner region. The scattering ratio is the same in both regions and $c = 0.9999$. The spatial grid is uniform with 40×40 cells. The numerically estimated spectral radii are listed in Table 5.6 and plotted on Figure 5.8. In this test, the QD method exhibits slowing down of convergence for some set of cross sections. The maximum of ρ occurs for $\sigma_{t,1} = 10^{-2}$ and $\sigma_{t,2} = 10$ and equals 0.46.

5.6 Conclusions

We have developed stability analysis of the nonlinear quasidiffusion method for infinite-medium problems with spatially periodic configurations of materials in 2D geometry. This theoretical analysis enabled us to study the convergence properties of the QD method in the vicinity of the solution for problems with periodic horizontal interface and learn about the influence of heterogeneity of the medium on the method convergence. It showed the loss of effectiveness and divergence of the QD method with the considered independent discretization in case of PHI problems consisted of layers with significantly different cross sections. The numerical results confirmed these theoretical predictions. Note that the effectiveness of the DSA method degrades but it still converges. The TSA method diverges for a wide range of parameters of heterogeneous problems. The divergence of the QD method in PHI problems occurs for rather small range of problem parameters. Some additional analysis of the QD method gives us a reason to expect that if the QD equations are discretized consistently, then its behavior will be similar to the one of the DSA method, and it will not diverge.

We now work on further analysis of the QD method for 2D heterogeneous problems and interpretation of the obtained theoretical results. We consider approaches for improving stability properties of the QD method in problems with strong heterogeneities and feasibility of applying Krylov subspace methods for this purpose.

Table 5.1: Theoretically Estimated Spectral Radii of the QD Method for PHI Problem with $c = 0.9999$.

$\sigma_{t,1}$	$\sigma_{t,2}$								
	10^{-4}	10^{-3}	10^{-2}	10^{-1}	1	10^{1}	10^{2}	10^{3}	10^{4}
1	9.97e-1*	9.84e-1	9.03e-1	5.10e-1	1.94e-1	1.99e-1	2.88e-1	6.36e-1	6.80e-1
10	9.88e-1	9.69e-1	8.95e-1	6.40e-1	1.99e-1	1.63e-1	2.16e-1	4.82e-1	5.44e-1
10^{2}	7.66e-1	7.41e-1	6.77e-1	5.22e-1	2.88e-1	2.16e-1	9.70e-2	1.06e-1	1.33e-1
10^{3}	4.93e-1	5.66e-1	1.00e+0	9.12e-1	6.36e-1	4.82e-1	1.06e-1	2.54e-3	1.85e-3
10^{4}	9.89e-1	1.84E+0	1.69e+0	1.02e+0	6.80e-1	5.44e-1	1.33e-1	1.85e-3	2.59e-5

*Read as 9.97×10^{-1}

Table 5.2: Numerically Estimated Spectral Radii of the QD Method for PHI Problem with $c = 0.9999$ and $\{0 \leq x, y \leq 40\}$.

$\sigma_{t,1}$	$\sigma_{t,2}$								
	10^{-4}	10^{-3}	10^{-2}	10^{-1}	1	10^{1}	10^{2}	10^{3}	10^{4}
1	7.11e-1	7.03e-1	6.63e-1	4.16e-1	8.64e-2	8.46e-2	1.86e-1	5.58e-1	6.91e-1
10	7.43e-1	7.40e-1	7.16e-1	5.67e-1	8.46e-2	1.23e-1	1.50e-1	4.36e-1	4.96e-1
10^{2}	4.06e-1	4.13e-1	4.21e-1	3.30e-1	1.86e-1	1.50e-1	6.56e-2	8.67e-2	1.13e-1
10^{3}	5.96e-2	6.33e-2	1.55e-1	6.51e-1	5.58e-1	4.36e-1	8.67e-2	1.29e-3	1.19e-3
10^{4}	8.46e-3	6.67e-2	5.17e-1	8.79e-1	6.91e-1	4.96e-1	1.13e-1	1.19e-3	4.79e-6

Table 5.3: Numerically Estimated Spectral Radii of the QD Method for PHI Problem with $c = 0.9999$ and $\{0 \leq x \leq 400, 0 \leq y \leq 12\}$.

$\sigma_{t,1}$	$\sigma_{t,2}$								
	10^{-4}	10^{-3}	10^{-2}	10^{-1}	1	10^{1}	10^{2}	10^{3}	10^{4}
1	9.24e-1	8.73e-1	7.23e-1	3.13e-1	7.20e-2	1.08e-1	2.11e-1	5.92e-1	6.49e-1
10	9.69e-1	9.48e-1	8.48e-1	5.68e-1	1.08e-1	1.28e-1	1.62e-1	4.38e-1	5.02e-1
10^{2}	7.16e-1	7.09e-1	6.34e-1	4.58e-1	2.11e-1	1.62e-1	6.92e-2	8.91e-2	1.15e-1
10^{3}	2.87e-1	3.31e-1	9.59e-1	9.58e-1	5.92e-1	4.38e-1	8.91e-2	1.71e-3	1.19e-3
10^{4}	1.24e-1	7.88e-1	1.05e+0	1.04e+0	6.49e-1	5.02e-1	1.15e-1	1.19e-3	4.79e-6

Table 5.4: Numerically Estimated Spectral Radii of the QD Method for PHI Problem with $c = 0.9999$ and $\{0 \leq x \leq 2000, 0 \leq y \leq 4\}$.

$\sigma_{t,1}$	$\sigma_{t,2}$								
	10^{-4}	10^{-3}	10^{-2}	10^{-1}	1	10^{1}	10^{2}	10^{3}	10^{4}
1	5.27e-1	4.64e-1	3.54e-1	2.27e-1	1.15e-1	1.53e-1	2.48e-1	5.94e-1	6.54e-1
10	6.20e-1	5.73e-1	4.68e-1	3.25e-1	1.53e-1	1.01e-1	1.78e-1	4.39e-1	5.11e-1
10^{2}	4.76e-1	4.59e-1	4.08e-1	3.43e-1	2.48e-1	1.78e-1	5.54e-2	8.93e-2	1.21e-1
10^{3}	3.97e-1	4.25e-1	1.00e+0	9.60e-1	5.94e-1	4.39e-1	8.93e-2	1.66e-3	1.51e-3
10^{4}	4.21e-1	9.92e-1	1.12e+0	1.10e+0	6.54e-1	5.11e-1	1.21e-1	1.51e-3	4.79e-6
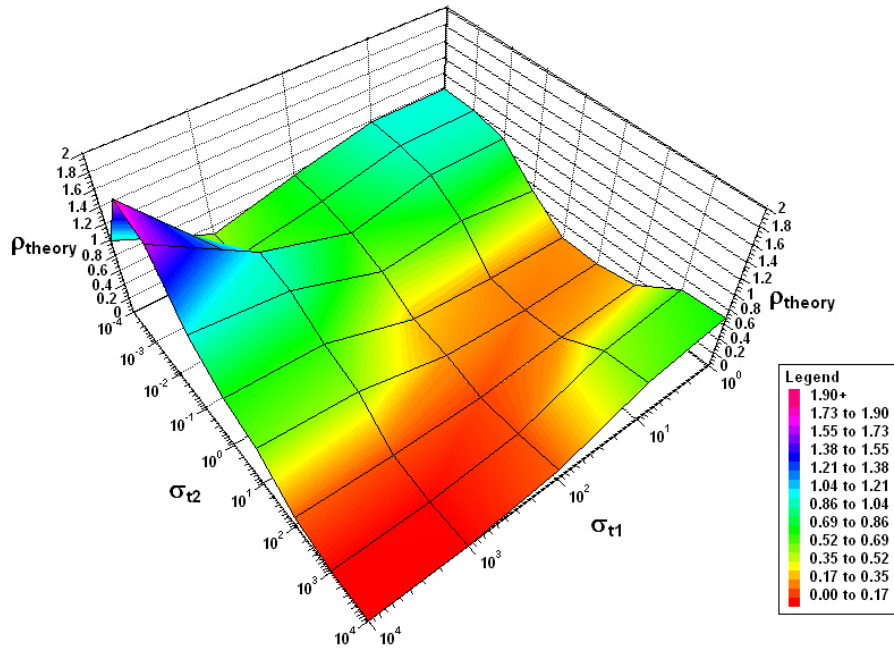
Figure 5.1: Theoretically Estimated Spectral Radii of the QD Method for PHI Problem with $c = 0.9999$
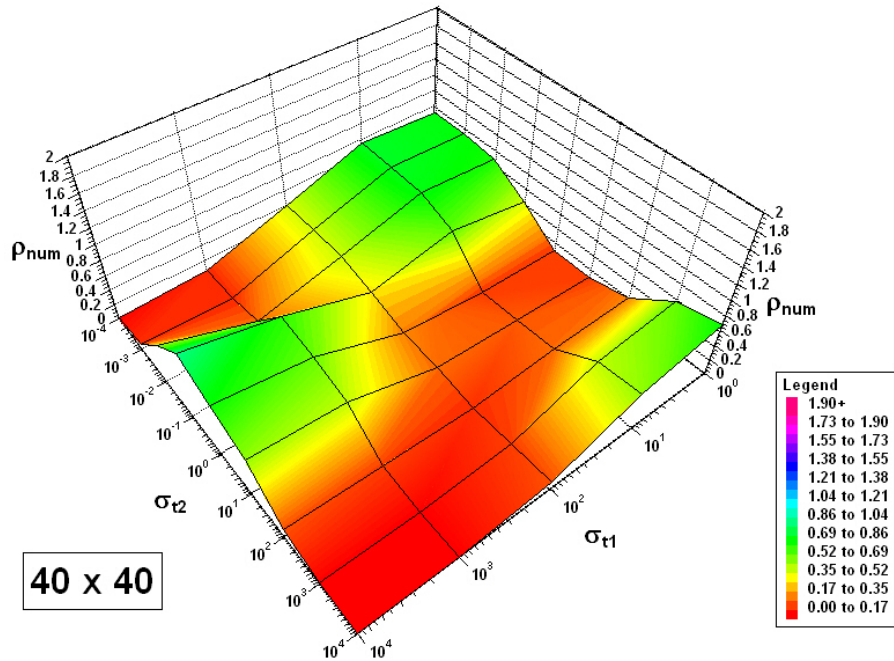
Figure 5.2: Numerically Estimated Spectral Radii of the QD Method for PHI Problem with $c = 0.9999$ and $\{0 \leq x, y \leq 40\}$.
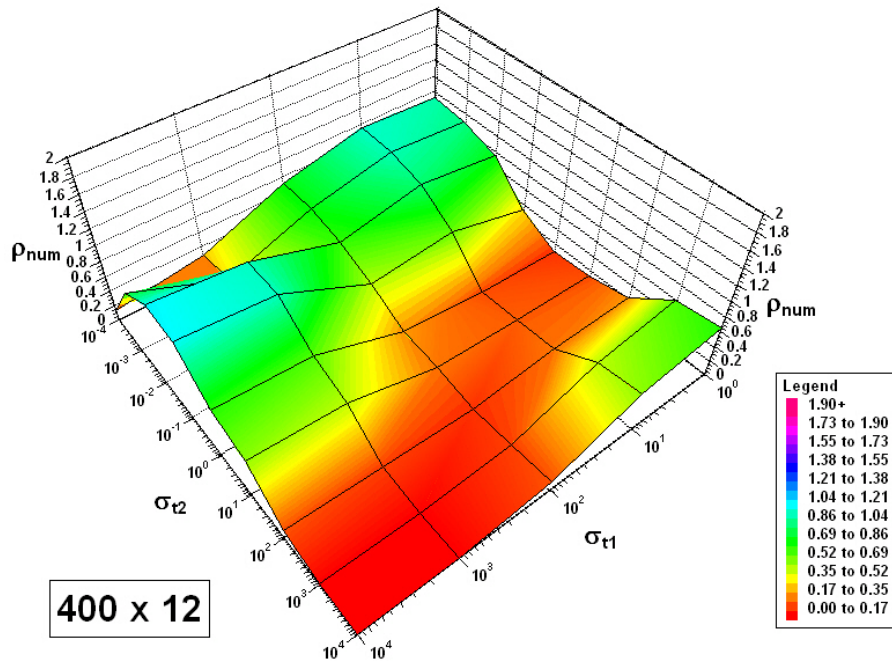
Figure 5.3: Numerically Estimated Spectral Radii of the QD Method for PHI Problem with $c = 0.9999$ and $\{0 \leq x \leq 400, 0 \leq y \leq 12\}$.
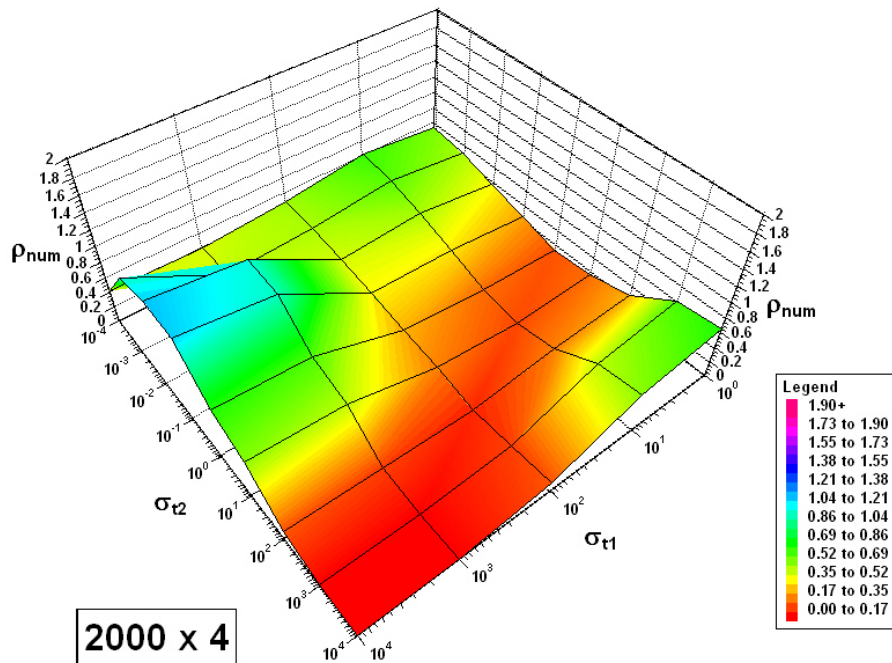
Figure 5.4: Numerically Estimated Spectral Radii of the QD Method for PHI Problem with $c = 0.9999$ and $\{0 \leq x \leq 2000, 0 \leq y \leq 4\}$.
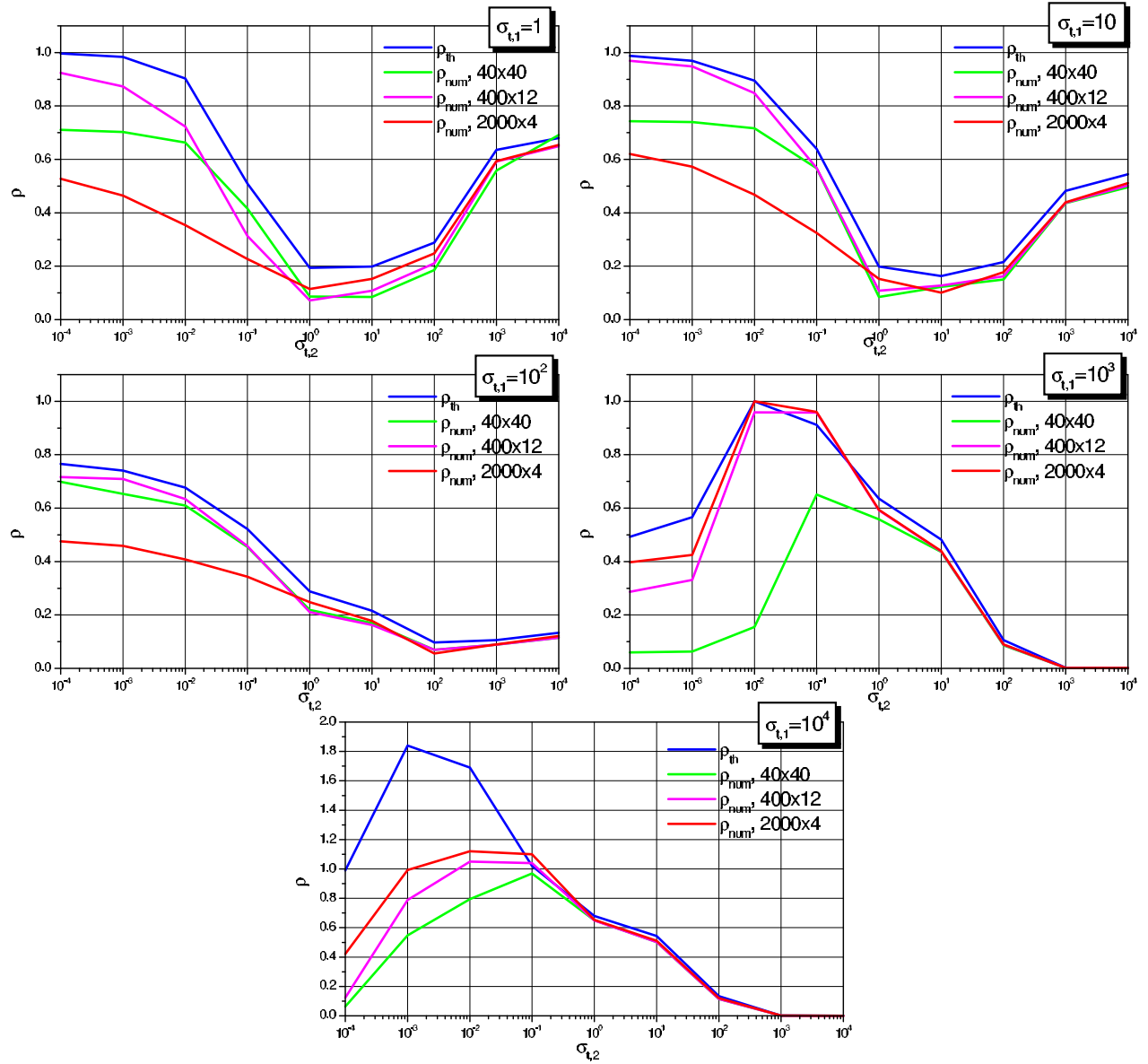
Figure 5.5: Theoretically (ρ_{th}) and numerically (ρ_{num}) estimated spectral radii of the QD method, $c = 0.9999$.
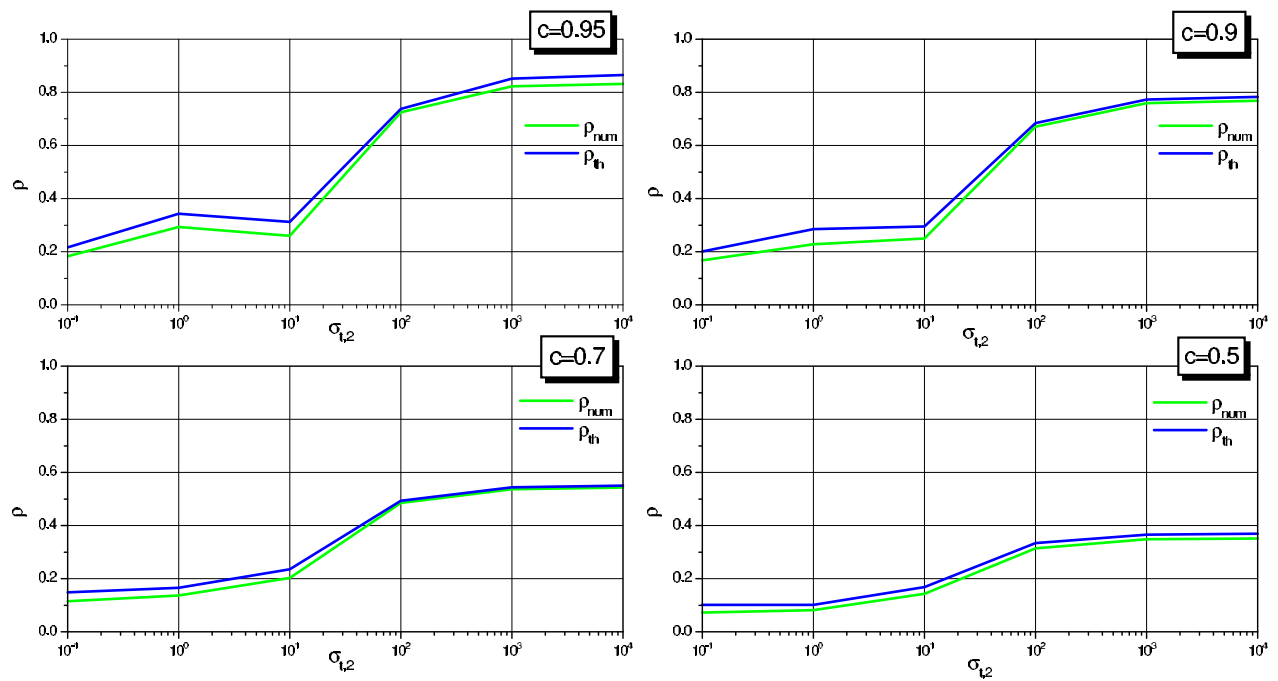
Figure 5.6: Theoretically (ρ_{th}) and numerically (ρ_{num}) estimated spectral radii of the QD method, $\sigma_{t,1} = 10^{-1}$, $\{0 \leq x, y \leq 40\}$.

Table 5.5: Numerically Estimated Spectral Radii of the QD Method for the Checker-Board Problem, $c = 0.9999$, and $\{0 \leq x, y \leq 40\}$.

$\sigma_{t,1}$	$\sigma_{t,2}$						
	10^{-2}	10^{-1}	1	10	10^2	10^3	10^4
10^{-2}	1.02e-1	6.22e-2	1.45e-1	2.39e-1	1.73e-1	3.06e-2	6.00e-3
10^{-1}	6.22e-2	2.01e-1	1.53e-1	1.80e-1	1.62e-1	3.67e-2	1.32e-2
1	1.45e-1	1.53e-1	1.20e-1	1.19e-1	1.24e-1	1.74e-2	6.97e-3
10	2.39e-1	1.80e-1	1.19e-1	1.28e-1	1.05e-1	1.20e-1	3.44e-2
10^2	1.73e-1	1.62e-1	1.24e-1	1.05e-1	6.98e-2	2.19e-2	2.92e-3
10^3	3.06e-2	3.67e-2	1.74e-2	1.20e-1	2.19e-2	1.29e-3	2.07e-4
10^4	6.00e-3	1.32e-2	6.97e-3	3.44e-2	2.92e-3	2.07e-4	9.35e-10

Table 5.6: Numerically Estimated Spectral Radii of the QD Method for the Two-Region Problem with $c = 0.9999$ and $\{0 \leq x, y \leq 40\}$.

$\sigma_{t,1}$	$\sigma_{t,2}$						
	10^{-2}	10^{-1}	1	10	10^2	10^3	10^4
10^{-2}	5.60e-2	1.20e-1	3.98e-1	4.60e-1	3.82e-1	2.70e-1	2.81e-1
10^{-1}	2.53e-1	2.00e-1	2.99e-1	3.41e-1	2.85e-1	3.06e-1	3.22e-1
1	3.91e-1	2.96e-1	8.63e-2	1.58e-1	1.96e-1	2.64e-1	2.68e-1
10	2.50e-1	2.44e-1	1.42e-1	1.22e-1	1.47e-1	2.00e-1	2.14e-1
10^2	1.71e-1	1.51e-1	1.54e-1	1.45e-1	6.55e-2	7.72e-2	8.52e-2
10^3	4.51e-2	2.28e-1	2.08e-1	1.69e-1	8.03e-2	1.29e-3	1.16e-3
10^4	5.16e-2	2.56e-1	2.16e-1	1.73e-1	8.37e-2	2.90e-5	4.79e-6
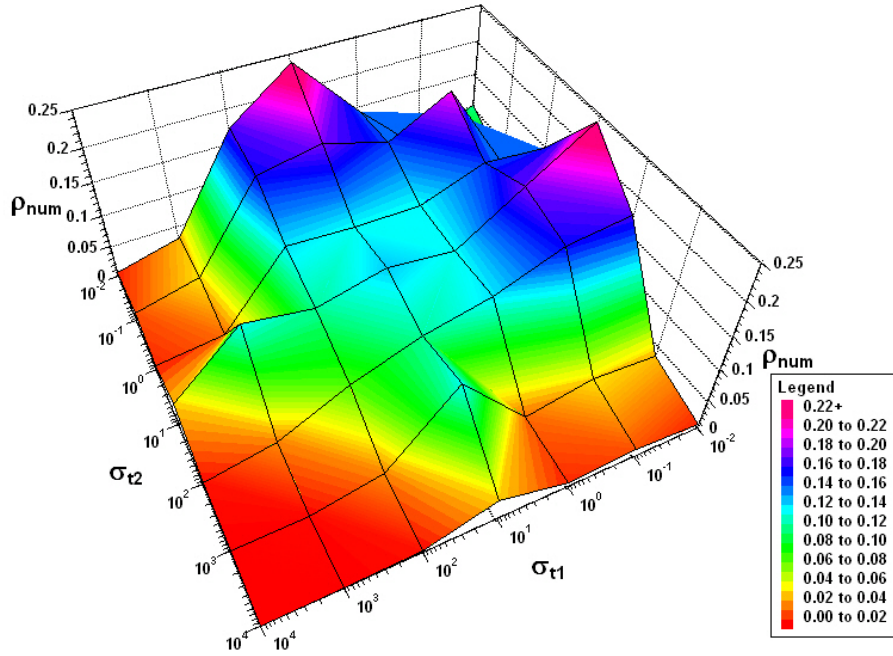
Figure 5.7: Numerically estimated spectral radii of the QD method for the checker-board problem, $c = 0.9999$.
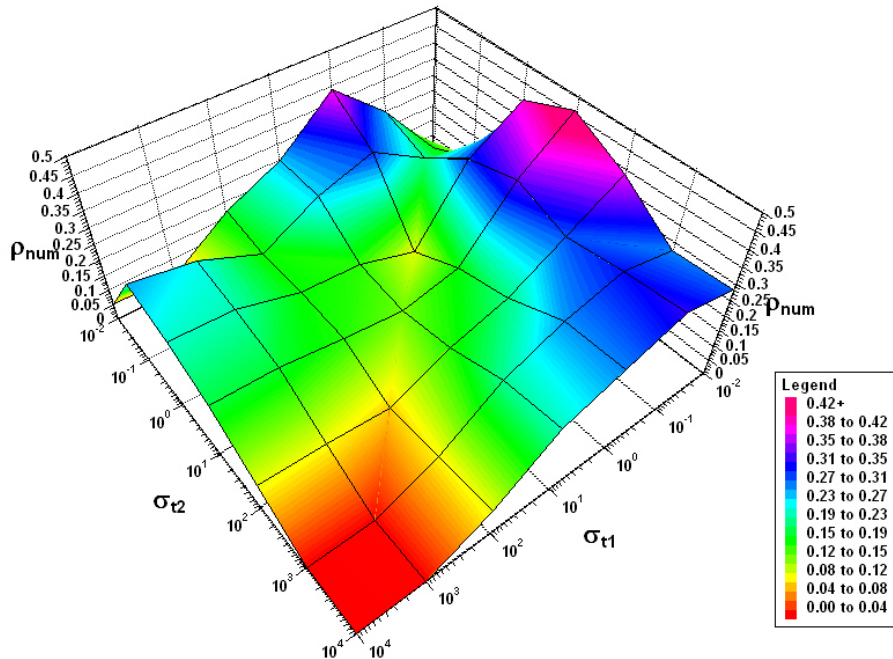
Figure 5.8: Numerically estimated spectral radii of the QD method for the two-region problem with $c = 0.9999$.

Chapter 6

The Quasidiffusion Method for Two-Dimensional Transport Problems on Unstructured Meshes

6.1   Introduction

In this paper we present the development of a method for solving transport problems on spatial grids used by adaptive mesh refinement (AMR) algorithms [43, 44]. Both orthogonal and non-orthogonal AMR grids with quadrilateral cells are considered. This type of meshes are utilized, for example, in radiative hydrodynamics problems in which radiative transfer is coupled to hydrodynamics processes that define the structure of spatial grids. An AMR algorithm determines the regions where the grid should be subdivided to satisfy certain accuracy requirements. As a result, a cell can share a face with two smaller cells.

We use the quasidiffusion (QD) method [4] to solve the transport equation. The system of equations of the QD method consists of two parts: (i) low-order QD (LOQD) equations for the scalar flux and current and (ii) the high-order (transport) equation for the angular flux. We developed a discretization of the LOQD equations for AMR grids based on the local approximation of these equations in each cell and interface continuity conditions on each cell face. The transport equation is discretized by means of the method of characteristics.

The results of the research presented in this chapter were published in

- W. A. Wieselquist (*Ph.D. student*) and D.Y. Anistratov, "The Quasidiffusion Method for 2D Transport Problems on AMR Grids," *Trans. Am. Nucl. Soc.,* **96** (2007) (to appear).

6.2   Formulation of the QD Method

Let us consider two-dimensional steady-state one-group transport problems with isotropic scattering and source in 2D Cartesian geometry:

$$\vec{\Omega} \cdot \vec{\nabla}\psi(\vec{r},\vec{\Omega}) + \sigma_t(\vec{r})\psi(\vec{r},\vec{\Omega}) = \frac{1}{4\pi}\sigma_s(\vec{r})\int_{4\pi}\psi(\vec{r},\vec{\Omega})d\vec{\Omega} + \frac{1}{4\pi}q(\vec{r}), \quad \vec{r} \in G, \qquad (6.1)$$

$$\psi(\vec{r}, \vec{\Omega}) = \psi^{in}(\vec{r}, \vec{\Omega}), \quad \vec{r} \in \partial G, \quad \vec{\Omega} \cdot \vec{n} < 0, \tag{6.2}$$

where G is the domain of the problem, ∂G is the boundary surface of G, $\vec{n}$ is the outward normal to ∂G. To derive the low-order QD (LOQD) equations, the transport equation (6.1) is integrated over all directions $\vec{\Omega}$ to get the balance equation. Then, it is integrated over all directions $\vec{\Omega}$ with weight $\vec{\Omega}$ to obtain the first moment equations. As a result, the complete system of the QD equations has the following form (k is the iteration index) [4, 45, 46]:

$$\vec{\Omega} \cdot \vec{\nabla}\psi^{(k+1/2)} + \sigma_t \psi^{(k+1/2)} = \frac{1}{4\pi}\sigma_s \phi^{(k)} + \frac{1}{4\pi}q, \tag{6.3}$$

$$\psi^{(k+1/2)}\big|_{\vec{r} \in \partial G} = \psi^{in}\big|_{\vec{r} \in \partial G} \text{ for } \vec{\Omega} \cdot \vec{n} < 0, \tag{6.4}$$

$$E_{\alpha\beta}^{(k+1/2)} = \int_{4\pi} \Omega_\alpha \Omega_\beta \psi^{(k+1/2)} d\vec{\Omega} \Big/ \int_{4\pi} \psi^{(k+1/2)} d\vec{\Omega}, \quad \alpha, \beta = x, y, \tag{6.5}$$

$$C^{(k+1/2)} = \int_{\vec{\Omega} \cdot \vec{n} \geq 0} (\vec{\Omega} \cdot \vec{n})\psi^{(k+1/2)} d\vec{\Omega} \Big/ \int_{\vec{\Omega} \cdot \vec{n} \geq 0} \psi^{(k+1/2)} d\vec{\Omega}, \quad \vec{r} \in \partial G, \tag{6.6}$$

$$\vec{\nabla} \cdot \vec{J}^{(k+1)} + \sigma_a \psi^{(k+1)} = q, \tag{6.7}$$

$$\frac{\partial}{\partial x}(E_{xx}^{(k+1/2)}\phi^{(k+1)}) + \frac{\partial}{\partial y}(E_{xy}^{(k+1/2)}\phi^{(k+1)}) + \sigma_t J_x^{(k+1)} = 0, \tag{6.8}$$

$$\frac{\partial}{\partial x}(E_{xy}^{(k+1/2)}\phi^{(k+1)}) + \frac{\partial}{\partial y}(E_{yy}^{(k+1/2)}\phi^{(k+1)}) + \sigma_t J_y^{(k+1)} = 0, \tag{6.9}$$

$$\vec{n} \cdot \vec{J}^{(k+1)}\big|_{\vec{r} \in \partial G} = \left[C^{(k+1/2)}(\phi^{(k+1)} - \phi^{in}) + J_n^{in}\right]\big|_{\vec{r} \in \partial G}, \tag{6.10}$$

$$\phi^{in} = \int_{\vec{\Omega} \cdot \vec{n} < 0} \psi^{in} d\vec{\Omega}, \quad J_n^{in} = \int_{\vec{\Omega} \cdot \vec{n} < 0} (\vec{\Omega} \cdot \vec{n})\psi^{in} d\vec{\Omega}, \quad \vec{r} \in \partial G, \tag{6.11}$$

where $\phi = \int_{4\pi} \psi d\vec{\Omega}$ is the scalar flux, $\vec{J}(\vec{r}) = \int_{4\pi} \vec{\Omega}\psi d\vec{\Omega}$ is the current. The iteration procedure for the QD method consists of the following three steps:

1. *High-order calculations:* Using the scalar flux $\phi^{(k)}$ from the previous iteration, the transport equation Eq. (6.3) is solved to determine the angular flux $\psi^{(k+1/2)}$.

2. *Calculations of the QD factors:* The angular flux $\psi^{(k+1/2)}$ is used to compute the QD factors $E_{\alpha\beta}^{(k+1/2)}$ and $C^{(k+1/2)}$ (Eqs. (6.5) and (6.6)).

3. *Low-order calculations:* Using the factors $E_{\alpha\beta}^{(k+1/2)}$ and $C^{(k+1/2)}$, the low-order QD problem (Eqs. (6.7)-(6.10)) is solved to obtain the scalar flux $\phi^{(k+1)}$ and current $\vec{J}^{(k+1)}$.

The LOQD equations (6.7)-(6.9) can be presented by means of tensor divergence in the following form:

$$\text{div } \vec{J}(\vec{r}) + \sigma_a \phi(\vec{r}) = q, \tag{6.12}$$

$$\text{DIV } (\bar{\bar{E}}\phi(\vec{r})) + \sigma_t \vec{J}(\vec{r}) = 0, \quad \vec{r} \in G. \tag{6.13}$$

In Eq. (6.13), the Quasidiffusion (Eddington) tensor is recognized as a symmetric, rank-2 tensor give by

$$\bar{\bar{E}} = \begin{pmatrix} E_{xx} & E_{xy} \\ E_{xy} & E_{yy} \end{pmatrix}.$$

In 3D Cartesian geometry, the QD tensor has the form

$$\bar{\bar{E}} = \begin{pmatrix} E_{xx} & E_{xy} & E_{xz} \\ E_{xy} & E_{yy} & E_{yz} \\ E_{xz} & E_{yz} & E_{zz} \end{pmatrix}.$$

The components of these tensors are QD (Eddington) factors (Eq. (6.5)) that can be interpreted as average values of $\Omega_\alpha \Omega_\beta$

$$E_{\alpha\beta} = \langle \Omega_\alpha \, \Omega_\beta \rangle$$

(see Fig. 6.2) where the averaging functions is the angular flux ψ.

Under diffusive conditions, $E_{\alpha\beta} = \frac{1}{3}\delta_{\alpha\beta}$ and as a result $\bar{\bar{E}}$ is diagonal so Eq. (6.13) becomes the familiar Fick's Law

$$\vec{J}(\vec{r}) = -\frac{1}{3\sigma_t}\vec{\nabla}\phi(\vec{r}).$$

6.3 Discretization of the LOQD Equations on Grids Composed of Arbitrary Quadrilaterals

6.3.1 Finite-Volume Discretization of the LOQD Equations

The LOQD equations for arbitrary quadrilaterals in 2D are discretized by a finite volume (FV) scheme of the second-order accuracy [39]. The spatial cell is referenced with one index i. Hereafter, we refer to this discretization as *GGK method*. The general cell on which this discretization is performed is shown in Figure 6.2. Within each cell, there are 4 unknown face-average scalar fluxes, $\{\phi_{iB}, \phi_{iR}, \phi_{iT}, \phi_{iL}\}$, 4 unknown face-average normal currents $\{J_{iB}, J_{iR}, J_{iT}, J_{iL}\}$, and one unknown cell-average scalar flux, ϕ_i.

To discretize the balance equation (6.7), it is integrated over the whole cell i and one obtains

$$J_{iB}h_{iB} + J_{iR}h_{iR} + J_{iT}h_{iT} + J_{iL}h_{iL} + \sigma_{a,i}\phi_i A_i = Q_i A_i, \tag{6.14}$$

where A_i is the area of cell i, $h_{i\omega}$ is the cell-edge length. To get the next four equations, the first moment equations (6.8) and (6.9) are added together and multiplied by $x-$ and $y-$direction components of the unit vector $\vec{n}$. The resulting equation is integrated over the area of half-cell $A_{i\omega}$

$$n_{x,i\omega} \iint_{A_{i\omega}} \frac{\partial}{\partial x}(E_{xx}\phi) \, dx \, dy + n_{y,i\omega} \iint_{A_{i\omega}} \frac{\partial}{\partial y}(E_{yy}\phi) \, dx \, dy$$

$$+ n_{x,i\omega} \iint_{A_{i\omega}} \frac{\partial}{\partial x}(E_{xy}\phi) \, dx \, dy + n_{y,i\omega} \iint_{A_{i\omega}} \frac{\partial}{\partial y}(E_{xy}\phi) \, dx \, dy + \sigma_{t,i} J_{i\omega} A_{i\omega} = 0, \tag{6.15}$$

where $\omega = \{B, R, T, L\}$, $\vec{n}_{i\omega}$ is the outward normal of face ω of cell i. Figure 6.3 shows the left half-cell and the direction of surface integration. Note that in each half-cell, the
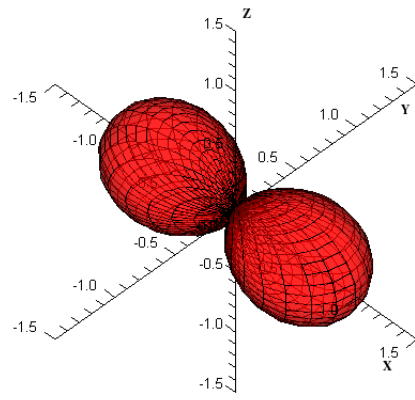
(a) $\Omega_{\mathbf{x}}^2$
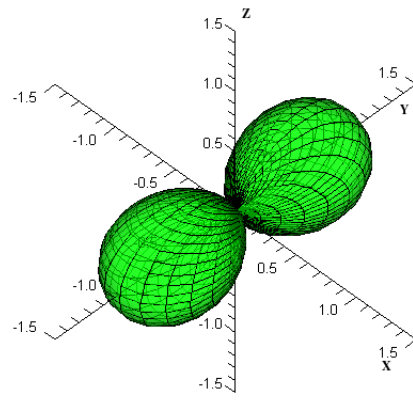
(b) $\Omega_{\mathbf{y}}^2$
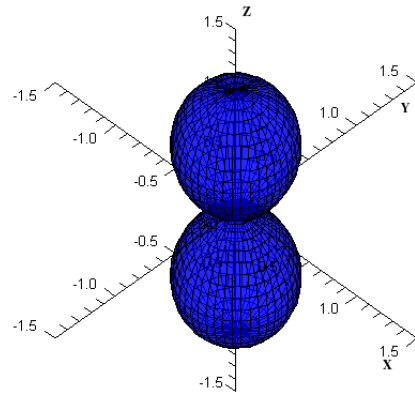
(c) $\Omega_{\mathbf{z}}^2$
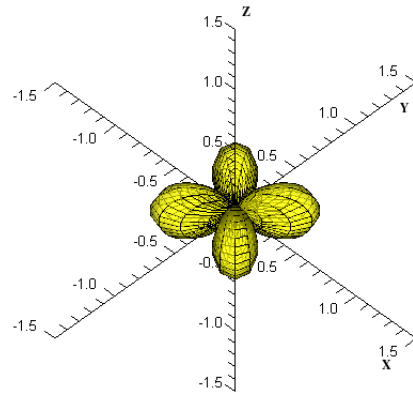
(d) $\Omega_{\mathbf{x}}\Omega_{\mathbf{y}}$
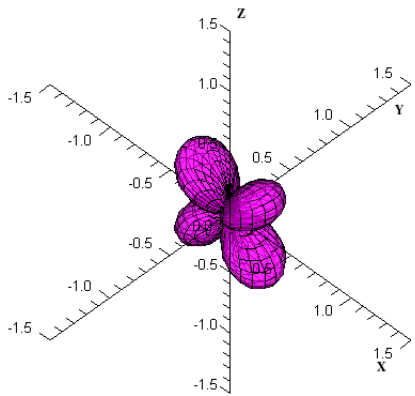
(e) $\Omega_{\mathbf{x}}\Omega_{\mathbf{z}}$
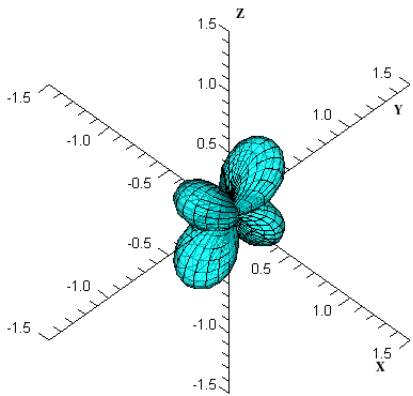
(f) $\Omega_{\mathbf{y}}\Omega_{\mathbf{z}}$

Figure 6.1: QD (Eddington) Factor Weight Functions, $\Omega_\alpha \Omega_\beta$
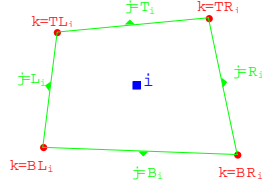
Figure 6.2: The skewed quadrilateral grid cell.
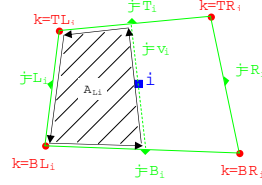
Figure 6.3: The left (L) half-cell integration.

face-average normal current appears for the full face, $J_{i\omega} = \vec{J} \cdot \vec{n}_{i\omega}$. When considering top and bottom subcells, cell i is split into half-cells with a line connecting midpoints of the left and right faces. When considering left and right subcells, cell i is split into half-cells with a line that connects midpoints of the top and bottom faces. In case of the left-half subcell, i.e. $A_{i\omega} = A_{iL}$ (Fig. 6.3) , we get

$$
\begin{aligned}
& \left[(n_{x,iL}E_{xx,iB} + n_{y,iL}E_{xy,iB})\frac{\ell_{y,iB}}{2} - (n_{x,iL}E_{xy,iB} + n_{y,iL}E_{yy,iB})\frac{\ell_{x,iB}}{2} \right] && \phi_{iB} \\
& - \left[(n_{x,iL}E_{xx,i} + n_{y,iL}E_{xy,i})\ell_{y,iv} - (n_{x,iL}E_{xy,i} + n_{y,iL}E_{yy,i})\ell_{x,iv} \right] && \phi_i \\
& + \left[(n_{x,iL}E_{xx,iT} + n_{y,iL}E_{xy,iT})\frac{\ell_{y,iT}}{2} - (n_{x,iL}E_{xy,iT} + n_{y,iL}E_{yy,iT})\frac{\ell_{x,iT}}{2} \right] && \phi_{iT} \\
& + \left[(n_{x,iL}E_{xx,iL} + n_{y,iL}E_{xy,iL})\ell_{y,iL} - (n_{x,iL}E_{xy,iL} + n_{y,iL}E_{yy,iL})\ell_{x,iL} \right] && \phi_{iL} \\
& && + \sigma_{t,i}A_{iL} \quad J_{iL} \quad = 0 \quad (6.16)
\end{aligned}
$$

$$
\ell_{y,iB} = y_{iBR} - y_{iLB}, \quad \ell_{y,iT} = y_{iTL} - y_{iTR}, \quad \ell_{y,iv} = y_{iT} - y_{iB}, \quad \ell_{y,iL} = y_{iLB} - y_{iTL} \quad (6.17)
$$

6.3.2 General Form of Discretization Methods for the LOQD Equations

To approximate the LOQD equations, we consider three different methods that utilize a *local* spatial discretization approach. In the local approach, the governing PDEs are approximated in some manner over a cell. Then *interface conditions* are imposed at intersections of faces of two or more cells and *boundary conditions* are imposed on faces which are on the domain boundary.

The unknowns in each discretization are identical: cell-average and face-average scalar fluxes, ϕ_i and $\phi_{i\omega}$, and face-average normal currents, $J_{i\omega} = \vec{J}_{i\omega} \cdot \vec{n}_{i\omega}$, where $\vec{n}_{i\omega} = \frac{\vec{A}_{i\omega}}{|\vec{A}_{i\omega}|}$ and $\vec{A}_{i\omega}$ is the area vector of face ω in cell i. The index pair $i\omega$ references a face locally to cell i, while a single index j may be used to reference a face globally. These discretization methods are can be expressed as a family:

$$\frac{1}{V_i} \sum_{\omega} J_{i\omega} |\vec{A}_{i\omega}| + \sigma_{a,i} \phi_i = q_i, \tag{6.18}$$

$$\frac{1}{V_{i\omega}} \left(\sum_{\omega'} \bar{\bar{E}}_{i\omega'} \phi_{i\omega'} \vec{A}_{i\omega'} \alpha_{i\omega'} \right) \cdot \vec{n}_{i\omega} + \sigma_{t,i} \beta_{i\omega} J_{i\omega} = 0, \quad \text{for each subcell } \omega, \tag{6.19}$$

for each cell i in the interior G, with boundary conditions

$$J_j = c_j \left(\phi_j - \phi_j^{in} \right) + J_j^{in}, \quad \text{for each boundary face } j, \tag{6.20}$$

on the boundary ∂G. In Eq. (6.18), the summation over ω indicates to sum over all faces of cell i. In Eq. (6.19), the summation over ω' indicates to sum over all a set of faces that define the subcell ω. The faces ω' may be actual faces of the cell or they may be imaginary faces that cut through the interior of the cell. Note that in order to have the same numbers of equations as unknowns, there must be one subcell (Eq. (6.19)) for each face, so the reference to the subcell ω corresponds to the subcell which has the face-average normal current $J_{i\omega}$. The parameters $\alpha_{i\omega'}$ and $\beta_{i\omega}$ define the family of discretizations.

6.3.3   GGK Method for Discretization of the LOQD Equations

Using our general form, the GGK method [39] on arbitrary quadrilaterals is 5 equations given by

$$\frac{1}{V_i} \left(J_{iB} + J_{iR} + J_{iT} + J_{iL} \right) + \sigma_{a,i} \phi_i = q_i, \tag{6.21}$$

$$\frac{1}{V_{i\omega}} \Big(\frac{1}{2} \bar{\bar{E}}_{i\omega-1} \phi_{i\omega-1} \vec{A}_{i\omega-1} + \bar{\bar{E}}_{i\omega} \phi_{i\omega} \vec{A}_{i\omega} +$$
$$\frac{1}{2} \bar{\bar{E}}_{i\omega+1} \phi_{i\omega+1} \vec{A}_{i\omega+1} + \bar{\bar{E}}_i \phi_i \vec{A}_{center,i\omega} \Big) \cdot \vec{n}_{i\omega} +$$
$$\sigma_{t,i} J_{i\omega} = 0, \quad \text{for each subcell } \omega = B, R, T, L. \tag{6.22}$$

Indices iB, iR, iT, iL denote the bottom (B), right (R), top (T), and left (L) faces of quadrilateral cell i, respectively. Counter-clockwise ordering of faces allows referencing adjacent faces—the next face counter-clockwise from ω is $(\omega + 1)$; the previous face counter-clockwise from ω is $(\omega - 1)$. Thus, in terms of our quadrilateral faces: $B + 1 = R$, $R + 1 = T$, $T + 1 = L$, and $L + 1 = B$. The balance equation (Eq. (6.21)) relates cell-average scalar flux ϕ_i and all face-average normal currents $J_{iB}, J_{iR}, J_{iT}, J_{iL}$. The half-cell equation (Eq. (6.22)) for cell i and face ω relates the cell-average scalar flux in cell i, face-average scalar flux for each face ω' in the subcell, face-average normal current for face ω, and adjacent faces' scalar fluxes $\phi_{i\omega-1}$ and $\phi_{i\omega+1}$. For example, the left (L) half-cell depends on cell-average scalar flux ϕ_i, face-average scalar fluxes ϕ_{iL}, ϕ_{iT}, ϕ_{iB}, and unknown face-average normal current J_{iL}.

6.3.4 AK Method for Discretization of the LOQD Equations

Another half-cell FV discretization [47, 38] uses the same half cells but expresses the integration of ϕ over adjacent faces $\omega - 1$ and $\omega + 1$ as the integration of a linear function based on $\phi_{i\omega}$ and ϕ_i (instead of just using $\phi_{\omega-1}$, $\phi_{\omega+1}$ as in the GGK method). Hereafter, we refer to this discretization as *AK method.*

Using our general form, the AK discretization method on arbitrary quadrilaterals is 5 equations given by

$$\frac{1}{V_i}\left(J_{iB} + J_{iR} + J_{iT} + J_{iL}\right) + \sigma_{a,i}\phi_i \ = \ q_i, \quad \text{for each cell } i \tag{6.23}$$

$$\frac{1}{V_{i\omega}}\Big(\frac{1}{4}\bar{\bar{E}}_{i\omega-1}(\phi_{i\omega} + \phi_i)\vec{A}_{i\omega-1} \ + \ \bar{\bar{E}}_{i\omega}\phi_{i\omega}\vec{A}_{i\omega} +$$

$$\frac{1}{4}\bar{\bar{E}}_{i\omega+1}(\phi_{i\omega} + \phi_i)\vec{A}_{i\omega+1} \ + \ \bar{\bar{E}}_i\phi_i\vec{A}_{center,i\omega}\Big) \cdot \vec{n}_{i\omega} +$$

$$\sigma_{t,i}J_{i\omega} \ = \ 0, \quad \text{for each face } \omega = B, R, T, L. \tag{6.24}$$

The balance equation in Eq. (6.23) is exactly the same as before in Eq. (6.21), but the half-cell equations corresponding to each face are now different. The new half-cell equations in Eq. (6.24) relate the cell-average scalar flux in cell i, face-average scalar flux for face ω, face-average normal current for face ω, *without* dependence on the scalar flux of adjacent faces $\phi_{i\omega-1}$ and $\phi_{i\omega+1}$ like in the original half-cell equation (Eq. (6.22).) Thus the left (L) half-cell in the AK method depends on cell-average scalar flux ϕ_i, face-average scalar flux ϕ_{iL} and unknown face-average normal current J_{iL}.

6.3.5 Morel's Cell-Centered Discretization Method

In [48], Jim Morel devises a cell-centered discretization for the diffusion equation on meshes of arbitrary polyhedrons by representing the gradient of the scalar flux at the center of a cell $\vec{\nabla}\phi_i$ in terms of face-average scalar fluxes. Then he represents the gradient at the faces of the cell $\vec{\nabla}\phi_{i\omega}$ in terms of the gradient $\vec{\nabla}\phi_i$ and cell- and face-average scalar flux unknowns. Then, to determine the face-average current at face α in cell i, Morel uses the face-average gradient of the scalar flux,

$$\vec{J}_{i\omega} = -\frac{1}{3\sigma_{t,i}}\vec{\nabla}\phi_{i\omega}.$$

In the LOQD equations, the representation for the current is given by

$$\vec{J}_{i\omega} = -\frac{1}{\sigma_{t,i}}\text{DIV}\,(\bar{\bar{E}}_{i\omega}\phi_{i\omega}).$$

We consider Morel's formulas in terms of components of the gradient, $\frac{\partial}{\partial x}\phi$ and $\frac{\partial}{\partial y}\phi$, and derive approximation of DIV $(\bar{\bar{E}}_{i\omega}\phi_{i\omega})$. Hereafter, we refer to this method as the $\hat{J}$M method.

6.3.6 Interface Continuity Conditions

Our local approach allows us to use the above discretizations for cells, combined with interface conditions (and boundary conditions) in order to fully specify the system of equations to

solve. For a structured mesh, in which an interface is composed of two and only two faces, interface conditions are to simply enforce continuity of face-average current and face-average scalar flux:

$$J_{i\omega} = -J_{i'\omega'}, \tag{6.25}$$
$$\phi_{i\omega} = \phi_{i'\omega'}, \tag{6.26}$$

for interface of faces $i\omega$ and $i'\omega'$.

For an unstructured mesh, such as the unstructured orthogonal (uo) mesh (also called an adaptive mesh refinement, or AMR mesh—see Fig. 6.6) we must do something different because cell may have a common face with more than ine cell. We enforce the same strong continuity of face-average current at each subface $i'\omega'$ of an interface, while we enforce a weak continuity condition on the scalar flux. We require the area-weighted sum of the subface face-average scalar fluxes, $\phi_{i'\omega'}$, to be equal to the master face-average scalar flux, $\phi_{i\omega}$.

$$J_{i\omega} = -J_{i'\omega'}, \tag{6.27}$$
$$\phi_{i\omega} = \frac{1}{|\vec{A}_{i\omega}|} \sum_{i',\omega'} |\vec{A}_{i'\omega'}| \phi_{i'\omega'}, \tag{6.28}$$

for interface of master face $i\omega$ and subfaces $i'\omega'$. Note that if one applies weak condition for the currents and strong conditions for the scalar fluxes, it results in interface relationships that are not valid for the scalar fluxes varying linearly along cell interfaces [49].

For example, in 2D, if the left face of i-th cell is a common face with the m-th and p-th cells, then we define strong continuity conditions for the normal components of the currents

$$J_{iL} = -J_{mR}, \tag{6.29}$$
$$J_{iL} = -J_{pR}, \tag{6.30}$$

and the weak continuity condition for the face-average scalar fluxes

$$\phi_{iL} h_{iL} = \phi_{mR} h_{mR} + \phi_{pR} h_{pR}, \tag{6.31}$$

where $h_{i\omega}$ is the cell-edge length.

6.3.7 Iterative Solution of the System of the Discretized LOQD Equations

In order to solve the resulting system of linear algebraic equations iteratively, we must use a method which can handle the non-symmetric structure of the LOQD system equations, like `BiCGstab`. However, in order for this solver to be efficient, we must use a preconditioner, thus we have another problem? What kind of preconditioner should one use for a non-symmetric system which is somewhat arbitrary? (This is because its structure depends on the mesh structure, which is arbitrary.)

<div align="center">

(a) Before Local Reordering   (b) After Local Reordering
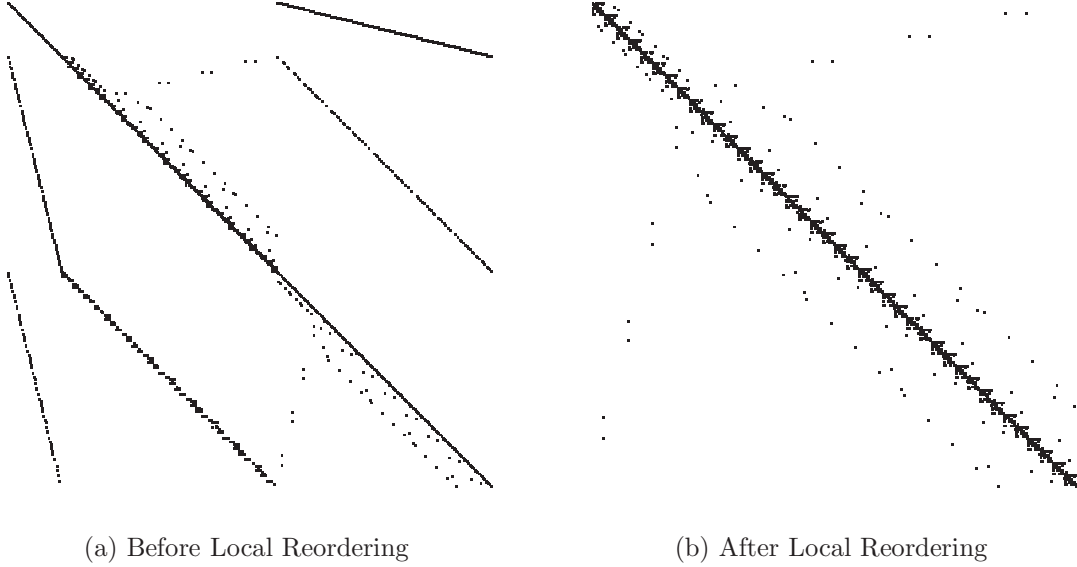
Figure 6.4: The sparse matrix of the discretized LOQD equations

</div>

We use incomplete LU factorization with truncation (ILUT) preconditioning and apply a simple local reordering (see Fig. 6.4) which forces the face-average scalar fluxes of a cell to have sequential columns. Currently generating the preconditioner takes a considerable amount of the low-order QD solution time, on the order of 50% and up. We have experimented with various standard reorderings, e.g. Reverse Cuthkill-McGee, to reduce the bandwidth and/or envelope of the QD system which would hopefully lead to an ILUT preconditioner which needs less fill in, so is smaller and reduces preconditioner generation time. However, we have not not seen much advantage in reordering strategies.

6.4 Discretization of the Transport Equation

The transport equation is used to determine the angular flux that will be utilized to evaluate the QD factors. To discretize the transport equation, we use the method of (short) characteristics with a second-order interpolation [40, 41, 50]. The scattering term is approximated by a linear function using the scalar flux from the LOQD problem. This is a vertex-based method. As a result, the QD factors are calculated in cell vertices, and the face-average values are defined as an average of the vertex values.

(a) Face-Parallel   (b) Perpendicular   (c) Diagonal
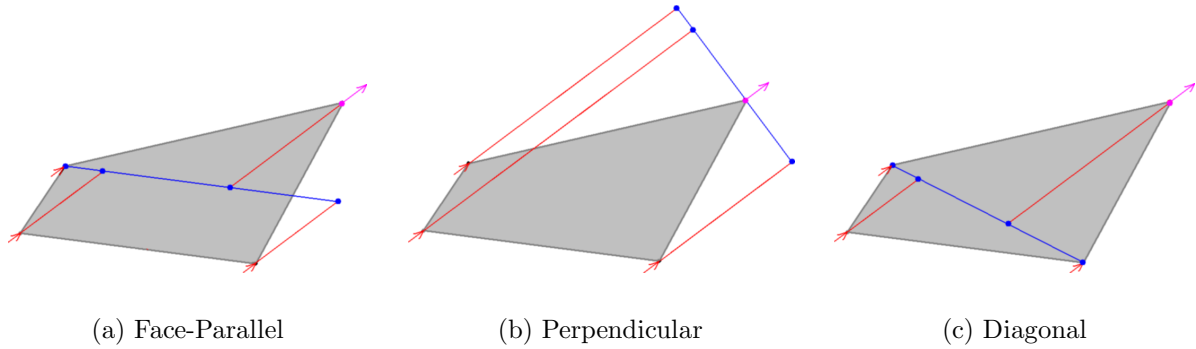
Figure 6.5: Parabolic Interpolation: interpolation planes (blue), with characteristics used (red), outgoing angular flux (magenta arrow), and incoming angular fluxes (red arrows).

6.4.1 Interpolation Plane in the Short Characteristics Method on Arbitrary Meshes

We use three different orientations of the *interpolation plane* for parabolic (second order) interpolation within a cell. The interpolation plane may be

- parallel to the face intersected by the backward-projected characteristic ray, Fig. 6.5(a),

- perpendicular to the characteristic ray, Fig. 6.5(b), and

- oriented on the diagonal of a quadrilateral cell, Fig. 6.5(c).

Only the diagonal interpolation plane results in all characteristics being completely contained within the cell, thus the properties needed for the characteristic solution (total cross section σ_t and source $Q = \sigma_s \phi + q$) also belong to the cell. With the other interpolation planes, one of the three characteristics in a second order interpolation scheme on quadrilaterals travels outside the cell. In such case, the transport equation is solved along characteristics with parameters of the current cell. Obviously, if the bordering cell's cross sections, scattering source, and/or external source are different, additional approximation is introduced by the face-parallel and perpendicular schemes. Lastly, the diagonal interpolation plane requires only 2 characteristic evaluations (the others require 3), which include costly exponential evaluations.

6.4.2 Representing the Scalar Flux within a Cell

At this point, it is convenient to introduce *barycentric coordinates*, $\vec{r}^* = \vec{r} - \vec{r}_i$. Then, the scalar flux within cell i may be represented as the linear function

$$\varphi_i(x^*, y^*, z^*) = ax^* + by^* + cz^* + d. \tag{6.32}$$

64

The source within a cell is then given by Eq. (6.33) as,

$$Q_i(x^*, y^*, z^*) = \frac{1}{4\pi}\left(q_i + \sigma_{s,i}(ax^* + by^* + cz^* + d) \right),\tag{6.33}$$

The goal then, is to determine coefficients a, b, c, and d from face-average and cell-average scalar fluxes in the cell, defined by the LOQD solution. In 3D with hexahedrons (2D with quadrilaterals), we have 4 (3) degrees of freedom in the coefficients, but 6 (4) face-average scalar fluxes and 1 cell-average scalar flux. Because the number of scalar fluxes outnumber the degrees of freedom, we cannot generate an exact fit, and must instead determine $\varphi_i(x^*, y^*, z^*)$ by minimizing residuals in some sense.

Linear Source via Least-Squares for Arbitrary Quadrilaterals in 2D

Consider the 2D case, where $c = 0$. We determine a and b based on a least-squares approximation to the 4 face-average values. We then choose d such that the cell-average flux is given by integrating the surface over the cell. We solve the rectangular system in Eq. (6.34) to determine a and b and determine c by Eq. (6.35).

$$\begin{pmatrix} x_B^* & y_B^* \\ x_R^* & y_R^* \\ x_T^* & y_T^* \\ x_L^* & y_L^* \end{pmatrix} \begin{pmatrix} a \\ b \end{pmatrix} = \begin{pmatrix} \phi_{iB} \\ \phi_{iR} \\ \phi_{iT} \\ \phi_{iL} \end{pmatrix},\tag{6.34}$$

where $\vec{r}_\omega^*$ is the centroid of face ω on cell i, in barycentric coordinates. With quadrilaterals in 2D, we have four faces, denoted bottom ($\omega = B$), right ($\omega = R$), top ($\omega = T$), and left ($\omega = L$). Then we calculate d from

$$d = \phi_i - \frac{1}{V_i} \iint_{V_i} ax^* + by^* \, dx \, dy\tag{6.35}$$

6.4.3   Characteristics Solution

Now, assuming that the angular domain has been discretized into N_m discrete ordinates, $\{\vec{\Omega}_m | m = 1, ..., N_m\}$. The angular flux a distance s along characteristic direction $\vec{\Omega}_m$, in cell i, is given by the method of characteristics as:

$$\psi(s) = \psi(0)e^{-\sigma_{t,i}s} + \int_0^s Q_i(s')e^{-\sigma_{t,i}(s-s')}ds'.\tag{6.36}$$

In order to calculate each $\psi_{k,m}$ we do the following for each vert k in each direction m. For simplicity, m and k subscripts are suppressed so $\vec{\Omega}$ is the direction of travel, ψ is the unknown angular flux, and $\vec{r}$ is the location of the unknown angular flux.

1. Get the cell i when we travel in the $-\vec{\Omega}$ direction and the distance s_0 to intersection with the interpolation plane. (The location of intersection is $\vec{r}_0 = \vec{r} - \vec{\Omega} s_0$.)

2. Determine the set of support verts $\{k_n | n = 1, ..., N_{interp}\}$ in cell i which correspond to *incoming* angular fluxes $\psi_n(0)$ for this direction.

3. Generate the source within cell i, $Q_i(x^*, y^*, z^*)$. (The linear source $Q_i(s)$, that depends only on the characteristic distance s, may be constructed by evaluating Q_i at any two points along the characteristic.)

4. Calculate the distance from each support vert to the interpolation plane, s_n.

5. Use Eq. (6.36) to project each incoming vert k_n to the interpolation plane:

$$\psi_n(s_n) = \psi_n(0)e^{-\sigma_{t,i}s_n} + \int_0^{s_n} Q_i(s')e^{-\sigma_{t,i}(s_n-s')}ds'.$$

6. Now that we have N_{interp} values of the angular flux all on the same plane (line in 2D) we may easily interpolate the angular flux to the point $\vec{r}_0$, $\psi_0(0)$.

7. With the angular flux at $\vec{r}_0$, we may simply apply Eq. (6.36) again over the distance s_0 to determine our unknown angular flux:

$$\psi = \psi_0(s_0) = \psi_0(0)e^{-\sigma_{t,i}s_0} + \int_0^{s_0} Q_i(s')e^{-\sigma_{t,i}(s_0-s')}ds'.$$

6.5 Numerical Results

To demonstrate the performance of the developed method, we solve two test problems with homogeneous and two-region domains. The results of computations on two-level AMR orthogonal and non-orthogonal grids are compared with those on regular rectangular (single-level) grids. The results on a set of sequentially refined grids are used to estimate numerically by means of Aitken process [51] the order of spatial convergence of the method on orthogonal grids .

6.5.1 Test 1

Description

The domain is a 5cm by 3cm rectangle, with $\sigma_t = 1\text{cm}^{-1}$ and $\sigma_s = 0.5\text{cm}^{-1}$. There are vacuum BC on all sides. The external source in the left half of the domain is $q = 0.5$, in the right half of the domain is $q = 0$. The scalar flux convergence criteria is $\epsilon = 1e - 8$.

Discretization Methods

We use the short characteristics with diagonal interpolation plane and min/max monotonization and all three methods for discretization of the LOQD equations.

Meshes

We use the following structured meshes: structured orthogonal (**so**) and structured perturbed (**sp**). We use the following unstructured meshes with left-side and right-side refinement, respectively: unstructured orthogonal (**uoL** and **uoR**), unstructured perturbed (**upL** and **upR**). (See Fig. 6.6.) Random perturbations of 20% are used to create the perturbed meshes.
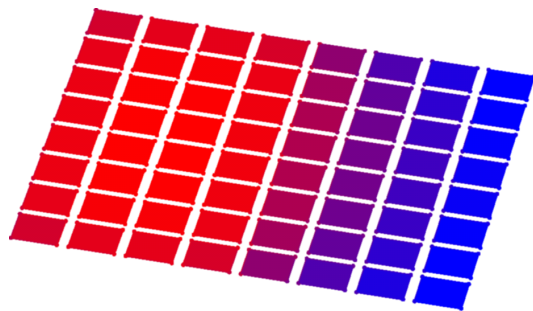
(a) structured orthogonal (**so**)
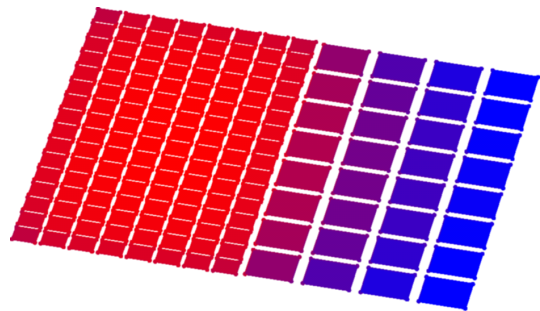
(b) unstructured orthogonal with left refinement (**uoL**)
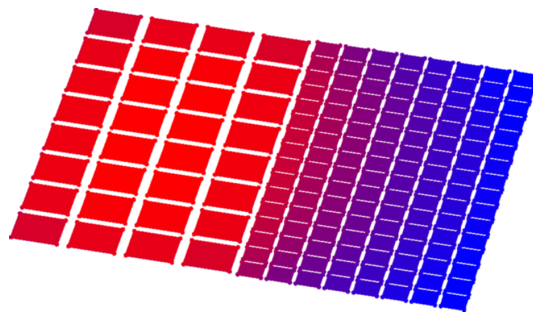
(c) unstructured orthogonal with right refinement (**uoR**)
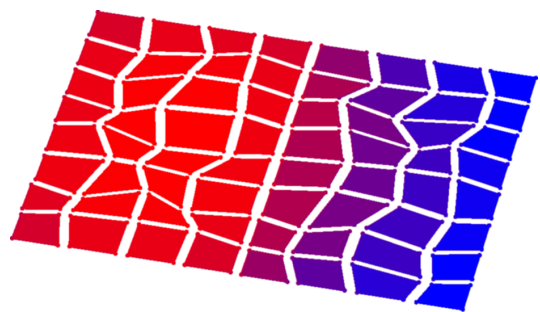
(d) structured perturbed (**sp**)
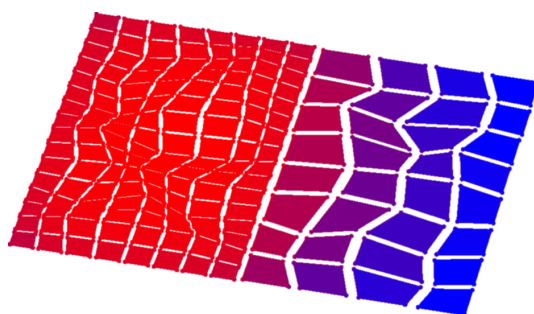
(e) unstructured perturbed with left refinement (**upL**)
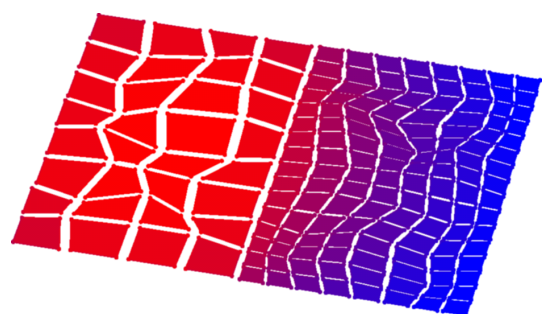
(f) unstructured perturbed with right refinement (**upR**)

Figure 6.6: Meshes for Test 1(cells colored with scalar flux)

Observables

We look at the scalar flux along the interface of the left and right sides ($\phi(x = 2.5cm, y)$), shown in Fig. 6.7, 6.8, and 6.9, for GKK, AK and JM methods, respectively. We show only reasonably coarse **so** and **sp** meshes, as increasing refinement leads to crowded graphs and the effect of the perturbations are more difficult to see. However, the relative quality of each FV variant remains the same as in the coarse meshes. For each of the three methods, we also calculate numerical convergence orders for the left-side scalar flux (Eq. 6.37), right-side scalar flux (Eq. 6.38), and average exiting current at the top right corner (Eq. 6.39) on **so**, **sp**, **uoL**, **uoR**, **upL**, and **upR** meshes.

$$\phi_{left} = \frac{1}{7.5} \int_{0.0}^{2.5} dx \int_{0.0}^{3.0} dy \phi(x, y) \tag{6.37}$$

$$\phi_{right} = \frac{1}{7.5} \int_{2.5}^{5.0} dx \int_{0.0}^{3.0} dy \phi(x, y) \tag{6.38}$$

$$J_{UR} = \frac{1}{4.0} \left(\int_{2.5}^{5.0} J(x, 3.0) dx + \int_{1.5}^{3.0} J(5.0, y) dy \right) \tag{6.39}$$

Discussion of the Results

The GGK method behaves very well on the traditional **so** mesh, exhibiting strong second order convergence. The **uoL** and **uoR** meshes also exhibit second order convergence of the scalar flux, except for ϕ_{right} on the **uoR** mesh where there is first order convergence. Current convergence is somewhat reduced (to about 1.5), probably because of the interface conditions imposed and the decent coupling between the left and right sides ($\sigma_s = 0.5$.) The perturbed meshes exhibit erratic convergence, especially the structured (**sp**) mesh, which had differences between successive iterations that changed signs, thus the Aitken process exploded.

The AK method also behaves very well on the traditional **so** mesh, exhibiting strong second order convergence. The **uoL** and **uoR** meshes also exhibit second order convergence of the scalar flux and better convergence of the current than the GGK method. However, convergence on perturbed meshes is highly erratic, with large differences exhibited between orders on structured (**sp**) and unstructured (**upL**,**upR**) meshes.

The JM method also behaves very well on the traditional **so** mesh, exhibiting strong second order convergence. On other meshes, this discretization leads to scalar flux convergence orders of approximately 2 and current convergence orders of approximately 1.5. Overall, this discretization appears most robust and will be used in the remaining tests.
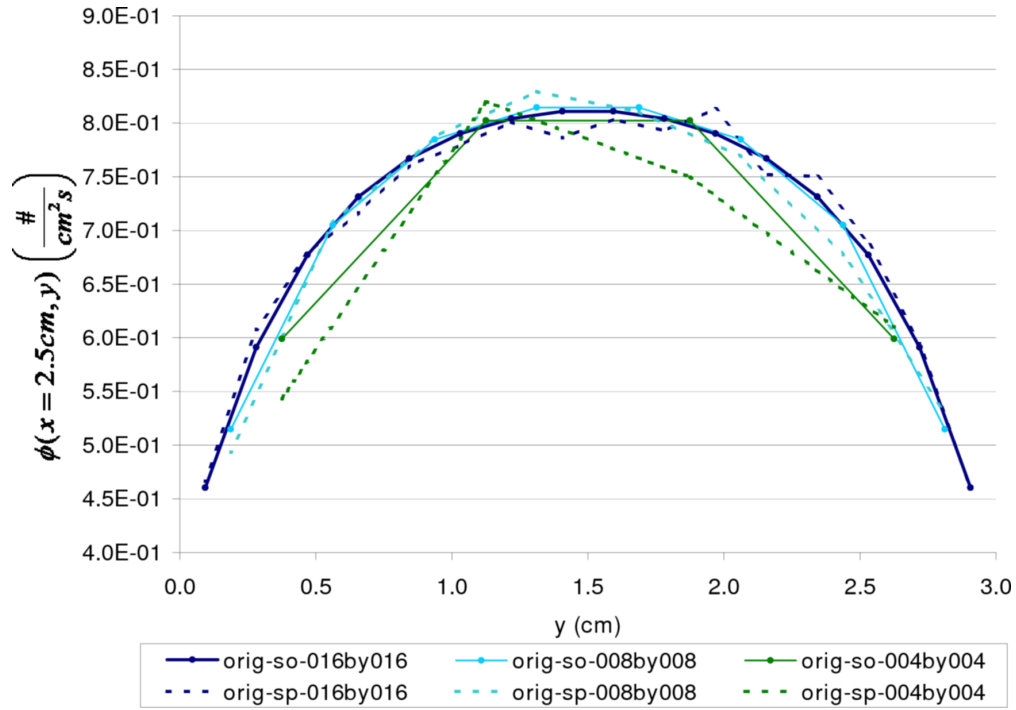
Figure 6.7: Test 1: Face-average Scalar Flux $\phi(x = 2.5cm, y)$ for the GGK Method
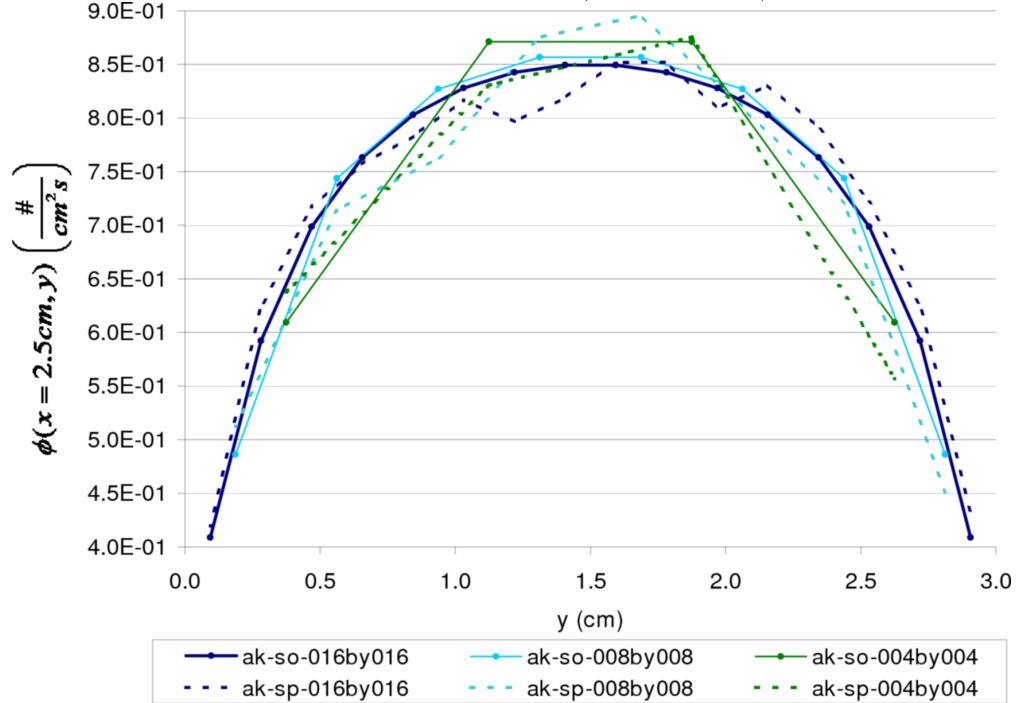
Figure 6.8: Test 1: Face-average Scalar Flux $\phi(x = 2.5cm, y)$ for the AK Method
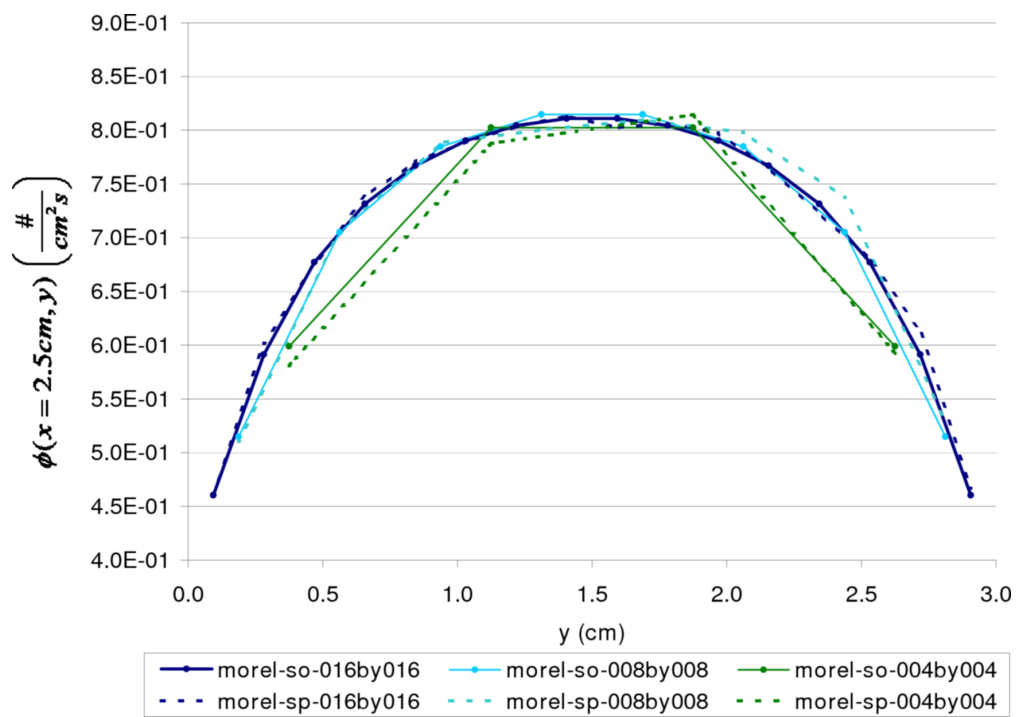
Figure 6.9: Test 1: Face-average Scalar Flux $\phi(x = 2.5cm, y)$ for the JM Method

Table 6.1: Test 1: Results for the GGK Method

Mesh	J_{UR}	ϕ_{left}	ϕ_{right}
so-002by002	2.237E-02	9.905	0.593
so-004by004	2.705E-02	8.909	0.893
so-008by008	2.998E-02	8.413	1.100
so-016by016	3.141E-02	8.266	1.173
so-032by032	3.194E-02	8.231	1.192
so-064by064	3.209E-02	8.224	1.195
sp-002by002	2.237E-02	9.905	0.593
sp-004by004	2.787E-02	8.887	0.904
sp-008by008	3.077E-02	8.382	1.110
sp-016by016	3.283E-02	8.184	1.210
sp-032by032	3.410E-02	8.129	1.242
sp-064by064	3.408E-02	8.105	1.255
uoL-004and002	2.275E-02	9.105	0.713
uoL-008and004	2.850E-02	8.515	0.996
uoL-016and008	3.071E-02	8.304	1.135
uoL-032and016	3.167E-02	8.242	1.181
uoL-064and032	3.201E-02	8.226	1.193
uoR-002and004	2.610E-02	9.751	0.736
uoR-004and008	2.829E-02	8.826	0.984
uoR-008and016	3.044E-02	8.376	1.139
uoR-016and032	3.155E-02	8.254	1.185
uoR-032and064	3.197E-02	8.228	1.194
upL-004and002	2.275E-02	9.105	0.713
upL-008and004	2.926E-02	8.488	1.016
upL-016and008	3.138E-02	8.283	1.145
upL-032and016	3.275E-02	8.201	1.205
upL-064and032	3.356E-02	8.171	1.228
upR-002and004	2.610E-02	9.751	0.736
upR-004and008	2.888E-02	8.820	0.981
upR-008and016	3.086E-02	8.352	1.144
upR-016and032	3.229E-02	8.191	1.209
upR-032and064	3.304E-02	8.156	1.222

Table 6.2: Test 1: Results for the AK Method

Mesh	J_{UR}	ϕ_{left}	ϕ_{right}
so-002by002	1.436E-02	10.097	0.612
so-004by004	1.884E-02	9.118	0.903
so-008by008	2.198E-02	8.564	1.124
so-016by016	2.349E-02	8.396	1.205
so-032by032	2.398E-02	8.356	1.227
so-064by064	2.409E-02	8.347	1.231
sp-002by002	1.436E-02	10.097	0.612
sp-004by004	1.804E-02	9.132	0.892
sp-008by008	2.258E-02	8.531	1.134
sp-016by016	2.545E-02	8.290	1.259
sp-032by032	2.660E-02	8.249	1.291
sp-064by064	2.682E-02	8.223	1.314
uoL-004and002	1.474E-02	9.374	0.640
uoL-008and004	2.058E-02	8.692	0.986
uoL-016and008	2.282E-02	8.442	1.155
uoL-032and016	2.378E-02	8.369	1.213
uoL-064and032	2.405E-02	8.350	1.228
uoR-002and004	1.873E-02	9.912	0.802
uoR-004and008	2.071E-02	9.011	1.018
uoR-008and016	2.274E-02	8.517	1.172
uoR-016and032	2.368E-02	8.381	1.219
uoR-032and064	2.400E-02	8.353	1.230
upL-004and002	1.474E-02	9.374	0.640
upL-008and004	1.992E-02	8.690	0.987
upL-016and008	2.340E-02	8.394	1.170
upL-032and016	2.572E-02	8.256	1.264
upL-064and032	2.664E-02	8.232	1.289
upR-002and004	1.873E-02	9.912	0.802
upR-004and008	1.953E-02	9.031	1.001
upR-008and016	2.310E-02	8.483	1.184
upR-016and032	2.549E-02	8.278	1.273
upR-032and064	2.657E-02	8.250	1.293

Table 6.3: Test 1: Results for the JM Method

Mesh	J_{UR}	ϕ_{left}	ϕ_{right}
so-002by002	2.237E-02	9.905	0.593
so-004by004	2.705E-02	8.909	0.893
so-008by008	2.998E-02	8.413	1.100
so-016by016	3.141E-02	8.266	1.173
so-032by032	3.194E-02	8.231	1.192
so-064by064	3.209E-02	8.224	1.195
sp-002by002	2.237E-02	9.905	0.593
sp-004by004	2.574E-02	8.912	0.914
sp-008by008	2.872E-02	8.447	1.076
sp-016by016	3.124E-02	8.284	1.157
sp-032by032	3.205E-02	8.233	1.186
sp-064by064	3.216E-02	8.223	1.194
uoL-004and002	2.275E-02	9.105	0.713
uoL-008and004	2.850E-02	8.515	0.996
uoL-016and008	3.071E-02	8.304	1.135
uoL-032and016	3.167E-02	8.242	1.181
uoL-064and032	3.201E-02	8.226	1.193
uoR-002and004	2.610E-02	9.751	0.736
uoR-004and008	2.829E-02	8.826	0.984
uoR-008and016	3.044E-02	8.376	1.139
uoR-016and032	3.155E-02	8.254	1.185
uoR-032and064	3.197E-02	8.228	1.194
upL-004and002	2.275E-02	9.105	0.713
upL-008and004	2.733E-02	8.512	1.022
upL-016and008	2.959E-02	8.326	1.118
upL-032and016	3.156E-02	8.254	1.169
upL-064and032	3.203E-02	8.229	1.188
upR-002and004	2.610E-02	9.751	0.736
upR-004and008	2.807E-02	8.833	0.986
upR-008and016	3.020E-02	8.395	1.126
upR-016and032	3.150E-02	8.264	1.178
upR-032and064	3.203E-02	8.228	1.192

Table 6.4: Test 1: Convergence Orders for the GGK Method

Mesh	J_{UR}	ϕ_{left}	ϕ_{right}
so	1.9	2.3	2.3
sp	∗	1.2	1.3
uoL	1.5	1.9	2.0
uoR	1.4	2.2	1.3
upL	0.8	1.5	1.3
upR	0.9	2.2	2.3

∗ Aitken process failed

Table 6.5: Test 1: Convergence Orders for the AK Method

Mesh	J_{UR}	ϕ_{left}	ϕ_{right}
so	2.1	2.3	2.2
sp	2.4	0.7	0.5
uoL	1.8	2.0	1.9
uoR	1.6	2.2	2.2
upL	1.3	2.6	1.9
upR	1.2	2.8	2.2

Table 6.6: Test 1: Convergence Orders for the JM Method

Mesh	J_{UR}	ϕ_{left}	ϕ_{right}
so	1.9	2.3	2.3
sp	2.8	1.9	1.9
uoL	1.5	2.0	2.0
uoR	1.4	2.3	2.3
upL	2.0	1.4	1.4
upR	1.3	1.8	1.8

6.5.2 Test 2

Description

The domain is a 0.1cm by 0.1cm square, with $\sigma_t = 1\text{cm}^{-1}$ and $\sigma_s = 0.5\text{cm}^{-1}$. There are reflective BC on the top and bottom, vacuum BC on the left and right. The external source everywhere is $q = 1$. The scalar flux convergence criteria is $\epsilon = 1e-8$. The fine spatial mesh is used in order to be able to more easily study asymptotic convergence.

Meshes

We use the following structured meshes: structured orthogonal (**so**), structured rotated (**sr**), and structured perturbed (**sp**). We use the following unstructured meshes with left-side refinement only: unstructured orthogonal (**uoL**), unstructured rotated (**urL**), unstructured perturbed (**upL**). (See Fig. 6.6 for mesh pictures.) Random perturbations of 30% are used to create the perturbed meshes. Rotations of verts about the center produce perturbations on the order of 15%. The random perturbation is extremely close to the maximum random perturbation allowed of 31.4% on quadrilateral meshes to prevent possibly having non-convex quadrilaterals, thus creating an invalid mesh. The rotation is close to the maximum rotation allowed which results in verts near the corners crossing over the domain boundary into the mesh exterior, thus again creating an invalid mesh.

Discretization Methods

We use the short characteristics method with diagonal interpolation plane and min/max monotonization and the JM method for discretization of the LOQD equations.

Observables

The global quantities of interest are the left-side and right-side average scalar flux, and the exiting current out of the right side, shown in Fig. 6.10, 6.11, and 6.12, respectively. The relative difference in these quantities with respect to the finest orthogonal mesh is shown in Fig. 6.13, 6.14, and 6.15, respectively.

Discussion of Results

All global quantities converge to the same value with increasing refinement, regardless of the mesh. The sudden drop off in relative differences of the **sp** mesh in Fig. 6.13, 6.14, and 6.15 is explained by the fact that at the finest level of refinement, the **sp** mesh has the same number of cells and so may be roughly considered as at the same approximate level of refinement as the **so** mesh (with which we calculate relative differences). So for this data point, we are really just looking at the "noise" introduced by the perturbed mesh versus an orthogonal mesh.

Unstructured meshes **uoL**, **urL**, and **upL** exhibit different convergence behavior than their structured counterparts, however in this case, the convergence orders are very similar—there appears to just be a small difference in the coefficient of convergence, i.e. it is smaller (better) for the structured meshes.
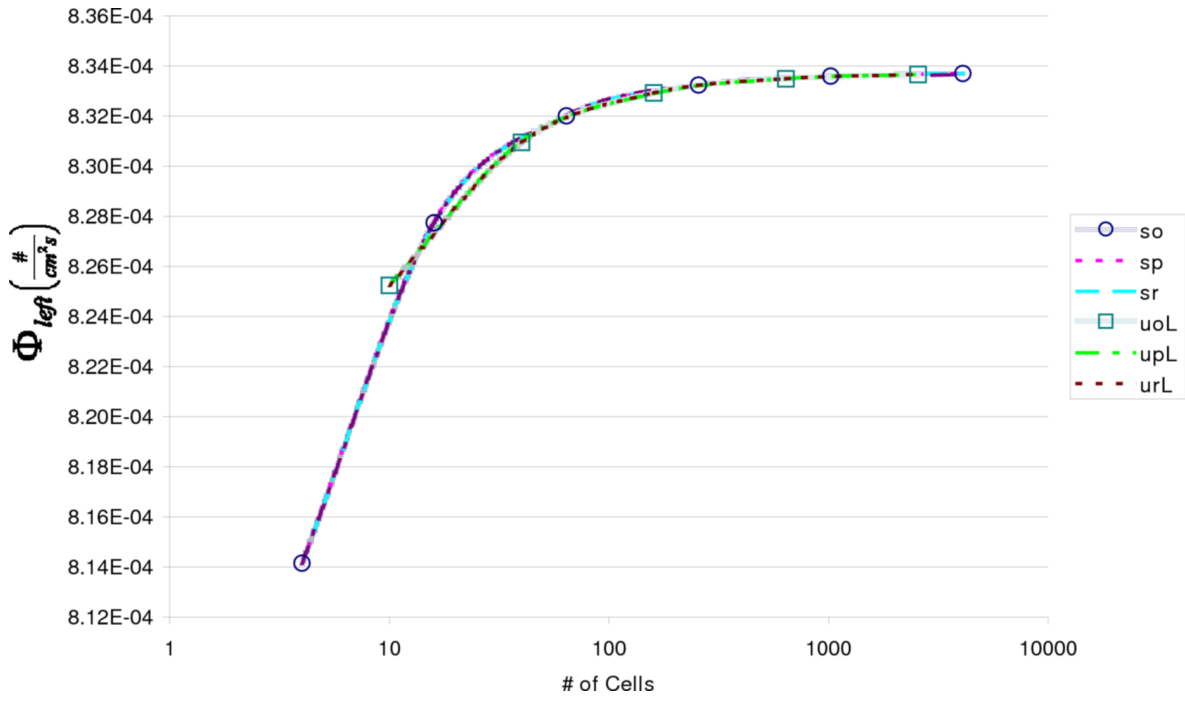
Figure 6.10: Test 2: Left-Side-Average Scalar Flux

Although global quantities on orthogonal and perturbed meshes converge to the same value, the convergence orders are similar to Test 1, despite a much smaller domain, and therefore less optically thick cells, conditions that we expected would lead to asymptotic convergence.
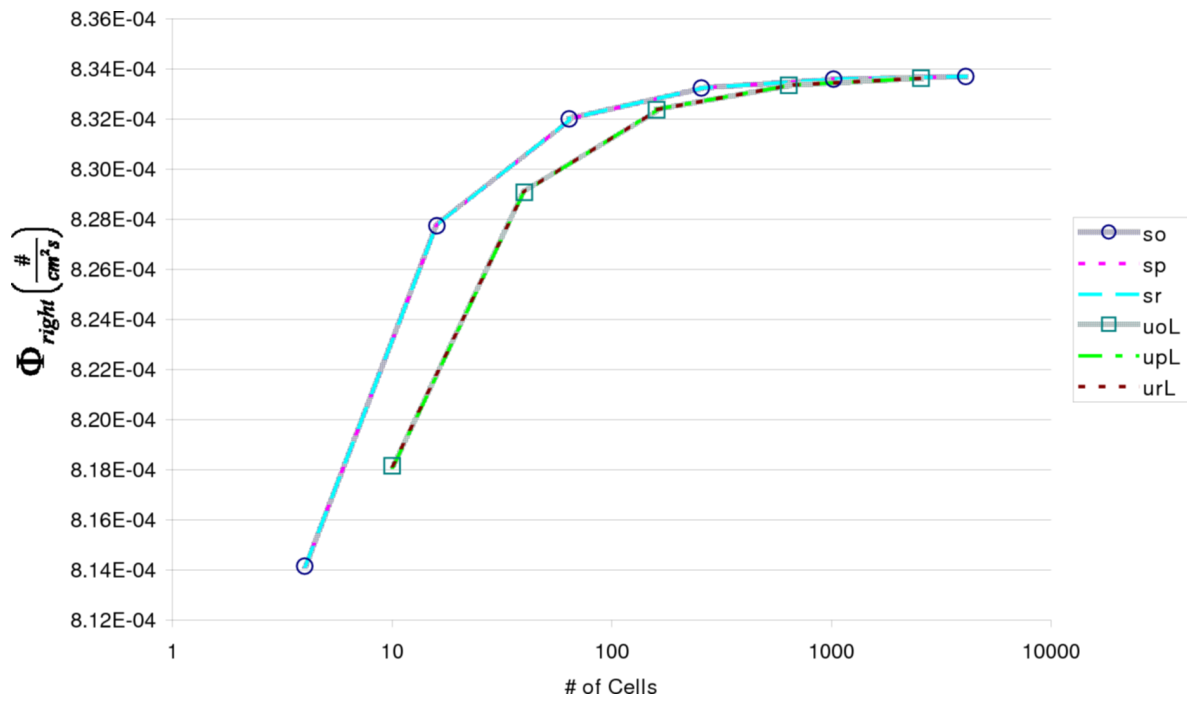
Figure 6.11: Test 2: Right-Side-Average Scalar Flux
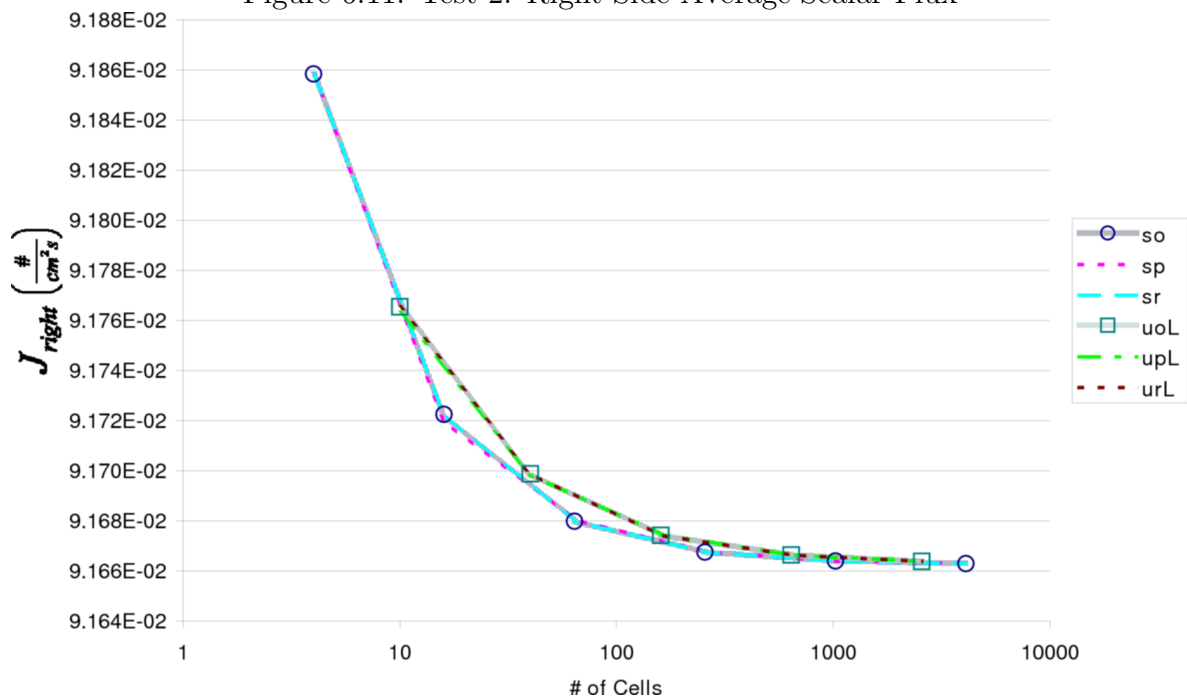
Figure 6.12: Test 2: Right-Side Exiting Currents
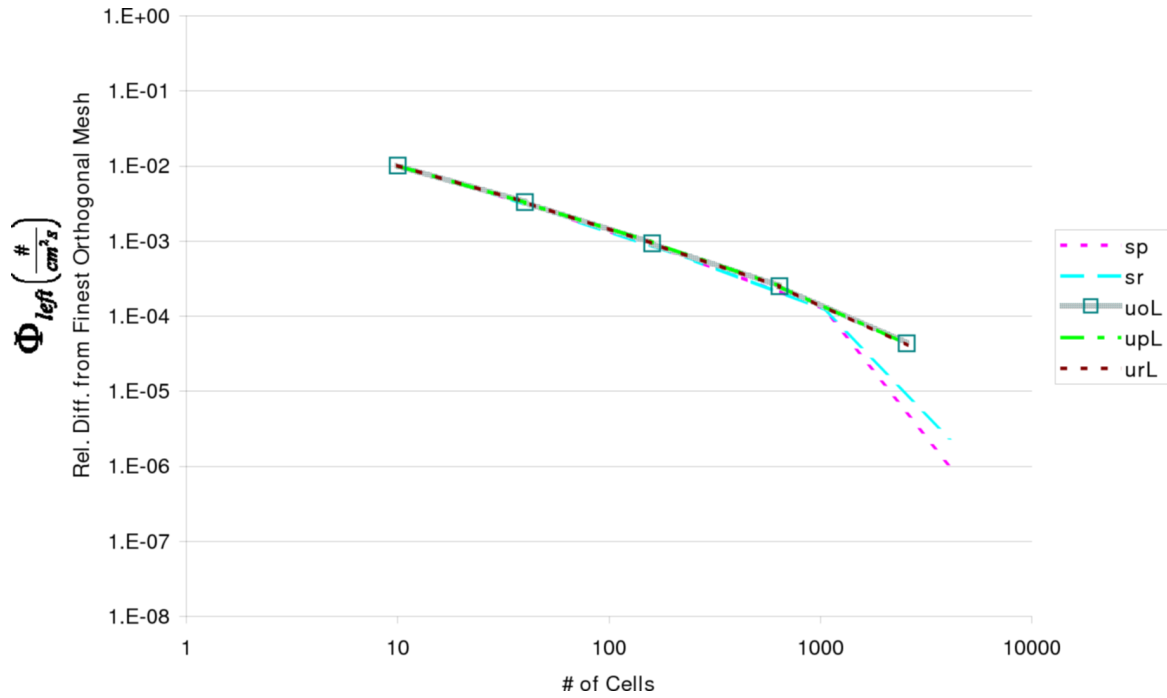
Figure 6.13: Test 2: Relative Differences in Left-Side-Average Scalar Flux with Respect to the Finest Orthogonal Mesh (64by64 cells)
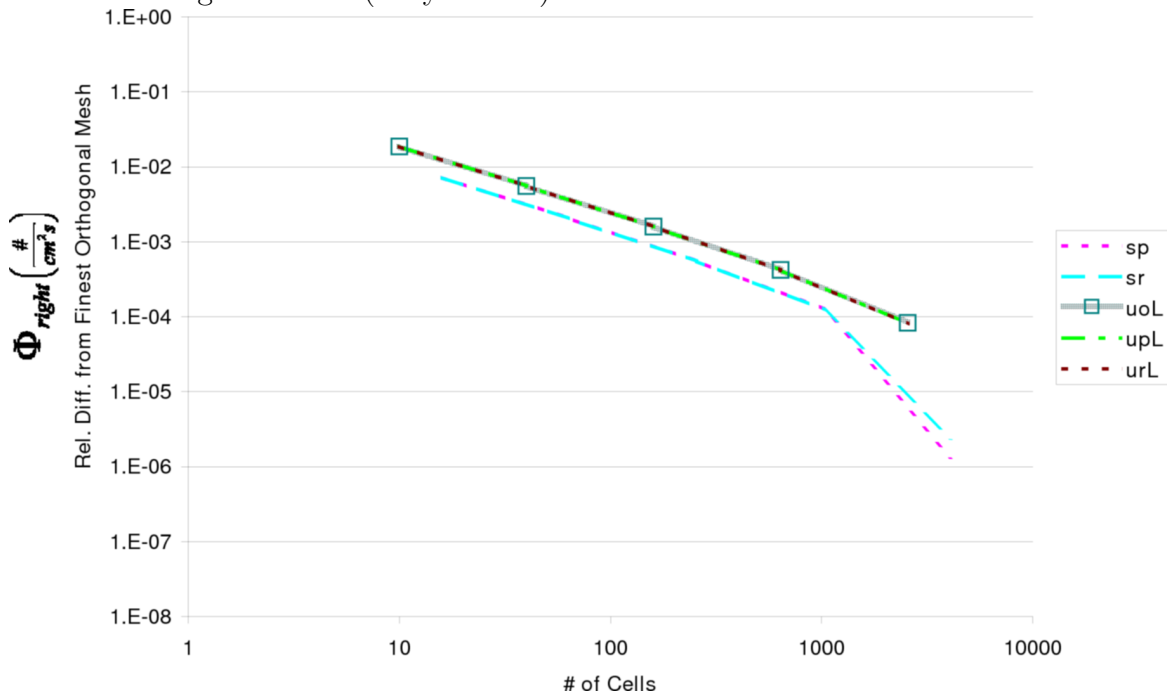
Figure 6.14: Test 2: Relative Differences in Right-Side-Average Scalar Flux with Respect to the Finest Orthogonal Mesh (64by64 cells)
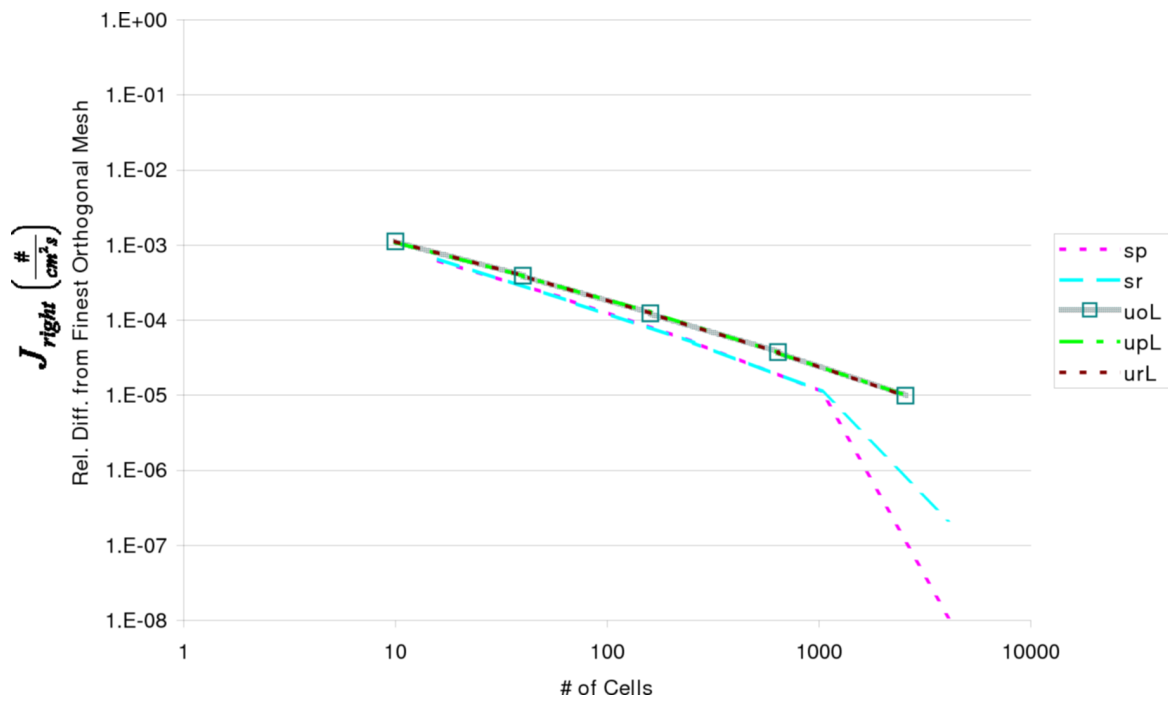
Figure 6.15: Test 2: Relative Differences in Right-Side Exiting Currents with Respect to the Finest Orthogonal Mesh (64by64 cells)

6.5.3 Test 3

Description

The domain is a 5cm by 3cm rectangle, with $\sigma_t = 1\text{cm}^{-1}$ and $\sigma_s = 0.5\text{cm}^{-1}$. There are vacuum BC on all sides except left where the incident flux is $\psi^{in} = 0.5$. The external source everywhere is $q = 0$. The scalar flux convergence criteria is $\epsilon = 1e - 8$ [52].

Meshes

We use the following structured meshes: structured orthogonal (**so**) and structured perturbed (**sp**) meshes (see Fig. 6.6) on a fine mesh of 64×64 cells.

Discretization Methods

We use the short characteristics method with diagonal interpolation plane and min/max monotonization and the JM method for discretization of the LOQD equations.

Observables

We have shown in previous tests that the unstructured meshes exhibit similar convergence to structured meshes, with the use of our special interface conditions. In this test we look at the behavior of different levels of random perturbations on the exiting flow out of the upper-right corner of the domain, shown in Fig. 6.16. The relative difference in the exiting flow on perturbed meshes versus the orthogonal mesh is shown in Fig. 6.17.

Discussion of Results

The exiting flow is relatively invariant with respect to perturbation as seen in Fig. 6.16, where the flow profiles overlap considerably. The small abrupt jump in flow at a distance of $2.5cm$ along the boundary from the top of the domain ($x = 2.5cm, y = 3cm$) is due the presence of a corner. Overall, the difference in flow between perturbed and orthogonal is excellent (see Fig. 6.17), exhibiting only a 1% difference from orthogonal for a 30% perturbation of verts. Also, for small perturbations, the "noise" introduced seems to have a strong pattern, while for larger perturbations, the effect seems more random.
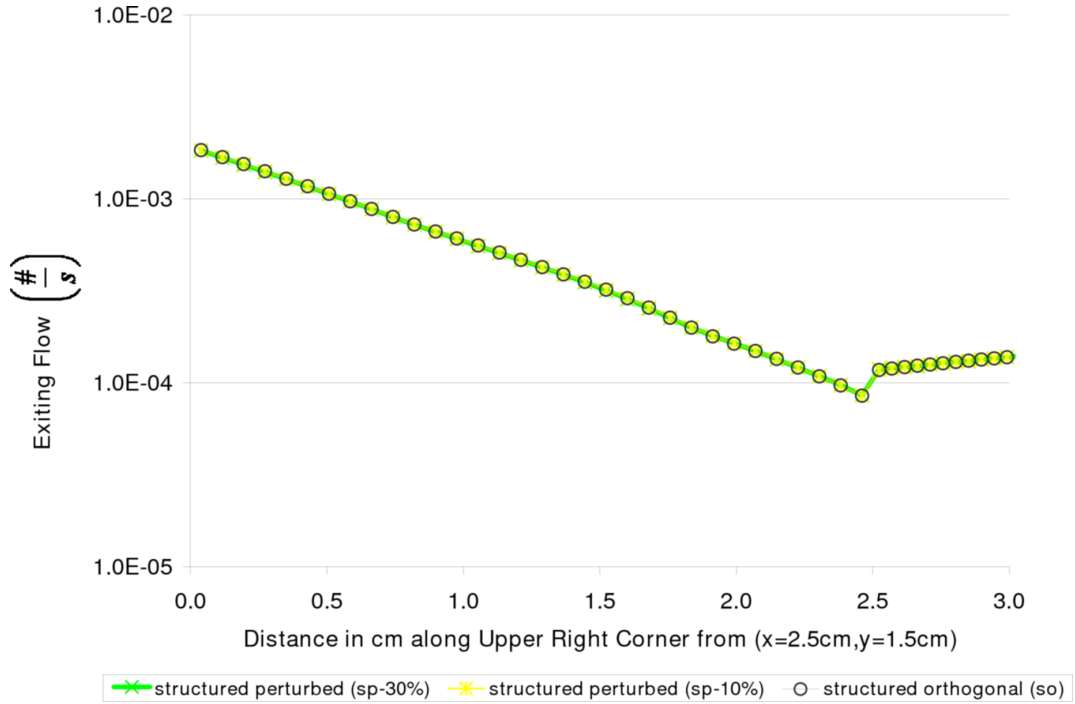
Figure 6.16: Test 3: Flow out of Upper Right Corner ($x \geq 2.5$,$y \geq 1.5$)
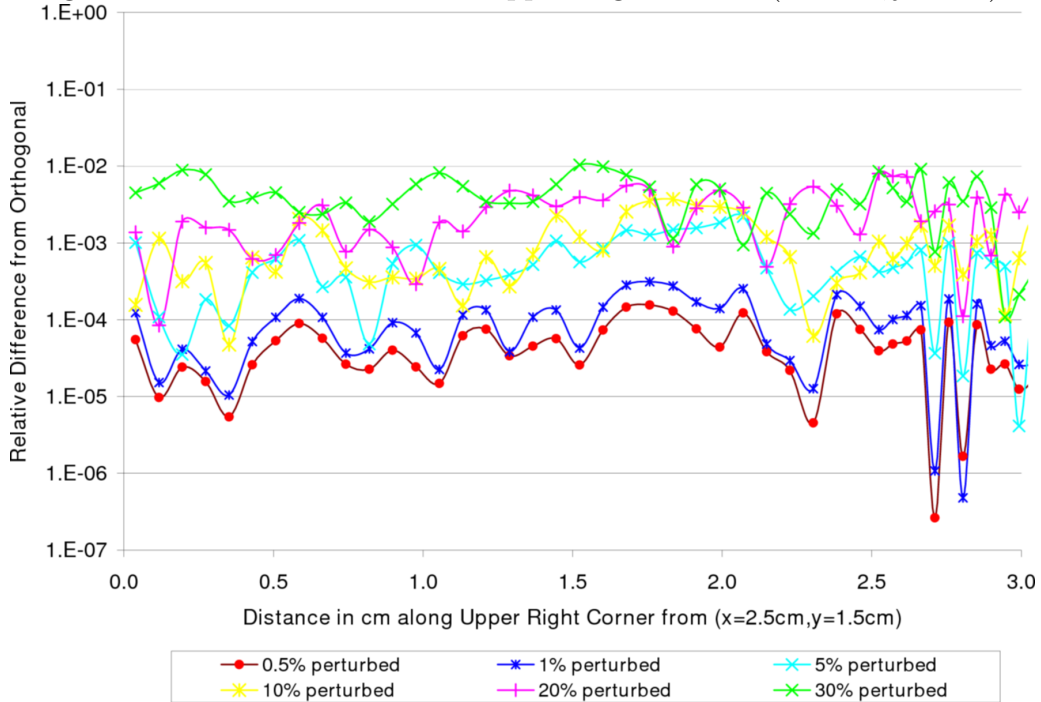
Figure 6.17: Test 3: Relative difference in Flow out of Upper Right Corner ($x \geq 2.5$,$y \geq 1.5$) on Perturbed Meshes with respect the Finest Orthogonal Mesh

6.6 The Transport Algorithms PACKage

In order to solve transport problems on arbitrary meshes we have created a code package, `TAPACK`. With `TAPACK`, we take a modular approach to programming, with the goals of producing code with the following attributes:

- "toolbox-style" routines targeted at performing specific tasks, while hiding most of the complexities from the user,

- expandable code, i.e. the code structure outlays a general sequence of processes and then within each process, specific routines are called (based on user input and/or internal logic) to carry out that process—thus new specific routines may be added easily,

- extendable in terms of number of dimensions considered and number of processors, made in order to provide the most general framework,

- visualization-ready.

We will discuss each of these aspects of `TAPACK` briefly.

To date, we have implemented the following capabilities into our transport code (TAPACK):

1. versatile unstructured mesh generation,

2. a short characteristics transport solver for arbitrary quadrilateral meshes in 2D,

3. three different finite volume discretizations of the LOQD equations on arbitrary quadrilateral meshes in 2D, and

4. solution of resulting QD linear system with iterative methods (BiCGstab with Incomplete LU preconditioning is current best technique).

6.6.1 Arbitrary 3D Mesh Representation

We represent an arbitrary 3D mesh *implicitly* as a set of *verts* $\{\vec{r}_k | k = 1, ..., N_k\}$ and the following relational elements: *edges*, *faces*, and *cells*.

1. Cells (volumes) are at the top of the hierarchy and composed of faces.

2. Faces (surfaces) are next, composed of edges.

3. Edges (lines) are composed of verts (points).

From this implicit representation, explicit representations of elements may be calculated as needed. For example, planar face coefficients a, b, c, and d from the equation for a plane $0 = ax + by + cz + d$ may be calculated from the edges (or verts) which create a face. Our methods for solving the LOQD equations require face area vectors and cell volumes, so as part of a setup phase, we get explicit representations of cells and faces, determine face area vectors and cell volumes, then discard the explicit representations.
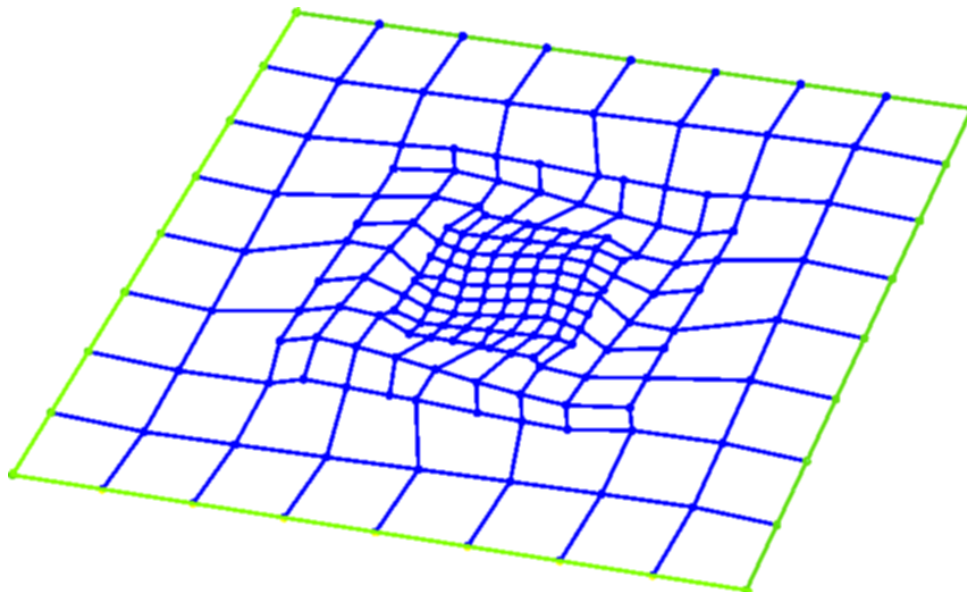
Figure 6.18: A 2D Mesh

6.6.2 Representing 2D (and 1D) Meshes

Obviously, the same complexity is not required for 2D (and 1D) arbitrary meshes as in 3D, so we may logically down-select the elements we consider in two ways: bottom-up selection (Table 6.7) and top-down selection (Table 6.8). Verts are not shown in the tables because they are a fundamental component of any mesh.

Both selections have advantages and disadvantages. Namely, the bottom-up selection has "geometric consistency", while the top-down selection has "solution referencing consistency". We choose the top-down selection, the conventional approach within the transport community.

Bottom-up Selection

The bottom-up selection has geometric consistency in that an edge is always 1D, a face always 2D, a cell always 3D. This leads to more straightforward coding of computational geometry algorithms for the mesh.

Top-down Selection

The top-down selection's "solution referencing consistency" has merits which arise from typical applications, i.e. approximations of solutions of PDEs with discretization methods which determine *average quantities* over faces and cells. With the top-down selection, a cell-average quantity from a 1D simulation is identical to a cell-average quantity from a 2D simulation with $\pm y$ or $\pm x$ symmetry. A face-average quantity is consistent among 2D and 3D with $\pm z$ symmetry.

It may be easier to understand the referencing problems that arise by considering what happens with the bottom-up selection. So by counter-example, consider a problem on a

Table 6.7: Bottom-Up Selection of Elements

dimensions	edges	faces	cells
1	✓		
2	✓	✓	
3	✓	✓	✓

Table 6.8: Top-Down Selection of Elements

dimensions	edges	faces	cells
1			✓
2		✓	✓
3	✓	✓	✓

2D mesh and another one on a 3D mesh with $\pm z$ symmetry. The two problems are of course equivalent, but using the bottom-up selection of the 2D mesh, a confusing situation results: a) the face-average scalar flux of the 3D mesh is equivalent to the edge-average scalar flux of the 2D mesh and b) even more confusingly, the cell-average scalar flux of the 3D mesh is equivalent to the face-average scalar flux of the 2D mesh. Often, symmetry is used to benchmark 3D methods against 2D results and 2D methods against 1D results—this is probably one of the reasons the top-down selection is the convention.

6.6.3 Toolbox-Style

In the development of `TAPACK`, we have found it advantageous to create various toolboxes in order to partition the operations that must be performed and create reusable software for future endeavors. Up to date, we have created an sequential input/output toolbox (`SIO`), a meshing toolbox (`Mesh`), a method of short characteristics toolbox (`MoCShort`), and a 2D visualization toolbox (`xyDraw`). These packages are integrated into `TAPACK` but are reusable on their own for sequential input/output; creating, querying, and modifying meshes (structured and unstructured); setting up and solving the transport equation with the method of short characteristics; and visualizing lines, polygons, and vectors in 2D using OpenGL; respectively.

6.6.4 Expandable

The structure of `TAPACK` is shown in Figure 6.19. This project implements short characteristics as the high-order solver and quasidiffusion as the low-order solver. To integrate additional solvers into `TAPACK`, we need to add a single line to each of the following: `SolverHO`, `SolverLO`, `Setup`, and `Wrapup`. Then a single additional input command should be defined (using the `SIO` toolbox) that sets parameters of the new routine (options, tolerances, etc.) Also additional outputs may be defined for these new routines using the `SIO` package, although the basic set of outputs for all transport calculations (angular flux and moments)

```
              ┌──────────────┐
              │    Input     │
              └──────────────┘
                     │
                     ▼
              ┌──────────────┐
              │    Setup     │
              └──────────────┘
                     │
                     ▼
              ┌──────────────┐
              │  InputEcho   │
              └──────────────┘
                     │
    ┌────────────────┼────────────────────────────┐
    │      ┌─────────▼────────┐     ┌───────────┐  │
    │  ┌──▶│     SOLVE        │────▶│  SolverLO │  │
    │  │   └──────────────────┘     └───────────┘  │
    │  │            │               ┌───────────┐  │
    │  │            │          ────▶│  SolverHO │  │
    │  │            ▼               └───────────┘  │
    │  │   ┌──────────────────┐                    │
    │  └───│     REFINE       │                    │
    │      └──────────────────┘                    │
    └──────────────────────────────────────────────┘
                     │
                     ▼
              ┌──────────────┐
              │    Output    │
              └──────────────┘
                     │
                     ▼
              ┌──────────────┐
              │    Wrapup    │
              └──────────────┘
```
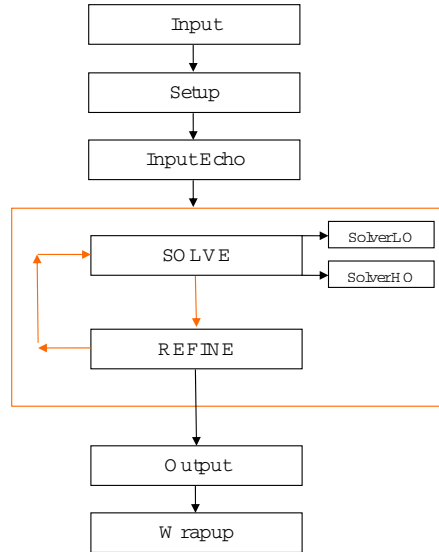
Figure 6.19: The framework of `TAPACK`.

may suffice.

6.6.5 Extendable

Currently, `TAPACK` is strictly a 2D code. However, the extension into 3D requires relatively few modifications to the code. All geometric considerations are relegated to the `Setup` stage and within that to calls to the meshing toolbox (`Mesh`). The meshing toolbox calls upon a library of 2D geometry routines. To extend the short characteristics transport from 2D to 3D would be fairly simple and involve only the task of creating 3D geometry routines (e.g. 3D ray-surface intersections, point-in-polyhedron checks, etc.) and modifying the meshing toolbox (`Mesh`).

Currently, `TAPACK` is strictly a serial code. However, it can be modified to perform parallel computations. In order to facilitate parallel computations with `TAPACK` we restrict the majority of runtime data to be contained in arrays. By doing this way we have a transparent (and portable) data structure on which to perform computations.

6.6.6 Visualization-Ready

We have found that visualization is especially useful when solving problems on unstructured meshes. A visual inspection of the mesh can immediately illuminate problems with the grid definition that would be difficult to find in tables of output data on the grid characteristics. We chose to use new Fortran bindings for the OpenGL API available through NIST. OpenGL is the industry standard in the world of 3D graphics, thus it is a portable graphics solution for the simple 2D unstructured mesh visualization, as well as easily extended into 3D unstructured mesh visualization, when `TAPACK` has 3D capability.
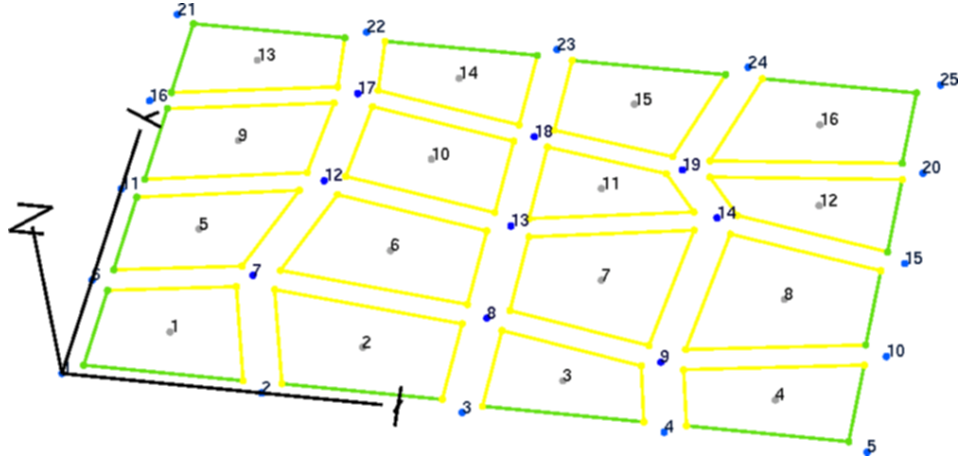
Figure 6.20: Vert and Cell Information needed for High Order Solve (Short Characteristics)
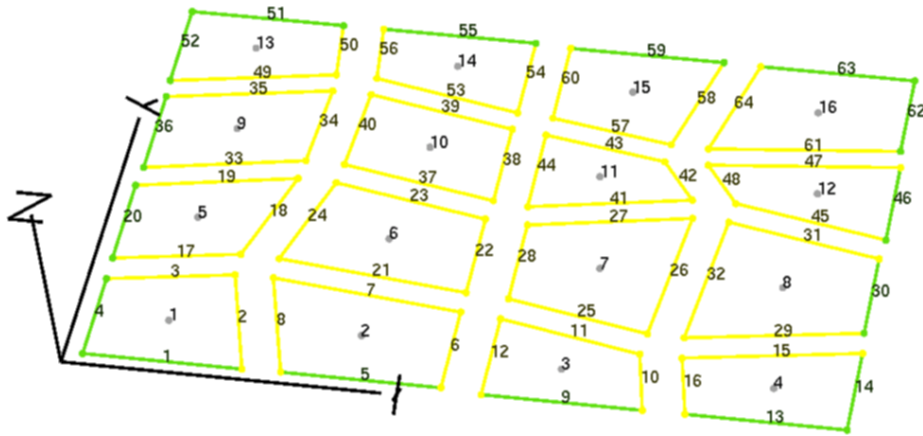
Figure 6.21: Face and Cell Information needed for Low Order Solve (Quasidiffusion)

Fig. 6.20 and 6.21 show example visualizations of a small, perturbed 2D mesh. Fig. 6.20 displays vert and cell numbers, while 6.21 displays face and cell numbers. These types of displays are useful in debugging newly implemented features as the identification numbers of verts, faces, and cells local to a particular area in an unstructured mesh are not usually related in any meaningful way—although, with that said, a reordering has been applied in Fig. 6.21 such that the faces belonging to a cell have sequential numbering.

6.7   Conclusions

We have developed a method for solving transport problems on unstructured meshes based on the QD method. To discretize the low-order QD equations, we apply local discretization to the equations in each cell. Then we couple cells at interfaces through strong continuity conditions for face-average normal currents and weak continuity conditions for face-average scalar fluxes. We have developed the following parts of the methodology:

1. new discretization method for the LOQD equations on arbitrary quadrilateral cells,

2. interface conditions for unstructured orthogonal or adaptive mesh refinement (AMR) meshes,

3. a sweeping order algorithm for arbitrary quadrilateral meshes,

4. method of short characteristics with local within cell interpolation along diagonal of a cell and linear approximation of the scattering source term, and

5. preconditioning and unknown reordering strategies for iteratively solving the the LOQD matrix system via `BiCGstab`.

Bibliography

[1] Y. Y. Azmy, "Unconditionally Stable and Robust Adjacent-Cell Diffusive Preconditioning of Weighted-Difference Particle Transport Methods is Impossible," *J. of Comp. Phys.*, **182**, 213-233 (2002).

[2] J. S. Warsa, T. A. Wareing, J. E. Morel, "Krylov Iterative Methods and the Degraded Effectiveness of diffusion Synthetic Acceleration for Multidimensional S_N Calculations in Problems with Material Discontinuities," *Nucl. Sci. Eng.*, **147**, pp. 218-248 (2004).

[3] J. Chang and M. L. Adams, "Analysis of Transport Synthetic Acceleration for Highly Heterogeneous Problems," *Proc. of M&C Topical Meeting*, Gatlinburg, TN, (2003).

[4] V. Ya. Gol'din, "A Qausi-Diffusion Method of Solving the Kinetic Equation," *USSR Comp. Math. and Math. Phys.*, **4**, 136-149 (1964).

[5] M. L. Adams and E. W. Larsen, "Fast Iterative Methods for Discrete-Ordinates Particle Transport Calculations," *Prog. Nucl. Energy*, **40**, 3-139 (2002).

[6] G.R. Cefus and E.W. Larsen, "Stability Analysis of the Quasidiffusion and Second Moment Methods for Iteratively Solving Discrete-Ordinates Problems," *Trans. Th. Stat. Phys.*, **18**, 493-511 (1989-90).

[7] K. S. Smith and J. D. Rhodes, III, *Proc. of PHYSOR*, Seoul, Korea (2002).

[8] D.Y. Anistratov and V.Ya. Gol'din, Nonlinear Methods for Solving Particle Transport Problems, *Transport Theory Statist. Phys.* **22**, 125 (1993).

[9] T.A. Germogenova, Convergence of Some Approximate Methods of Solving the Transport Equation, *Soviet Mathematics - Doklady* **9**, 855 (1968).

[10] V.Ya. Gol'din, G.V. Danilova and B.N. Chetverushkin, Approximate Method of Solving the Time-Dependent Kinetic Equation, in *Computational Methods in Transport Theory* (Atomizdat, Moscow, 1969) pp. 50-57 (in Russian).

[11] V.V. Gorskii and S.T. Surzhikov, Use of the Semimoment Method to Solve the Shock Layer Radiative Heat-Transfer Problem, *J. of Eng. Physics*, **42**, No. 1, 108 (1982).

[12] D.Y. Anistratov and E. W. Larsen, "Nonlinear and Linear α-Weighted Methods for Particle Transport Problems," *J. of Computational Physics*, **173**, 664-684 (2001).

[13] M.L. Adams, New Nonlinear Methods for Linear Transport Calculations, in *Proceedings of Joint International Conference on Mathematical Methods and Supercomputing in Nuclear Applications, April 19-23, 1993, Karlsruhe, Germany* pp. 683-694.

[14] S.G. Hong and N.Z. Cho, "A Rebalance Approach to Nonlinear Iteration for Solving the Neutron Transport Equation," *Ann. Nucl. Energy*, **24**, 147 (1997).

[15] E.W. Larsen and J.E. Morel, Asymptotic Solution of Numerical Transport Problems in Optically Thick Diffusive Regimes II, *J. of Computational Physics*, **83**, 212 (1989).

[16] E. W. Larsen, "The Asymptotic Diffusion Limit of Discretized Transport Problems," *Nucl. Sci. Eng.*, **112**, 336 (1992).

[17] M.M. Miften and E.W. Larsen, The Quasi-Diffusion Method for Solving Transport Problems in Planar and Spherical Geometries, *Transport Theory Statist. Phys.*, **22**, 165 (1993).

[18] T.R. Hill, Technical Report No. LA-5990-MS, Los Alamos Scientific Laboratory, June 1975 (unpublished).

[19] R.E. Alcouffe, E.W. Larsen, W.F. Miller and B.R. Wienke, Computational Efficiency of Numerical Methods for the Multigroup, Discrete-Ordinates Neutron Transport Equations: The Slab Geometry Case,", *Nucl. Sci. Eng.* **71**, 111 (1979).

[20] E.W. Larsen and J.B. Keller, "Asymptotic Solution of Neutron Transport Problems for Small Mean Free Paths," *J. Math. Phys.*, **15**, 75 (1974).

[21] G.J. Habetler and B.J. Matkowsky, "Uniform Asymptotic Expansions in Transport Theory with Small Mean Free Paths, and the Diffusion Approximation," *J. Math. Phys.*, **16**, 846 (1975).

[22] K.M. Case and P.E. Zweifel, **Linear Transport Theory**, Addison-Wesley, Reading, MA (1967).

[23] V.Ya. Goldin, V.A. Kuzyuk, and A.K. Rakhmatulina, "Nonlinear Method of Electron Transport Calculation," *USSR Comp. Math. and Math. Phys.*, **16**, No. 2, 131 (1976).

[24] M.L. Adams, Discontinuous Finite Element Transport Solutions in Thick Diffusive Problems, *Nuclear Science and Engineering*, **137**, pp. 298-333 (2001).

[25] L. Roberts and D.Y. Anistratov, "Nonlinear Weighted Flux Methods for Particle Transport Problems," Proceedings of *M&C 2005, International Conference on Mathematics and Computations, Supercomputing, Reactor Physics and Nuclear Biological Applications,* American Nuclear Society Topical Meeting of M&C Division, Avignon, France, September, 2005, 10 pp.

[26] M.L. Adams and W.R. Martin, "Diffusion Synthetic Acceleration of Discontinuous Finite Element Transport Iterations," *Nuclear Science and Engineering*, **111**, 145 (1992).

[27] J.E. Morel, J.E. Dendy, Jr., and T.A. Waring, "Diffusion-Accelerated Solution of the Two-Dimensional S$_n$ Equations with Bilinear-Discontinuous Differencing," *Nuclear Science and Engineering*, **115**, 304-319 (1993).

[28] V.Ya. Gol'din, "Characteristic Difference Scheme for Non-Stationary Kinetic Equation," *Soviet Mathematics - Doklady*, **1**, 902 (1960).

[29] V.Ya. Gol'din, N.N. Kalitkin , and T.V. Shishova, "Nonlinear Difference Schemes for Hyperbolic Equations," *USSR Comp. Math. and Math. Phys.* **5**, 229 (1968).

[30] K.Takeuchi, "A Numerical Method for Solving the Neutron Transport Equation in Finite Cylindrical Geometry," *J. Nucl. Sci.*, **6**, 446 (1969).

[31] I.K. Abu-Shumays, Angular Quadratures for Improved Transport Computations, *Transport Theory Statist. Phys.*, **30**, pp. 169-204 (2001).

[32] K.M. Case and P.E. Zweifel, **Linear Transport Theory**, Addison-Wesley, Reading, MA (1967).

[33] C.D. Levermore, "Relating Eddington Factors to Flux Limiters," *J. Quant. Spectrosc. Radiat. Transfer*, **31**, 149-160, (1984)

[34] C.D. Levermore and G.C. Pomraning, "A Flux-Limited Diffusion Theory," *Astrophys. J.*, **248**, 321-334, (1981).

[35] G.N. Minerbo, "Maximum Entropy Eddington Factors," *J. Quant.Spectrosc. Radiat. Transfer*, **20**, 541-545 (1978).

[36] R. Sanchez, "On the Spectral Analysis of Iterative Solutions of the Discretized One-Group Transport Equation," *Annals of Nuclear Energy*, **149**, pp. 2059-2075 (2004).

[37] A. Constantinescu and D.Y. Anistratov, "Stability Analysis of the Quasidiffusion Method for 1D Periodic Heterogeneous Problems," *Trans. Am. Nucl. Soc.,* **95**, 2006.

[38] E.N.Aristova, V.Ya. Gol'din, and A.V.Kolpakov, "Multidimensional Calculations of Radiation Transport by Nonlinear Quasi-Diffusion Method," *Proceeding of ANS International Conference on Mathematics and Computation, Reactor Physics and Environmental Analysis in Nuclear Applications*, Sept. 27-30, 1999, Madrid, Spain, 667-676 (1999).

[39] V.Ya. Gol'din, D. A. Gol'dina and A.V. Kolpakov, "The Solution of Two-Dimensional Stationary Quasidiffusion Problem," *Preprint of the Keldysh Institute for Applied Mathematics*, the USSR Academy of Sciences, No. 49 (1982) (in Russian).

[40] V.Ya. Gol'din, "Characteristic Difference Scheme for Non-Stationary Kinetic Equation," *Soviet Mathematics - Doklady*, **1**, 902 (1960).

[41] V.Ya. Gol'din, N.N. Kalitkin , and T.V. Shishova, "Nonlinear Difference Schemes for Hyperbolic Equations," *USSR Comp. Math. and Math. Phys.* **5**, 229 (1968).

[42] K.Takeuchi, "A Numerical Method for Solving the Neutron Transport Equation in Finite Cylindrical Geometry," *J. Nucl. Sci.*, **6**, 446 (1969).

[43] M. J. Berger & P. Colella, *J. of Comp. Phys.*, **88**, 64 (1989).

[44] J.P. Jessee, W.A. Fiveland, L.H. Howell, P. Colella, & R.B. Pember, *J. of Comp. Phys.*, **139**,380 (1998).

[45] V.Ya. Goldin. and B.N. Chetverushkin, "Methods of Solving One-Dimensional Problems of Radiation Gas Dynamics," *USSR Comp. Math. and Math. Phys.*, **12**, No. 4, 177 (1972).

[46] N. N. Aksenov and V. Ya. Gol'din, "Computation of the Two-Dimensional Stationary Equation of Neutron Transfer by the Quasi-Diffusion Method," *USSR Comp. Math. and Math. Phys.*, **19**, No. 5, 263-266 (1979).

[47] E.N.Aristova and A.V.Kolpakov, "A Combined Finite Difference Scheme for an Elliptic Operator in an Oblique-Angled Cell," *Mathematical Modeling*, **8**, 3 (1991) (in Russian). English translation was published in *Mathematical Modeling and Computational Experoment*, **1**, 187 (1993).

[48] J.E. Morel, "A 3-D Cell-Centered Diffusion Discretization for Arbitrary Polyhedral Meshes," Los Alamos National Laboratory Research Note, CCS-4:02-40(U) (2002).

[49] K.Lipnikov, J. Morel, M. Shashkov, "Mimetic finite difference methods for diffusion equations on non-orthogonal non-conformal meshes," *J. of Comp. Phys.*, **199**, 589-597 (2004).

[50] V.Ya. Gol'din, A.V. Kolpakov, and A.V. Misyurev, "Front Capturing Solution of Unstationary Transport Equation," *Preprint of the Keldysh Institute for Applied Mathematics*, the USSR Academy of Sciences, No. 68 (1983) (in Russian).

[51] C. Brezinski, M. Redivo Zaglia, **Extrapolation methods. Theory and practice** , North-Holland (1991)

[52] M. L. Adams, "Subcell Balance Methods for Radiative Transfer on Arbitrary Grids," *Transport Theory and Statistical Physics*, 26(4&5), 385-431 (1997).